TÉCNICO LISBOA

Numerical modeling of cardiovascular physiology

Study of dynamic changes during autonomic reflexes and applications to acute myocardial infarction

João Nuno Gaspar Apura

Thesis to obtain the Master of Science Degree in

Biomedical Engineering

Supervisors: Prof.ª Adélia da Costa Sequeira dos Ramos Silva
Prof. Dr. Luís Afonso Brás Simões do Rosário

Examination Committee

Chairperson:	Prof. Ana Luísa Nobre Fred
Supervisor:	Prof. Dr. Luís Afonso Brás Simões do Rosário
Member of the Committee:	Prof. Jorge Filipe Duarte Tiago

December 2016

Acknowledgments

I would like to use this section to acknowledge the contribution of a few people who were fundamental to the successful elaboration of this thesis.

First and foremost, I would like to express my heartfelt gratitude to my adviser and supervisor Professor Luís Brás Rosário, for his immense support and help during my Master thesis, for his huge patience and encouragement, and for never giving up on me. His immense knowledge and passion for research was the key factor which kept me motivated. I could not have been more lucky regarding my mentor and adviser!

I also thank my supervisor Adélia Sequeira for all the knowledge, guidance and fondness during the elaboration of this thesis, always available for me.

Even though Professor Jorge Tiago has not been directly related to this thesis, I would like to thank him for his support, persistence and availability in other projects we developed together. Jorge is definitely one of the best scientific researchers I have already met, everything he does breeds precision and excellence.

I wish to express a deep thank you to Mário Apura, Donzília Gaspar, Cristina Apura, Nuno Garrinhas, Gustavo Garrinhas, Miguel Garrinhas and Tiago Garrinhas, who have never gave up supporting me all the way through and have picked me up in all those moments of shaken confidence. Thank you for your unconditional love and emotional support.

I also want to share the enormous gratitude I feel for Inês Ferreira. I am truly grateful for her enormous support during the final weeks of this thesis. Without her, I would never have understood how a sound mind needs a sound body. Thank you for teaching me how to *trust and believe*!

Finally, I would like to gratefully acknowledge the research grant funded by FCT Project EXCL/MAT-NAN/0114/2012: "PHYSIOMATH - Mathematical and Computational Modelling of Human Physiology".

Abstract

The autonomous nervous system maintains the cardiac output and arterial blood pressure within a narrow homeostatic range through a closed-loop network of cardiovascular reflexes, including the cardiac baroreflex, arterial chemoreflex and von Bezold-Jarisch reflex. These are cardioprotective reflexes and their effect has been extensively evaluated on heart rate and arterial blood pressure. Cardiac stroke work and total energy consumption are tightly regulated and it is hypothesized that these reflexes can participate in this regulation.

This thesis aimed at studying left ventricular mechanical properties of the heart during reflex cardiovascular responses, in order to better understand the autonomic balance of the cardiac system in the point of view of cardiovascular efficiency and ventriculo-arterial coupling, and how these can be compromised after the acute phase of myocardial infarction. Reflexes were evoked in anesthetized, paralyzed and artificially ventilated rabbits, and heart ischemia was provoked by ligation of the descending coronary artery. An intraventricular impedance catheter was used to measure simultaneously left ventricle pressure and volume.

It was developed a pressure-volume computational framework to manage physiological data and to accurately characterize instantaneous left ventricular and arterial physiologic properties. This custom software estimated single-beat left ventricle end-systolic elastance, arterial elastance and their ratio to analyze ventriculo-arterial coupling. From this data, left ventricle stroke work, total energy expenditure (pressure-volume area), ratio of the stroke work to its theoretical maximum and cardiac energetic efficiency were estimated.

In the intact cardiovascular system, the reflexes in study revealed a balanced control of induced homeostatic perturbations by simultaneously modeling arterial input impedance and left ventricle performance, as demonstrated by changes in contractility and stroke work, in such a way that ventriculo-arterial coupling, mechanical ratio and cardiac energetic efficiency were maintained close to optimal values. Each reflex optimized the cardiac work and energetic efficiencies in a different way.

Acute myocardial infarction contributed to a significant depression in cardiac contractility, which resulted in a deterioration of the ventriculo-arterial coupling. Due to myocardial necrosis, cardiac stroke work was augmented as an effort to maintain the arterial tone within the optimal physiological range, at the expense of a higher oxygen consumption. An unbalanced increase in workload and oxygen consumption resulted in a depression of cardiac work and energetic efficiencies. Activation of cardiovascular reflexes in infarcted hearts revealed similar hemodynamic responses as in the control group for arterial input impedance, left ventricle performance and oxygen intake. Cardiac efficiency and energy transmission to the arterial system were optimized differently according to each reflex.

Keywords: Cardiovascular reflexes – Acute myocardial infarction – Single-beat method – Ventriculo-arterial coupling – Cardiac efficiency

Resumo

O sistema nervoso autónomo mantém o débito cardíaco e a pressão arterial no intervalo homeostático através de uma rede fechada de reflexos cardiovasculares, incluindo o barorreflexo cardíaco, quimioreflexo arterial e reflexo von Bezold-Jarisch. Sendo reflexos cardioprotetores, o seu efeito tem sido extensivamente estudado na frequência cardíaca e pressão arterial. O trabalho cardíaco e o consumo total energético são rigorosamente regulados, e é colocada a hipótese que estes reflexos possam participar nesta regulação.

O objetivo principal desta tese é estudar as propriedades mecânicas do ventrículo esquerdo do coração durante as respostas cardiovasculares enunciadas, com o intuito de compreender melhor o equilíbrio autónomo do sistema cardíaco do ponto de vista da eficiência cardiovascular e do acoplamento ventriculo-arterial, e como estes podem ser comprometidos após isquémia cardíaca. Os reflexos foram evocados em coelhos anestesiados, paralisados e ventilados artificialmente, e o enfarte agudo do miocárdio foi provocado através da ligação da artéria coronária descendente. Para medir simultaneamente a pressão e o volume do ventrículo esquerdo foi utilizado um cateter de impedância intraventricular.

Foi desenvolvido um programa computacional de gestão e análise de dados fisiológicos de pressão-volume, de forma a caracterizar com precisão as propriedades fisiológicas ventriculares e arteriais instantâneas do sistema cardiovascular. Este software permitiu estimar, através do método de contração individual, a elastância de fim de sístole no ventrículo esquerdo, elastância arterial e o seu rácio, com o intuito de analisar o acoplamento ventriculo-arterial. A partir destes dados, estimou-se o trabalho cardíaco do ventrículo esquerdo, consumo total de energia (área pressão-volume), razão entre o trabalho cardíaco e o seu máximo teórico, e eficiência energética cardíaca.

Para um sistema cardiovascular intacto, os reflexos em estudo revelaram um controlo equilibrado das perturbações homestáticas induzidas através da modelação simultânea da impedância arterial, contractilidade do miocárdio e trabalho cardíaco, de tal forma que o acoplamento ventriculo-arterial e eficiência energética se mantiveram no intervalo de valores ótimos. Cada reflexo optimizou as eficiências mecânica e energética de forma diferente.

O enfarte agudo do miocárdio contribuiu para uma depressão significativa da contractilidade cardíaca, o que consequentemente contribuiu para uma deterioração do acoplamento ventriculo-arterial. Devido à morte de células musculares do coração, o trabalho cardíaco foi reforçado de forma a manter o tónus arterial dentro do intervalo fisiológico ideal, à custa de um aumento do consumo de oxigénio. Um aumento discordante no trabalho cardíaco e consumo total de oxigénio contribuiu para uma depressão das eficiências mecânica e energética do coração. A ativação de reflexos cardiovasculares em corações infartados relevou respostas hemodinâmicas semelhantes às no grupo de controlo, para a impedância arterial de entrada, desempenho do ventrículo esquerdo e consumo de oxigénio total. A eficiência cardíaca e a transmissão de energia para o sistema arterial foram otimizadas em função de cada reflexo.

Palavras-chave: Reflexos cardiovasculares – Enfarte agudo do miocárdio – Método de contração individual – Acoplamento ventriculo-arterial – Eficiência cardíaca

Table of Contents

List of Figures

List of Tables

List of Abbreviations

AIC	Akaike information criterion
ANOVA	Analysis of variance
ANS	Autonomic Nervous System
BJR	Bezold-Jarisch
BR	Baroreflex
CR	Chemoreflex
ECG	Electrocardiogram
EDPVR	End-diastolic pressure-volume relationship
ESPVR	End-systolic pressure-volume relationship
FIR	Finite impulse response
GUI	Graphical User Interface
LMM	Linear mixed-effect model
LV	Left ventricle
MA	Moving-average
MI	Myocardial infarction
ML	Maximum likelihood
NTS	Nucleus Tractus Solitarius
PE	Potential energy
PNS	Parasympathetic Nervous System
PRSW	Preload recruitable stroke work
PV	Pressure-volume
SA	Sinoatrial
SG	Savitzky-Golay
SNR	Signal-to-noise ratio
SNS	Sympathetic Nervous System
V-A	Ventricular-arterial
VCO	Vena cava occlusion

List of Symbols

BP	$[\, mm\ Hg \,]$	Arterial blood pressure
CO	$[\, mL/min \,]$	Cardiac output
CWE	$[\ ]$	Cardiac work efficiency
$E(t)$	$[\, mm\ Hg/mL \,]$	Time-varying left ventricle elastance
EF	$[\, \% \,]$	Ejection fraction
$E_N(t_N)$	$-$	Normalized elastance curve
E_a	$[\, mm\ Hg/mL \,]$	Effective arterial elastance
E_{es}	$[\, mm\ Hg/mL \,]$	End-diastolic elastance
E_{max}	$[\, mm\ Hg/mL \,]$	Maximum of time-varying left ventricle elastance
HR	$[\, min^{-1} \,]$	Heart rate
MVO_2	$[\, J \,]$	Myocardial oxygen consumption
$P(t)$	$[\, mm\ Hg \,]$	Time-varying left ventricle pressure
PVA	$[\, mm\ Hg \cdot mL \,]$	Pressure-volume area
P_{MAX}	$[\, mm\ Hg \,]$	Theoretical maximal isovolumic pressure
P_{ed}	$[\, mm\ Hg \,]$	End-diastolic pressure
P_{es}	$[\, mm\ Hg \,]$	End-systolic pressure
Q_{load}	$[\ ]$	Ratio of the stroke work to its maximum
SV	$[\, mm\ Hg \,]$	Stroke volume
SW	$[\, mm\ Hg \cdot mL \,]$	Stroke work
SW_{max}	$[\, mm\ Hg \cdot mL \,]$	Maximal stroke work
$T_{50\%}$	$[\, ms \,]$	Time required for pressure to decline to 50% of the value at $\mathrm{d}P/\mathrm{d}t_{min}$
$V(t)$	$[\, mL \,]$	Time-varying left ventricle volume
V_0	$[\, mL \,]$	Volume intercept of the end-systolic pressure-volume relationship
V_{ed}	$[\, mL \,]$	End-diastolic volume
V_{es}	$[\, mL \,]$	End-systolic volume
τ	$[\, ms \,]$	Isovolumic relaxation constant
τ_L	$[\, ms \,]$	Isovolumic relaxation constant from Logistic method
τ_W	$[\, ms \,]$	Isovolumic relaxation constant from Weiss's method
τ_{RG}	$[\, ms \,]$	Isovolumic relaxation constant from Raff & Glantz's method
$\mathrm{d}E_N(t_N)$	$-$	Physiological variance of $E_N(t_N)$
$\mathrm{d}P/\mathrm{d}t$	$[\, mm\ Hg/s \,]$	Rate of pressure change
$\mathrm{d}P/\mathrm{d}t_{max}$	$[\, mm\ Hg/s \,]$	Maximum rate of pressure change
$\mathrm{d}P/\mathrm{d}t_{min}$	$[\, mm\ Hg/s \,]$	Minimum rate of pressure change
$\mathrm{d}V_0$	$[\, mL \,]$	Variance about V_0 estimate
t_{max}	$[\, ms \,]$	Time to maximum left-ventricle elastance

CHAPTER 1

Introduction

1-1 Motivation

The normal cardiovascular system maintains the cardiac output and arterial blood pressure within a narrow homeostatic range, despite a number of internal and external perturbations. Some of these internal perturbations include processes such as respiration and fluctuations in peripheral resistance, while external perturbations include level of exercise, ambient temperature and postural shifts (Berne et al., 2008). The autonomous nervous system compensates for these perturbations through a closed-loop network of cardiovascular reflexes, including the cardiac baroreflex, arterial chemoreflex and von Bezold-Jarisch reflex. Unfortunately, while the basic mechanisms of cardiac system's autonomic balance are determined, the integrated regulatory system remains to be well understood (Mullen et al., 1997).

To assess the left ventricular systolic and diastolic mechanical properties of the heart, there is a wide variety of indexes that can characterize and quantify chamber contractility and performance. The development and validation of the conductance catheter method for the measurement of pressure-volume PV loops, based on the electrical conductance of the blood contained in the left-ventricle, allowed the determination of these indexes (Baan et al., 1981). However, determination of PV-based contractile indexes requires the recording of several PV loops while gradually decreasing the blood that enters the left-ventricle, using a balloon occlusion of the vena cava (Gupta et al., 1989). In humans, this procedure may be hazardous and raises ethical criticism. To circumvent this necessity, several single-beat methods have been proposed for the left-ventricle, based on data measured during hemodynamic steady-state conditions (Chen et al., 2001; Takeuchi et al., 1991).

Given its experimental advantages, the single-beat methods provide a reasonable approach to understand the role of ventriculo-arterial coupling in the assessment of cardiovascular function, offering new and complementary perspectives for understanding how both heart and arterial systems work together, in order to optimize cardiovascular efficiency (Guarracino et al., 2013). Analysis of single-beat ventriculo-arterial coupling during cardiovascular reflex responses can help characterize how the regu-

latory system decides whether to optimize cardiovascular performance or cardiac energetics, and how these altered hemodynamic profiles can be affected in the acute phase of myocardial infarction.

1-2 Objective and proposed approach

This thesis is focused on the mechanical properties of the heart during reflex cardiovascular responses, evoked by stimulation of carotid chemoreceptors, cardiac chemosensitive fibers and baroreceptors, before and after acute myocardial infarction (MI). Although blood pressure and heart rate had already been studied in Rocha et al. (2003a), this study provides a complementary and extensive framework to study other cardiovascular properties and, consequently, better understand the autonomic balance of the cardiac system in the point of view of ventriculo-arterial coupling and cardiovascular efficiency.

This work has two main goals. First, it aims at developing a computational framework in Matlab® to provide a powerful and easy-to-use software for researchers to manage physiological PV data and to compute beat-by-beat left ventricular and arterial physiologic properties. This framework should be able to automatically identify end-diastolic and end-systolic points for each cardiac cycle, estimate left-ventricle elastance using the single-beat method, compute left-ventricle mechanical properties, and dynamically visualize results.

Second, this study aims at accurately using the computational framework and a custom complementary statistical tool to characterize and analyze ventriculo-arterial coupling and cardiac performance in healthy hearts from rabbits, during three cardiovascular reflex responses: cardiac baroreflex, arterial chemoreflex and cardiopulmonary reflex. The developed framework will be also used to understand how acute interventions in the circulatory system, such as myocardial infarction, might compromise the heart's response to the altered hemodynamic profiles in study. As such, it will be attempted to identify temporal patterns during reflex responses and compare the results between healthy and pathological conditions.

This thesis was developed in Associação para a Investigação e Desenvolvimento da Faculdade de Medicina (AIDFM), from Faculty of Medicine, University of Lisbon, and Center for Computational and Stochastic Mathematics (CEMAT), from Instituto Superior Técnico, University of Lisbon. The work was supported by project grant "PHYSIOMATH - Mathematical and Computational Modelling of Human Physiology", FCT Project EXCL/MAT-NAN/0114/2012.

Some of the contents of this thesis have been submitted in abstract form and are detailed below.

Apura J., Rocha I., Pinto F., Sequeira A., and Bras-Rosario L. (2016), 'Cardiac Chemoreflex Control of Cardiac Stroke Work and Energy Consumption', Abstract - Experimental Biology 2016, San Diego, USA. *The FASEB Journal* **30**, 1286-5.

Apura J., Rocha I., Pinto F., Sequeira A., and Bras-Rosario L. (in submission), 'Arterial Chemoreflex influence in Cardiac Energetics', Abstract - Experimental Biology 2017, Chicago, USA.

1-3 Structure

This thesis is divided in six chapters: 1. Introduction, 2. State of Art, 3. Numerical Methods and Implementation, 4. Results, 5. Discussion, and 6. Conclusions and Future Work.

Chapter 1 presents the motivation of the project, concrete goals, contributions of this thesis and a summary of the work presented afterwards.

Chapter 2 begins with the physiological background necessary for the understanding of the applied methodology. The chapter focuses in the mechanical properties of the heart and important cardiovascular parameters are presented. The ventricular-arterial coupling concept is addressed. The chapter further details on how the heart function is regulated by the autonomous nervous system, focusing on three simple reflexes. In the last section, it is conducted a brief literature review on myocardial infarction.

In **Chapter 3**, numerical methods for PV data analysis and their computational implementation are fully explained. First, it is enlightened how the physiological data was acquired. Afterwards, a thorough description of the PV data analysis software is presented, from data preparation to estimation of hemodynamic properties. In each stage, a detailed overview of the implemented numerical methods is presented, along with a brief literature review.

Chapter 4 comprises the results obtained from statistical analysis, along with the respective remarks of each analysis.

In **Chapter 5**, a widespread discussion of the results is performed, with a parametric comparison between the healthy and pathological groups.

Finally, in **Chapter 6**, methodological considerations and final remarks concerning this work are presented. Future research developments in this field of study are explored.

CHAPTER 2

State of the Art

This chapter is designed to provide the reader with the essential background information needed to understand the discussions and explanations in the following chapters. It begins with a brief description of the cardiac cycle. Then, the most important cardiovascular parameters of the heart are presented, including ventricular elastance, effective arterial elastance, stroke work and cardiac work efficiency. Ventricular-arterial coupling is addressed, due to its importance in understanding how both heart and arterial systems work together. The chapter further details on cardiovascular regulation, focusing on three reflexes: cardiac baroreflex, arterial chemoreflex and Bezold-Jarisch reflex. In the last section, it is conducted a brief literature review on myocardial infarction.

2-1 Cardiac cycle

The heart is the muscular organ responsible for pumping blood throughout the circulatory system by rhythmic contractions, assuring appropriate quantities of oxygen and nutrients are delivered through the body to the tissue cells, and removing carbon dioxide and other waste products from them. In the systemic circuit, oxygenated blood is pumped from the left ventricle (LV) and flows throughout the body, returning deoxygenated to the heart via the right atrium. In pulmonary circuit, blood leaves the right ventricle, travels through the lungs and then returns oxygenated, through the left atrium. For a further description of the heart's anatomy and physiology, it is recommended to read McKinley and O'loughlin (2012, ch. 22).

A cardiac cycle comprehends all the cardiac events which occur from the beginning of one heartbeat to the beginning of the next. Each cycle, in itself, is composed of different phases. A summary of these phases is described in the Wiggers' diagram (Wiggers, 1915) and still used today, giving an opportunity to view electrical and mechanical temporal relationships throughout a heartbeat.

A cardiac cycle can be divided into two parts: a period of relaxation called diastole, during which the heart fills with blood, followed by a period of contraction called systole. Its total duration, including systole and diastole, is reciprocal of the heart rate. Each cycle begins with the early diastole, when the

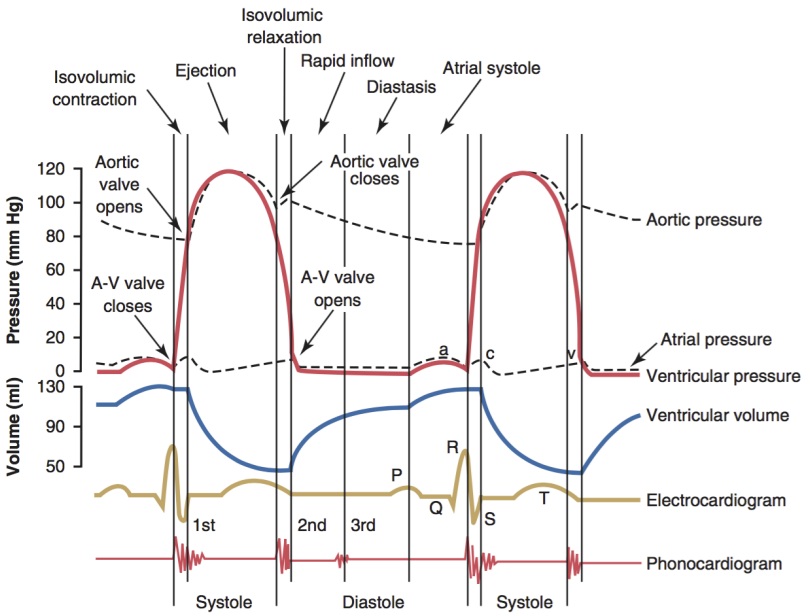

Figure 2-1: Wiggers' diagram: a set of events from the cardiac cycle, measured in a human's left ventricle (Hall, 2015). The top three curves show the pressure changes in the aorta, left ventricle and left atrium, respectively. Ventricular volume is depicted in the forth curve, whereas the fifth represents the electrocardiogram. The last curve depicts a phonocardiogram, which is a recording of the sound produced by the heart. A-V: atrioventricular.

blood from the two atria passively flow into the two ventricles, while both pulmonary and aortic valves remain closed. The atria then contract and force all the blood in them into the ventricles, a stage called atrial systole. After this, both tricuspid and mital (atrioventricular) valves close, preventing backflow of blood from the ventricles to the atria. Since there is no flow of blood into or out of the heart, it is called isovolumic contraction. This stage is followed by ventricular ejection: a rapid ejection of blood, due to contraction of the ventricles and opening of the semi-lunar valves (one located at the opening of the aorta and the other at the opening of the pulmonary artery). In this stage, the pressure in the ventricle decreases until it reaches the aortic pressure. The fifth stage, isovolumic ventricular relaxation, begins when the semi-lunar valves close. Since no blood enters the ventricles, they stop contracting and begin to relax. When the pressure in the ventricles falls below the pressure in the atria, both atrioventricular valves open, creating a stage of rapid filling followed by a period of diastasis, in which the filling almost stops.

2-2 Mechanical properties of the heart

Assessment of left and right ventricular systolic and diastolic mechanical properties is vital for understanding cardiovascular physiology. The first cardiovascular investigations, regarding the characterization of the pressure-volume (PV) relationship of an isolated frog ventricle, dates back to a 1895 article by the German physiologist Otto Frank (Frank, 1895). Frank made important observations about this relationship, which were well-received in Europe. In a series of articles from 1912 to 1914 (Knowlton and Starling, 1912; Markwalder and Starling, 1914; Patterson et al., 1914; Patterson and Starling, 1914),

Ernest Starling published what led to the well-known Frank-Starling law of the heart, which describes the ability of the heart to compensate for varying end-diastolic volumes by varying its force of contraction and external work accordingly, while all other factors remain constant. When an extra amount of blood flows into the ventricles, the cardiac muscle is stretched to a greater length. This stretching in turn causes the muscle to contract with increase force because the actin and myosin filaments are brought to a more nearly optimal degree of overlap for force generation (Sonnenblick et al., 1964).

Later force-velocity relations were investigated by Sonnenblick (1962), who concluded that an increase in myocardial contractility would not only result in an increase of the force developed by the muscle and velocity of contraction, but also in a decrease of the contraction time. Sonnenblick showed the possibility of relating force and velocity of myocardial contraction through a curve with maximum shortening velocity at zero load and at maximum tension developed by the muscle.

Since then, numerous articles have been published on the topic, resulting in a greater insight not only into the fundamental concepts of cardiovascular physiology and pathophysiology, but also mechanics of the heart muscle in different stages. Instead of displaying the LV pressure and volume independently as in a Wiggers' diagram, the gold standard is through simultaneous assessment of both, resulting in a counter-clockwise PV loop.

2-2-1 Pressure-volume loop

Figure 2-2 shows a diagram in which the red lines form a rectangular loop called PV loop of the cardiac cycle, for a normal left ventricle. Four phases of the heart cycle can be distinguished in the loop, which are described below for the left ventricle.

The first phase is the *filling period*. The loop begins with the opening of the mitral valve (point **A**), allowing the arterial blood to flow into the left ventricle from the left atrium. The ventricular volume in-

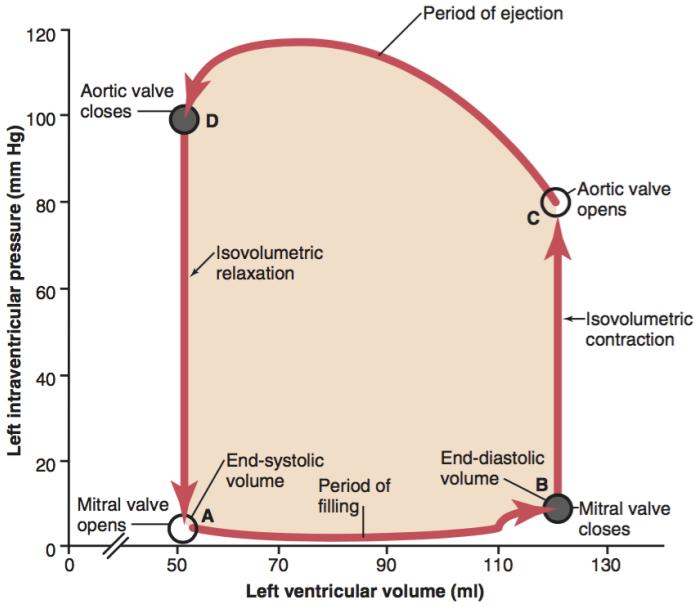

Figure 2-2: PV loop demonstrating the critical points and actions in a single cardiac cycle of a man. Adapted from Hall (2015).

creases to a maximum, designated end-diastolic volume (V_{ed}), and there is a slight increase in pressure in this period. This phase ends when the semi-lunar valve close (point **B**). Between points **B** and **C** is the *period of isovolumic contraction*, in which there is no flow of blood into or out of the left ventricle. Although the volume does not change, the pressure inside the ventricle increases to equal the pressure in the aorta. The *ejection period* starts at point **C**, with the opening of the aortic valve. During ejection, the ventricle contraction allows systolic pressure to rise and, at the same time, its volume decreases because the blood is now flowing into the aorta. At the end of the ejection period, the ventricle stops contracting and begins to relax. The ventricular volume and pressure at point **D** is called end-systolic volume (V_{es}) and end-systolic pressure (P_{es}), respectively. During this *period of isovolumic relaxation*, the left ventricle's pressure falls back to the diastolic pressure level, returning to the starting point **A** (Hall, 2015).

The end-systolic and end-diastolic points of a family of PV loops delineate two distinct curves (boundaries), namely the end-systolic (ESPVR) and end-diastolic pressure-volume relationship (EDPVR). The EDPVR is more commonly associated with LV's passive state, while the ESPVR provides information regarding the active mechanical properties of the LV. Interest in pressure-volume relationships of the heart experienced a resurgence in 1950s and 1960s, from studies in mammalian hearts (Hild and Sick, 1955; Ullrich et al., 1954) and canine hearts (Holt et al., 1957; Monroe and French, 1960, 1961). Although there were considerable differences regarding the volume measurement method, these studies proved to be different than the previous using the frog ventricle. While in the case of dog's ventricle under the control condition the ESPVR was almost linear, the frog's studies showed strong dependence of ESPVR on the loading conditions and inotropic (contractile) states. Later, some authors proposed possible reasons for the differences between these studies, which were summarized in Sagawa (1978). One reason could have been the difficulty to access the quantitative validity of the results, since they were presented in schematic diagrams. Another reason, with more consent, focused on the possibility of the frog's myocardium could have been in an ischemic condition during the determination of the PV relation curve, because its myocardium does not depend on coronary arteries, and obtains O_2 from intraluminal blood.

The most substantial work on the characterization of ESPVR comes from authors Suga, Sagawa and Sunagawa, in the 1970s and 1980s. This was due to advances in catheter technology and the advent of the conductance catheter, which allowed instantaneous and simultaneous volume and pressure measurements of the left ventricle in-vivo (Baan et al., 1981). The work on the in-vivo canine hearts further confirmed and refined the linearity of ESPVR in the physiologic range and helped advance understanding a wide set of other properties which could be obtained from these measurements (Suga, 1969, 1970; Sunagawa et al., 1983, 1985). More importantly, Suga et al. (1973) and Suga and Sagawa (1974) noticed the ESPVR was relatively insensitive to changes in heart rate and whether the ventricle was contracting isovolumically or ejecting blood against varying aortic pressure, providing a valuable index of systolic cardiac function. Furthermore, as end-diastolic volume (V_{ed}) increased and the PV loops shifted to the right, end-systolic pressure (P_{es}) would increase along the ESPVR line up to a maximum pressure for isovolumic contraction. However, results also showed PV loops were very sensitive

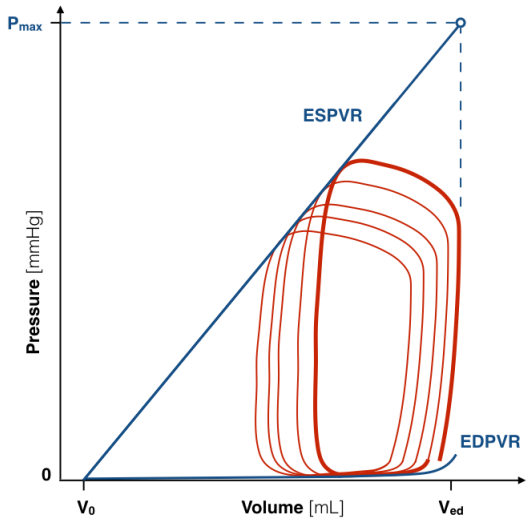

Figure 2-3: The PV loops are confined by the end-diastolic pressure volume relationship (EDPVR) and the end-systolic pressure volume relationship (ESPVR). In case of VCO, the PV shifts to the left due to a decrease of V_{ed} (Gupta et al., 1989). The theoretical P_{MAX} value is the maximum pressure reached by LV if ejection did not take place (maximum pressure at the isovolumic phase).

to dysfunctions, or changes in the contractile state of the ventricle. For example, through a vena cava occlusion (VCO), the PV loop would change in a characteristic way: the V_{ed} would decrease and thus the loops would shift to the left, but nothing else would be modified about the heart or arterial system properties (see **Figure 2-3**) (Gupta et al., 1989).

2-2-2 Preload and afterload

Basic concepts such as preload and afterload are of importance when characterizing the inotropic properties of the heart. In fact, in many abnormal functional states of the heart these concepts are altered from normal to severe degree. Similarly as in a skeletal muscle, preload specifies the degree of tension on the muscle when it begins to contract; afterload specifies the load against the muscle exerts its contractile force (Hall, 2015).

In the case of the heart, LV preload is correlated to end-diastolic pressure (P_{ed}), pressure when the ventricle has become filled with blood, and thus is influenced by the flow coming from the pulmunary circulation into the left atrium. To achieve a change in preload, balloon occlusion of the inferior vena cava has shown to be a rapid and practical way. This purely mechanical procedure prevents reflex mechanisms and is easily reversed by deflation of the balloon. Changes in ventricular preload have a crucial effect on cardiac output. When an extra amount of blood flows into the ventricles, the cardiac muscle stretches to a greater length and, in turn, this causes it to contract with increased force. This is the Frank-Starling mechanism and it can be seen easily in a PV loop diagram (see **Figure 2-4**).

Afterload is related to the force the ventricle must overcome to eject blood, imposed by the arterial system under normal, healthy conditions. There are various measurements that can help determine or characterize the afterload, such as the arterial pressure (or blood pressure, BP) and the systemic resistance, but none is as reliable as the effective arterial elastance, E_a, which can be obtained directly from a PV loop. E_a, which is discussed in section **Section 2-2-5**, is represented by the slope of the orange

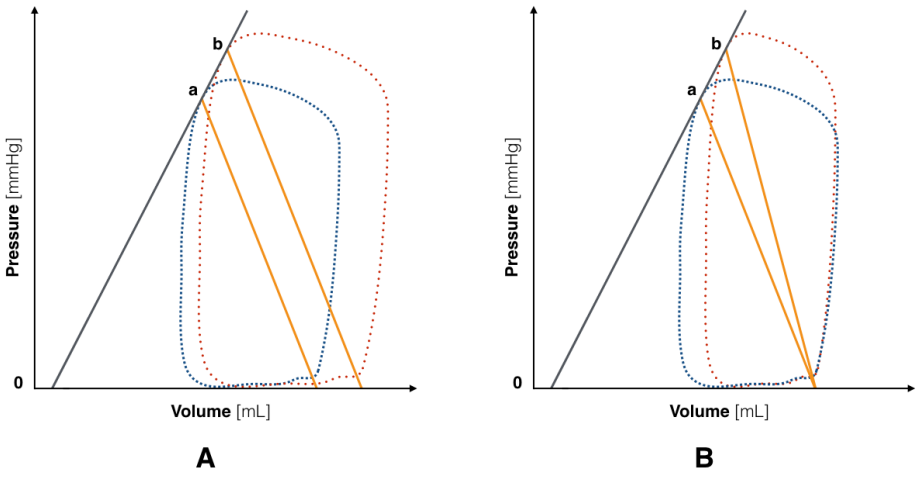

Figure 2-4: In both figures, the red dotted PV loop occurs after the blue dashed PV loop. At both points **a** and **b**, the ventricular volume and pressure are V_{es} and P_{es}, respectively. **(A)** Preload influences V_{ed} and PV loop's area, though the slope of the ESPVR (E_{es}) and E_a remain unchanged. **(B)** An increase in afterload is represented by an increased E_a, an unchanged ESPVR slope (Maughan et al., 1985) and, since the aortic resistance is higher, a decreased cardiac output.

lines in **Figure 2-4**, connecting end-systolic points **a** and **b** with V_{ed} on the volume-axis. Nevertheless, afterload can be changed, for example, by injection of phenylephrine (Yamazaki et al., 1982), which increases blood pressure, or by mechanically occluding part of the aorta. Loading alterations should be performed by interventions that minimally affect intrinsic myocardial function.

2-2-3 Stroke volume, ejection fraction and cardiac output

When addressing the pump function of the heart, there are some straightforward indexes: stroke volume (SV), ejection fraction (EF) and cardiac output (CO). SV (mL) yields the amount of blood ejected in one heart cycle, estimated as the difference between V_{ed} and V_{es}.

$$SV = V_{ed} - V_{es} \tag{2-1}$$

The ratio of stroke volume to the total blood volume present in the ventricle at end-diastole (V_{ed}) defines the ejection fraction (EF, in $\%$). Since low EF is usually indicative of heart failure (Curtis et al., 2003), monitoring this parameter could be useful when evaluating the heart's function. However, this was contradicted by recent studies (Gaddam and Oparil, 2009; Maeder and Kaye, 2009). Due to EF's load dependency, it cannot solely characterize contractility and cardiac response, and thus should not be relied on for detecting cardiac dysfunctions.

$$EF = \frac{SV}{V_{ed}} = 1 - \frac{V_{es}}{V_{ed}} \times 100 \tag{2-2}$$

The cardiac output (CO, mL/min) defines the quantity of blood pumped by the heart per time unit and it is computed by multiplying SV and heart rate (HR, min^{-1}).

$$CO = SV \cdot HR \tag{2-3}$$

Though intuitive and simple, these parameters are not sufficient for evaluation of the whole cardiac function. In the next subsections, other cardiovascular parameters are presented.

2-2-4 Left ventricular elastance

ESPVR connects the points of multiple PV loops when the left ventricle is in an activated state of contraction (one point from each loop), establishing a linear relationship between P_{es} and V_{es} (see **Figure 2-3**). The slope of this curve is referred to end-systole elastance (E_{es}) and it provides a measurement of the tendency of the heart to return to its original dimensions upon removal of a distending or compressing force. This simplified, but quite general, relation was defined and verified experimentally by Suga (1969, 1970, 1971), which led him and others (Sagawa et al., 1977; Templeton et al., 1972) to conclude that elastance could be a reliable physiological index of ventricular stiffness (contractility) and, thus, ventricular contractile efficiency. Since LV performance is not only influenced by ventricular stiffness, but also influenced by biochemical and geometric properties (Borlaug and Kass, 2011), E_{es} should be considered as a measure which integrates LV systolic function, as well as the complex and modulating effects of the functional, structural and geometric characteristics of the LV and its contractile efficiency (Kass, 2002).

Due to time-varying nature of the pressure and volume, elastance is also represented in function of time. $E(t)$ is the ratio of change in pressure to the change in volume ($\Delta P/\Delta V$) over time and represents changes in ventricular stiffness throughout the cardiac cycle. The equation is as follows:

$$E(t) = \frac{P(t)}{V(t) - V_0} \tag{2-4}$$

in which $P(t)$ is time-varying LV pressure ($mm\ Hg$), $V(t)$ is time-varying LV volume (mL) and V_0 is the intercept of the ESPVR (mL) in the volume axis. Since ventricular pressure in the beginning of diastole is close to $0\ mm\ Hg$, the numerator is simplified with $P(t)$.

The elastance increases with time from EDPVR to ESPVR during systole, reaching its maximum E_{max} at end of the ejection, and decreases with time during diastole (see **Figure 2-5**). Between these two states, the elastance lines are kept approximately linear and share the same volume-axis intercept V_0, which is a theoretical volume when no pressure is generated.

E_{es} and E_{max} have been used interchangeably in the literature, and this may result in some confusion. Although in most of the cases they are identical, since $E(t)$ varies for each beat, E_{max} may not necessarily occur at the end-systole (Kass and Maughan, 1988). For example, if afterload increases, E_{max} may occur before E_{es} (Maughan et al., 1985). The best way to distinguish both is that E_{max} corresponds to the maximum value of elastance of individual beats and E_{es} is the slope of the ESPVR, obtained from multiple PV loops in a stable inotropic state, regardless of the actual timing (Kass and Maughan, 1988; Suga, 1995). E_{es} is, however, a more useful measure of ventricular contractility.

Still today, the interpretation of V_0 is source of controversy in the scientific literature. Whereas some studies showed V_0 is unaffected by the contractile state (Sodums et al., 1984; Suga and Sagawa, 1974; Suga et al., 1973), others showed significant change, either influenced by afterload (Maughan et al.,

1985; Sodums et al., 1984), either shifting to the left due to enhanced contractile states (Borow et al., 1982; Mahler et al., 1975; Sagawa et al., 1977) – although in the latter end-systolic LV diameter was used instead of LV volume. Kono et al. (1984) proposed a method to determine V_0 by an iterative procedure. Initially, V_0 value is assumed zero, but then it is adjusted based on the volume intercept of the extrapolated linear relation from ESPVR. This new V_0 value is used to recalculate the maximal elastance. This continues until V_0 no longer significantly changes. V_0 can have negative values, because elastance has some degree of curvilinearity, especially during high inotropic states or when subject to loading conditions which are non-physiologic (Kass et al., 1989).

2-2-5 Effective arterial elastance

E_a $(mm\ Hg/mL)$ represents the total afterload imposed on the left ventricle, covering the complex association of different arterial properties, including total arterial compliance, characteristic impedance, peripheral arterial resistance (PVR) and diastolic time intervals (Sunagawa et al., 1983). Physiologically, it represents the capability of the arterial vessels to increase pressure when LV volume increases.

Traditionally, the arterial load was characterized in the frequency domain (Milnor, 1975; O'Rourke, 1967), but due to Sunagawa et al.'s pioneering work using a three-element Windkessel model in isolated canine hearts, an estimation in the time domain was introduced, allowing a cross-talk analysis between the left ventricle and the arterial system. A Windkessel model is a closed hydraulic circuit with a water pump connected to a chamber with air, and was first described by Frank (1899). By compressing the air in the chamber, it simulates the pump's compliance (distensibility) and the resistance encountered by the outflowing water. One limitation of this model is that it does not contemplate the effects of pressure wave reflection, originated from areas of major bifurcation. With aging or with hypertension, these waves arrive earlier in the cardiac cycle and, thus, they can substantially augment the pulsatile load on the heart. Later, Kelly et al. (1992) showed their net effects were functionally accounted for in PV loops,

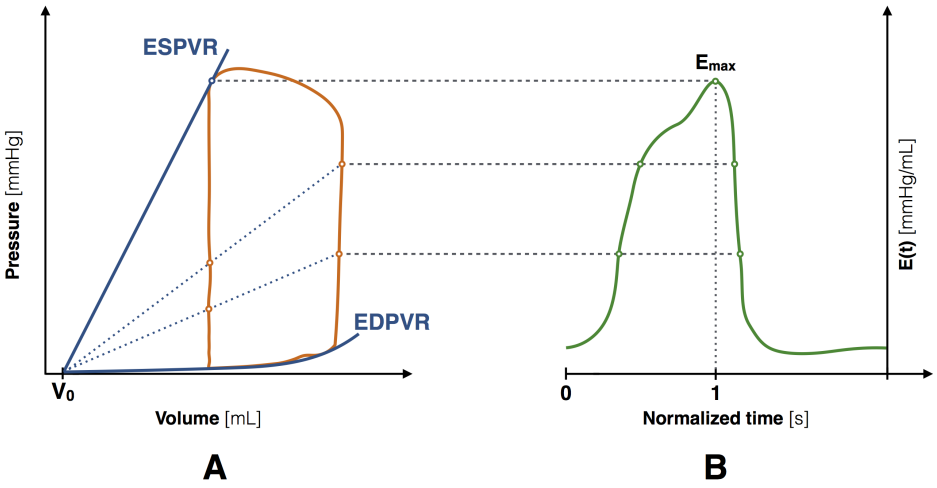

Figure 2-5: (A) There is a relatively smooth transition from the EDPVR towards the ESPVR (contraction phase), and back (relaxation phase). Elastance is considered to be linear and to intersect at a common point, V_0. **(B)** A rough approximation of the instantaneous ventricular elastance $E(t)$ throughout a cardiac cycle, with normalized time. E_{max} is also represented. The minimum value of the elastance corresponds to the slope of the EDPVR in the low volume range.

which helped accepting Sunagawa et al.'s proposal for an approximation of E_a.

Effective arterial elastance is determined as the negative slope of the line joining V_{ed} point in the volume axis and P_{es} point on the PV loop, represented in orange in **Figure 2-4**, and it can be approximated by the ratio of P_{es} to stroke volume SV (Kelly et al., 1992).

$$E_a = \frac{P_{es}}{SV} \tag{2-5}$$

Because arterial elastance shares common units with ventricular elastance E_{es}, it rendered as a convenient, useful method to assess arterial load and its impact on the human ventricle (Kelly et al., 1992). In **Figure 2-4 B**, given a contractile state (E_{es}) and a given preload (V_{ed}), if E_a increases (arteries become stiffer), P_{es} increases and SV decreases, reflecting the effect of enhanced afterload.

2-2-6 Myocardial energetics

It is important to quantify the systolic myocardial energetic performance, not only for a thorough understanding of cardiac pathophysiology, but also for evaluating processes that alter the contractile state (Glower et al., 1985).

2-2-6-1 Stroke work

The area inside the PV loop, with units of energy, characterizes the external mechanical energy of contraction (work) produced by the ventricle to eject blood, which is transferred to the arterial system as hydraulic energy (see **Figure 2-6**). SW ($mm\ Hg \cdot mL$) is maximal when all the energy from the ventricles is transferred to the arterial system, which only happens if both have the same elastance. Accordingly, SW_{max} occurs when $E_a = E_{es}$ (Burkhoff and Sagawa, 1986; Glower et al., 1985).

$$SW \approx P_{es} \cdot SV = E_a \cdot SV^2 \tag{2-6}$$

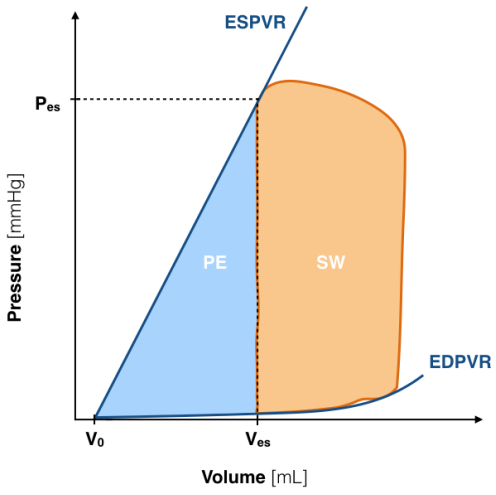

Figure 2-6: The orange shade in the PV loop represents stroke work by the left ventricle, during the cardiac cycle. The blue shade corresponds to potential energy, the mechanical energy available in the ventricle at end-systole. Pressure volume area (PVA) is obtained by summing up both energies.

As mentioned, the Frank-Starling mechanism describes the ability of the heart to compensate for changes in V_{ed} by varying its force of contraction and SW accordingly, while other factors remain unchanged. If the ventricle fills with more quantities of blood during systole, the cardiac muscle stretches to a greater length and, in turn, the ventricle contracts with greater pressure. Therefore, the area of the PV loop becomes larger, extending both rightwards and upwards, while E_a remains unchanged. This means SW is very sensitive to preload and varies very slightly with afterload (Kass et al., 1987).

The linear relationship between V_{ed} and SW is designated the preload recruitable stroke work (PRSW), a linear expression of Frank-Starling's law of the heart, which slope is a measure of ventricle stiffness (**Figure 2-7**). Unlike ESPVR, which represents end-systolic information only, PRSW integrates data from the whole cardiac cycle: it is less sensitive to afterload, its slope is more reproducible and its volume intercept is much more stable. Although the PRSW is less responsive to alterations in contractility than ESPVR, PRSW qualifies as a more robust contractility index (Glower et al., 1985; Little, 1985).

2-2-6-2 Pressure-volume area

Pressure volume area (PVA) ($mm\ Hg \cdot mL$) is equal to the sum of LV potential energy (PE) and stroke work (LV kinetic energy), representing all the energy that the ventricle needs to contract and pump blood under the given loading conditions (**Figure 2-6**). It corresponds to the total mechanical energy of a ventricular beat.

$$PVA = SW + PE \tag{2-7}$$

PE is the mechanical energy available in the ventricle at end-systole, which could produce external mechanical work if there were no afterload. Because the aortic valve closes after ejection, this energy is not converted into external work and dissipates as heat during relaxation, so it cannot be used for the next contraction cycle.

Similarly as a Hookean spring, at the end-systole, the ventricle has a certain pressure P_{es} for a given volume V_{es}, with stiffness E_{es}. Its stored energy will only depend on its elongation, or change in volume

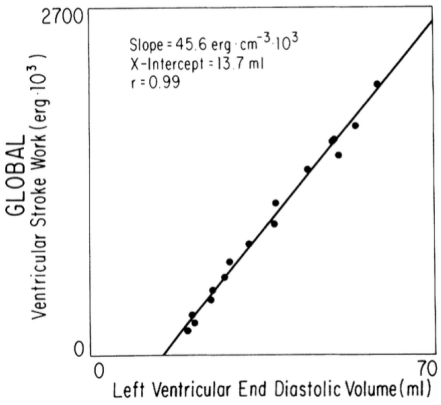

Figure 2-7: Glower et al. compared V_{ed} and SW from their experiments with dogs (global study) and noticed a linear relationship between these two variables. This relationship is known as preload recruitable stroke work (PRSW). Adapted from Glower et al. (1985)

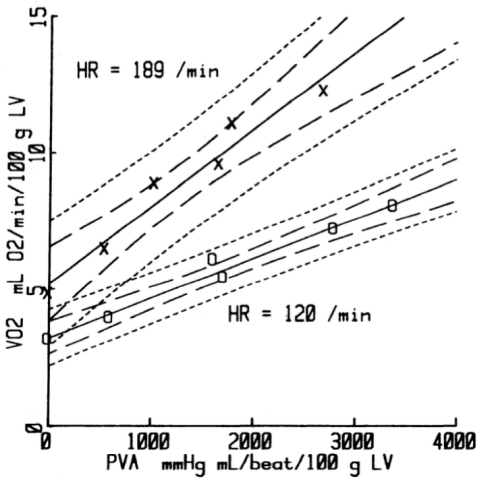

Figure 2-8: Suga et al. (1983) correlates V_{O_2} per minute with PVA at the control and at a higher HR, for the same dog's heart. HR changes the slope of the linear relation between V_{O_2} and PVA. Inner pair of dashed curves represent 95% confidence limit of the regression line; outer pair of dotted curves represent 95% confidence limit of sampled data points. Source: Suga et al. (1983)

($V_{ed}-V_0$), and elastance. Thus, PE is given by $\frac{1}{2}E_{es}(V_{ed}-V_0)^2$, representing the area under ESPVR spanning from V_0 to V_{es}. However, the area beneath EDPVR should not be considered in potential energy calculation, as it is not actively supplied and results from passive stretching. If E_{es} value, filling behavior or afterload (E_a) value changes, PE will certainly change as well.

Experimental studies have shown there is a very strong linear correlation between PVA and myocardial oxygen consumption, MVO_2, in ejecting as well as in isovolumic beats (Suga et al., 1981, 1983) (see **Figure 2-8**). Increasing (or decreasing) contractility shifts up (or down) the linear relation MVO_2-PVA, without changing its slope (Suga, 2003).

$$MV_{O_2} = \alpha + \beta \cdot PVA \qquad \alpha \text{ and } \beta \text{ constants} \tag{2-8}$$

The MVO_2-PVA relation contains useful information on energy conversion (Suga, 1990). The constant term α is considered the energy needed mainly for the non-contractile activities (basal metabolism and excitation-contraction coupling) (Suga et al., 1984), required by the heart even when the LV is not developing any pressure. The excess of energy from oxygen is applied for PVA.

Additionally, PVA combined with E_{es} can be used to assess the total amount of Ca^{2+} released and removed for contraction (Suga, 2003).

2-2-6-3 Cardiac work efficiency

LV mechanical performance is defined by its ability to convert metabolic energy into external mechanical work. It can be decomposed in two stages: **(1)** efficiency of energy transfer from oxygen to total mechanical energy PVA/MVO_2 (%), or metabolic efficiency, and **(2)** efficiency of energy transfer from the ventricle to the arterial system SW/PVA (%), or mechanical efficiency.

According to **Equation (2-8)**, the reciprocal slope of the MVO_2-PVA relation ($1/\beta$) yields the contractile efficiency of energy conversion. For a given PVA, the ratio PVA/MVO_2 shifts upwards when

contractility increases, implying more oxygen is consumed for the same PVA (Kameyama et al., 1992). Therefore, an increased contractility contributes to a lower oxygen conversion efficiency.

The ratio of external work (SW) to total mechanical energy (PVA) is called the efficiency of cardiac contraction (CWE), also known as efficiency of the heart. This ratio is a function of ventricular loading and inotropic state, increasing with contractility enhancement and decreasing with afterload.

$$CWE = \frac{SW}{PVA} \tag{2-9}$$

2-2-7 $\mathrm{d}P/\mathrm{d}t_{max}$ and $\mathrm{d}P/\mathrm{d}t_{min}$

The maximum and minimum rate of pressure change in the ventricle are represented by $\mathrm{d}P/\mathrm{d}t_{max}$ and $\mathrm{d}P/\mathrm{d}t_{min}$, respectively.

$\mathrm{d}P/\mathrm{d}t_{max}$ occurs early during isovolumic contraction and it is sensitive to the contractile state. However, it is known to be influenced by preload, afterload, heart rate and myocardial hypertrophy (Grossman et al., 1972; Kass et al., 1987), which makes it a poor contractility index. Rather than considering only $\mathrm{d}P/\mathrm{d}t_{max}$, Little (1985) proposed a relationship between the maximum rate of pressure change and V_{ed}, which slope was more sensitive to inotropic changes and would increase in response to positive contractile stimuli. Regarding its afterload dependency, Little (1985) showed the slope of $\mathrm{d}P/\mathrm{d}t_{max}$-$V_{ed}$ relation would remain unchanged in response to increase in aortic pressure, whereas ESPVR would shift to the left and its slope would decrease slightly. Unfortunately, this relation depends on heart rate. So, although E_{es} still has its downsides, it is more advantageous to use it instead of $\mathrm{d}P/\mathrm{d}t_{max}$ vs V_{ed} (Kass et al., 1987).

$\mathrm{d}P/\mathrm{d}t_{min}$ occurs early in diastole, usually shortly after the aortic valve closure (Weiss et al., 1976), and it has been used to reflect the relaxation properties of the heart independent of changes in volume (isovolumic relaxation). However, it is known to be influenced by preload (Cohn et al., 1972) and afterload (Weiss et al., 1976), so it cannot be qualified as an intrinsic relaxation index. In the next subsection, an alternative for the measurement of early diastolic function is discussed.

2-2-8 Isovolumic relaxation constant

LV relaxation begins during late ejection and continues throughout an early rapid filling and ends fully relaxed by diastasis, before the atrial systole begins. Different mathematical models have described this rate of myocardial relaxation and one of them is the time constant of relaxation, tau (τ). τ (in ms) was first proposed as a time constant during a monoexponential decay of the isovolumic LV pressure (Weiss et al., 1976), from the time of $\mathrm{d}P/\mathrm{d}t_{min}$ to the time in which pressure reaches P_{ed} – approximately two thirds of its initial value. In this model, τ_W equals the negative reciprocal of the slope of the natural logarithm of pressure against time.

$$P(t) = P_0 \cdot e^{-\frac{t}{\tau_W}+\alpha} \tag{2-10}$$

with P_0 and α constant.

However, Weiss et al.'s model assumed the LV pressure in the ventricle would simply decline to zero asymptotically. Subsequent modifications of this calculation include a non-zero variable asymptote, P_∞, as proposed by Raff and Glantz (1981). In this model, the LV pressure is related to the first derivative of pressure with respect to time ($\mathrm{d}P/\mathrm{d}t$).

$$P(t) = P_0 \cdot e^{-\frac{t}{\tau_{RG}}} + P_\infty \tag{2-11}$$

with P_0 and P_∞ constant.

These different methods led to discrepancies in literature, because there has been no agreement as to which is the most accurate. In fact, even though the curve experimentally observed resembles a monoexponential curve, some investigators recognized the limitation of these models and proposed other methdos to analyze LV relaxation (Matsubara et al., 1995; Mirsky, 1984; Rousseau et al., 1980). A logistic model was proposed by Matsubara et al. (1995), providing a better curve fit to the LV pressure decrease during isovolumic relaxation (**Figure 2-9**). In this model, the parameters P_0, τ_{RG} and P_∞ correspond to P_A, τ_L and P_B, respectively, with the same theoretical meanings. τ_L is the logistic isovolumic relaxation constant.

$$P(t) = \frac{P_A}{1 + e^{\frac{t}{\tau_L}}} + P_B \tag{2-12}$$

with P_A and P_B constant.

Although it is afterload dependent, τ is independent of preload and of peak aortic pressure, meaning it is more reliable than $\mathrm{d}P/\mathrm{d}t_{min}$ as a relaxation index of early diastolic function. An increase in τ indicates impairment of active properties of diastolic relaxation, for instance LV hypertrophy, LV ischemia, among others (Varma et al., 1989).

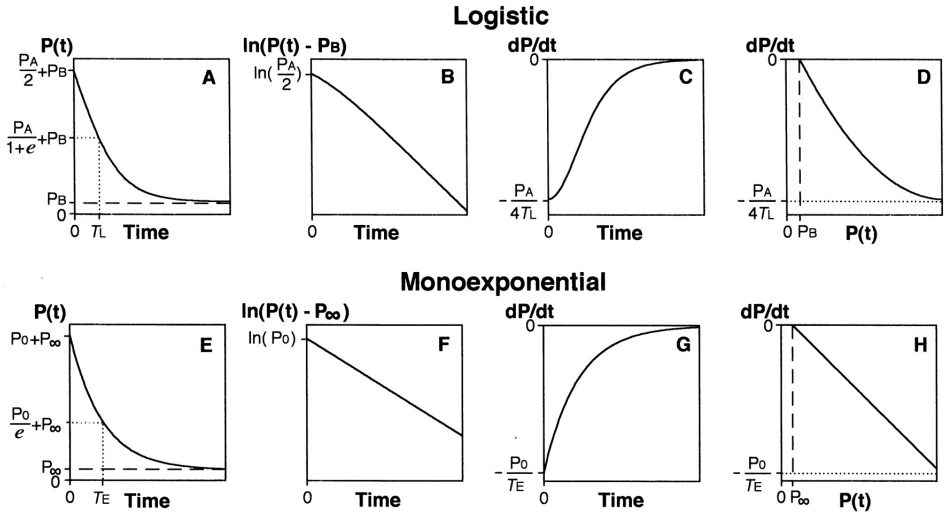

Figure 2-9: Comparison between Matsubara et al. (1995)'s logistic (A through D) and Raff and Glantz (1981)'s monoexponential (E through H) models. Schematic of pressure-time curves (A and E), semilogarithmic curves of P(t)-P_B and P_∞ (B and F, respectively), $\mathrm{d}P/\mathrm{d}t$ curves (C and G), and $\mathrm{d}P/\mathrm{d}t$ phase-plane curves (D and H). Although the differences may seem small, they lead to substantial differences between the two models. Source: Matsubara et al. (1995).

2-3 Ventricular-arterial coupling

In the previous section, both heart and arterial systems were characterized by variables in time domain, which facilitate studying them to assess their interaction. Assessment of ventricular-arterial (V-A) coupling determines whether or not cardiovascular performance (Kass, 2002) and cardiac energetics (Starling, 1993) are optimized, helping to understand how LV contractility match the afterload it must eject against.

Previous studies have shown that V-A coupling is related to both metabolic and mechanical efficiency. On one hand, CWE is optimized when E_a is approximately half E_{es} (Asanoi et al., 1989; Starling, 1993). On the other hand, SW is optimized when both elastances are equal ($SW = SW_{max}$), which is when all the energy from the ventricles is transferred to the arterial system. Since afterload is regulated to extract nearly maximal stroke work, while the heart is regulated to minimize oxygen consumption, except during ventricular dysfunctions (Sugimachi and Sunagawa, 1997), the normal heart at rest operates at neither maximal CWE, nor SW_{max}. In fact, it finds an optimal working point between these two (Asanoi et al., 1989; Starling, 1993). Appropriate coupling results in an optimal blood flow from LV to the periphery without excessive changes in pressure, an optimal SW and an optimal energy consumption to achieve the required SW (Borlaug and Kass, 2011). Decoupling occurs when E_{es} or E_a is too high or too low, leading to cardiac failure independent of myocardial ischemia and related systemic disease processes (Guarracino et al., 2013).

In the PV loop, V-A coupling can be studied using the ratio of elastances (E_a/E_{es}), a unit-less measure. E_a/E_{es} ratio is inversely related to EF[1], with the advantage of intrinsically evaluating whether variations in E_a/E_{es} are due to alterations in LV properties, arterial properties, or both (Cohen-Solal et al., 1994).

This ratio has been consistently demonstrated to be a reliable and effective measure of cardiovascular performance by several researchers. De Tombe et al. (1993) showed the dependence of ventricular and efficiency on V-A coupling in isolated canine hearts, by comparing these properties with the E_a/E_{es} ratio. Both stroke work and cardiac efficiency were optimal between ratios spanning $0.3 - 1.3$, whereas both would decline at much lower or higher ratios (see **Figure 2-10**). Interestingly, this range is also observed in dogs and cats, suggesting that it has been conserved through mammalian evolution (Chantler et al., 2008). Others investigators have demonstrated that the efficiency of the cardiovascular system is optimal when the coupling ratio is near unity, in which case the left ventricle provides an adequate stroke volume with the lowest possible energetic consumption (Burkhoff and Sagawa, 1986; Sunagawa et al., 1985). Either way, in a case of congestive heart failure, it is expected the ratio to rise due to relative decline in ventricular contractility (lower E_{es}) and concomitant rise in arterial resistance (Asanoi et al., 1989). Additionally, estimation of E_a/E_{es} provides more detailed information regarding hemodynamics. For instance, in hypotension, if a decrease in blood pressure is detected, the cases with preserved E_{es} (contractility) and low E_a (afterload) can be differentiated from those with low E_{es} and high E_a (Hayashi et al., 2000).

[1] $E_a/E_{es} \approx \frac{1}{EF} - 1$ (Cohen-Solal et al., 1994).

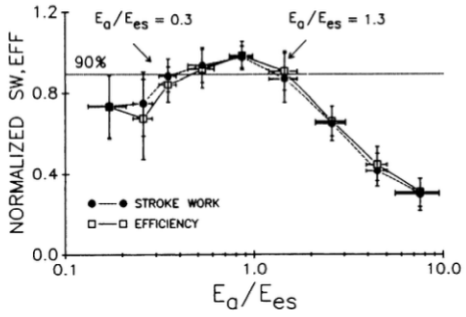

Figure 2-10: Average normalized SW and CWE as a function of E_a/E_{es}, plotted in a semilogarithmic scale. The solid line represents the range of coupling ratios above with both SW and CWE are optimal ($\geq 90\%$). Mean and $\pm$ standard deviation bars are also shown. Source: De Tombe et al. (1993).

The role of V-A coupling in the assessment of cardiovascular function is becoming very clear, offering new and complementary perspectives for understanding how both heart and arterial systems work together, in order to optimize cardiovascular efficiency. E_a/E_{es} ratio has become considerably useful in characterizing pathophysiology of altered hemodynamic profiles and testing the effectiveness of treatments (Guarracino et al., 2013).

2-4 Cardiovascular regulation

A suitable cardiac muscle contraction, which ensures the correct blood flow, results of the generation and transmission of electrical impulses. This can be recorded in an electrocardiogram (ECG) and is very useful in the diagnosis of an important number of conduction abnormalities.

The cardiac rhythm of the heart, or , is generated in the sinoatrial (SA) node, and it is mediated by the autonomic nervous system (ANS) (Berne et al., 2008). ANS is responsible to maintain a constant internal environment (homeostasis) and make the central nervous system to issue commands that lead to compensatory actions when internal environment regulation is required (Berne et al., 2008). ANS has two major divisions: sympathetic (SNS) and parasympathetic (PNS) nervous systems(Dodd and Role,

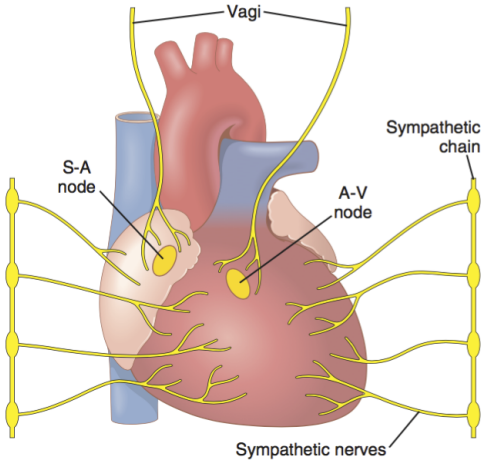

Figure 2-11: Representation of cardiac sympathetic and parasympathetic nerves (Hall, 2015). S-A: sinoatrial. A-V: atrioventricular.

1991). While PNS inhibits heart's automaticity via the vagus nerves, slowing atrial myocytes' conduction velocity, SNS enhances it via the sympathetic cardiac nerves, by allowing the SA node to reach its threshold more quickly. Changes in HR usually involve a reciprocal action of these two systems: an increase in HR occurs with a combined decrease in PNS and increase in SNS (Berne et al., 2008).

HR is modified together with other controlled cardiovascular variables, such as vascular resistance and, consequently, arterial blood pressure BP (Cavalcanti and Belardinelli, 1996). As a result of the activity of different mechanisms involved, HR and arterial BP fluctuations are observed in physiological conditions, on a beat-to-beat basis (short timescale, i.e., seconds to minutes). Occupational factors (emotions, sleep,...), mechanical factors (ventilation) and thermoregulatory factors evoke continuous fluctuations of the BP and HR. Even in the absence of motor behavior, as in paralysed animals, these fluctuations can be found (Dworkin et al., 2000), reflecting both the presence of various natural physiological perturbations to homeostasis and the dynamic response of the cardiovascular control systems to these perturbations (Akselrod et al., 1985).

Parasympathetic cardiac activation is considered an index of successful treatment of cardiovascular disease, though there is no cause-effect relationship between both (Townend and Littler, 1995). Hunt et al. (2001) showed the benefits of reducing sympathetic activity in cardiovascular disease. Vanoli et al. (1991) noticed outcome improvements after myocardial infarction (MI) in dogs posteriorly of enhancing parasympathetic activity. Therefore, these mechanisms are of interest for their therapeutic potential in cardiovascular disease.

In the next subsections, three mechanisms of autonomic balance of the cardiac system are briefly discussed: **(1)** cardiac baroreflex, **(2)** arterial chemoreflex and **(3)** von Bezold-Jarisch reflex.

2-4-1 Cardiac baroreflex

The cardiac baroreflex is one of the main mechanisms involved in BP regulation, acting as an effective buffer of short-team BP fluctuations and preventing excessive BP variations (Jordan et al., 2002).

Baroreceptors detect changes in stretch (or distention), as opposed to BP *per se* (Shepherd, 1982), and fire pulses at a tonic rate through the afferent pathways towards the central nervous system. They are divided in two types, depending their localization either in a high or low pressure zones of the circulatory system: low pressure baroreceptors are located mainly in the walls of the left and right atria, whereas high pressure baroreceptors are found mainly in the carotid sinus, at the bifurcation of external and internal carotids, and in the aortic arch. Afferent information is sent to the central nervous system by different pathways, depending of each type: low pressure baroreceptors use the vagus nerve; aortic high pressure baroreceptors use the aortic depressor nerve; and carotid high pressure baroreceptors use the carotid sinus nerve (Kandel et al., 2000).

Both aortic depressor and carotid sinus nerves synapse in the cardiovascular center of the nucleus tractus solitarius (NTS), located at the medulla oblongata, the central core of the baroreflex loop. Based on its input (increased or decreased firing), the NTS sends signals to the nucleus ambiguus, which controls vagal activity (Benarroch, 2008), and the rostral ventrolateral medulla, which controls vasomotor activity (Dampney et al., 2003). Together, these two regulatory pathways provide an integrated response

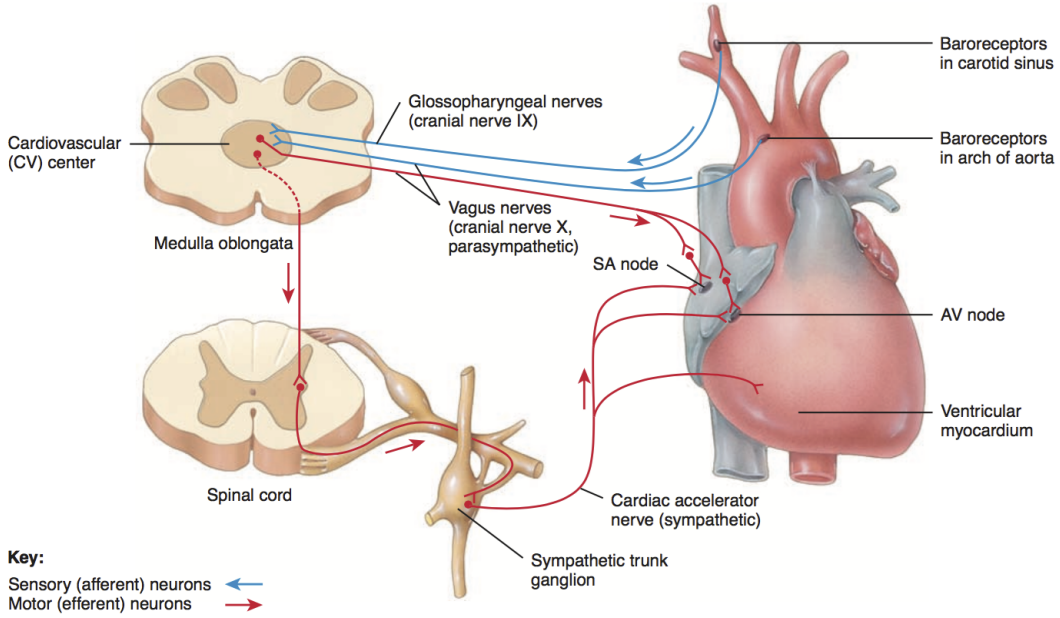

Figure 2-12: Schematics of heart innervation by autonomic nervous system, with some of the structures involved in the cardiac baroreflex. Baroreceptor impulses travel to the cardiovascular center through different paths, depending of its origin. After integration in the medulla, efferent signals are sent using two different branches: **(1)** through the vagus nerve, directly to the SA node (parasympathetic); **(2)** through the spinal cord (interneuron) until they reach the cardiac accelerator nerve, which in turn send them to heart's SA and atrioventricular nodes (sympathetic). For simplification, the aortic depressor nerve and carotid sinus nerve are not represented. Source: Tortora and Derrickson (2008).

to attenuate BP fluctuations.

The effector pathways of the cardiac baroreflex are modulated via two ANS branches: sympathetic and parasympathetic (Rowell, 1993). Sympathetic baroreflex signals are sent to both heart and peripheral vessels, whereas parasympathetic neural signals are only sent to the heart (see **Figure 2-12**). Due to the different dynamics of neurotransmitter release, SNS is slower with respect to PNS (Levy and Martin, 1996). The lack of impulses from sympathetic pathways allows PNS to act fast, change the firing rate of the SA node via the vagus nerve and, thus, counteract the sympathetic cardiac component of the baroreflex (Schwartz and De Ferrari, 2011). This results in a change of not only the pumping activity of the heart, but also the quantity of blood flow through peripheral vessels.

For example, when BP is elevated, baroreceptor afferents increase their firing rate, which consequently results in a decrease of impulses transmitted from the vasomotor center to the heart and blood vessels, through the efferent sympathetic pathways. This causes the heart rate to slow down and peripheral blood vessels to dilate, thus decreasing BP back to normal (Spyer, 1989). Conversely, a decrease in BP relaxes the baroreceptors, allowing the vasomotor center to become more active than usual. This results in an increase in sympathetic activity to the systemic vasculature, contributing to an augmented vasoconstriction and increased total peripheral resistance, and to the heart, contributing to an increased heart rate and contractility. As a result, BP raises to normal.

Thus, the cardiac baroreflex transforms a spontaneous fluctuation in the BP in an opposite fluctuation of HR. This regulation is done by a negative feedback loop, **Figure 2-13**, which attempts to maintain minute-to-minute BP around a mean value (set-point) of arterial blood pressure, or within normal limits.

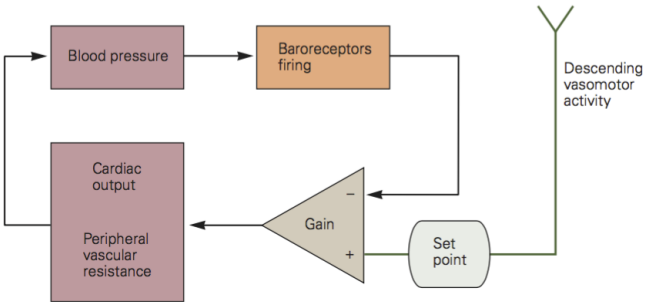

Figure 2-13: The cardiac baroreflex is a negative feedback control of the cardiovascular system. A sudden change in BP can be accurately regulated by tuning the cardiac output and vascular resistance. Source: Kandel et al. (2000).

This set-point varies under different physiological (i.e. exercise) (Rowell, 1993) and pathophysiological (i.e. hypertension) (Korner et al., 1993) conditions. An altered baroreflex control may carry an adverse prognosis in cardiac patients (La Rovere et al., 1998; Osterziel et al., 1995), resulting in reduced cardiac baroreflex sensitivity and poor outcome in cardiovascular diseases (La Rovere et al., 1998; Vanoli et al., 1991). A low baroreflex sensitivity is associated with high mortality after MI (La Rovere et al., 1998). Interventions that improve the sensitivity of the cardiac baroreflex, such as physical training, are known to reduce the risk of cardiovascular events (Hull et al., 1994).

2-4-2 Arterial chemoreflex

The arterial chemoreflex is a critical mechanism of control and regulation of the ventilatory responses to the changes in arterial oxygen (O_2) and carbon dioxide (CO_2) concentrations (Wade et al., 1970). This reflex modifies ventilation ensuring the demand of aerobic metabolism throughout the body is met in various physiological conditions, including exercise, high altitude, and pregnancy (Kumar and Prabhakar, 2012). Since the pulmonary system interacts directly with the cardiovascular system, any change in ventilation results in simultaneous complex cardiovascular effects, contributing to changes in HR and BP. Chemical agents, such as cyanide, nicotine or lobeline, can also mimic these effects (Calvelo et al., 1970; Heymans, 1958), by temporarily inducing changes in tissue respiration and in the ability of the chemoreceptors to utilize O_2 from the bloodstream. An injection of lobeline mimics the effect of an increase in arterial pressure of O_2.

Chemoreceptors are chemosensitive cells with a very high sensitivity to low O_2 content, CO_2 excess and hydrogen cation excess (blood pH) (Boulpaep et al., 2009; Hall, 2015). These fast-acting receptors are located peripherally in the carotid sinus and aortic arch, and centrally at the brainstem, with unique detection and response characteristics to each location. The peripheral chemoreceptors respond primarily to hypoxia[2] (Fitzgerald and Lahiri, 1986; Wade et al., 1970), whereas the central receptors are predominantly responsive to changes in hypercapnia[3] and acidosis[4] (Bowes et al., 1981; Gelfand and Lambertsen, 1973), by detecting hydrogen ions ($[H^+]$) in the blood. There is no consensus on how the

[2]Condition in which the body or a region of the body is deprived of adequate O_2 supply.
[3]Condition of abnormally elevated CO_2 levels in blood.
[4]An increase in $[H^+]$ concentration.

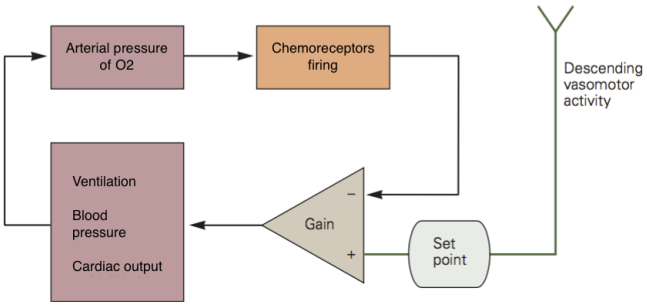

Figure 2-14: The arterial chemoreflex is a negative feedback control of the cardiovascular system. A sudden decrease in arterial pressure of O_2 cause the chemoreceptors to increase their firing rate, inducing an increase in the sympathetic nervous activity, which translates in a higher ventilation rate and higher cardiac output. Adapted from Kandel et al. (2000).

peripheral and central chemoreceptors interact with each other (Kara et al., 2003; Smith et al., 2010).

Whenever arterial pressure of O_2 falls below a critical level, chemoreceptors become stimulated due to a decrease of O_2 levels and an excess buildup of CO_2 and $[H^+]$. The signals transmitted from the receptors travel through afferent pathways to the pulmonary centers in the NTS, located at the medulla oblongata. By activating the vasomotor centers in the brain stem, the sympathetic nervous activity increases, which results in an increase of ventilation rate, mean arterial BP and HR, and consequently CO, to compensate the low arterial pressure of O_2 (Marshall, 1994).

Arterial chemoreflex plays a crucial role in maintaining perfusion when other mechanisms, such as the cardiac baroreflex, do not detect abnormalities. This is because the chemoreflex allows cardiovascular modulation in situations where circulating O_2 and CO_2 levels may be inadequate, despite a normal blood flow and pressure (Somers et al., 1991). However, other reflexes influence chemoreflex responses. Autonomic and ventilatory responses of the chemoreflex can be buffered by pulmonary afferents triggered by increased ventilation (Somers et al., 1989) and increased baroreceptor firing in response to increased blood pressure (Somers et al., 1991). In normal conditions of oxygen content and carbon dioxide content, it is generally assumed that BP modulation is predominantly associated with the cardiac baroreflex, without significant influence of the cardiac chemoreflex (Somers et al., 1991).

2-4-3 Bezold-Jarisch reflex

The Bezold-Jarisch (BJR) reflex, or cardiopulmonary reflex, is an inhibitory reflex induced by the stimulation of heart's receptors, either chemical or mechanical. This reflex was originally described by von Bezold and Hirst, in 1867, and characterized further by Jarisch and Richter in 1940, as the cardiorespiratory response to the intravenous injection of veratrum alkaloids or several biologically active chemicals, such as serotonin. By activating the cardiopulmonary afferent fibers, the reflex would promote parasympathetic activity, leading to bradycardia, hypotension and either excessively shallow breathing or an abnormally low respiratory rate (Thorén, 1979). This reflex was thought to be the basis of some unusual reactions where hyperstimulation of the myocardium paradoxically lead to profound

bradycardia[5] or asystole[6] (Parent and Lepage, 2015).

When the heart's receptors sense stimuli, due to the presence of difference substances either injected or released during cardiovascular emergency situations, cardiopulmonary afferent fibers are activated. Though the afferent fibers are mainly located within the left ventricular wall, they can also be found in the right ventricle, atria, pulmonary artery, and aorta. They respond by sending signals to the NTS, via the vagus nerve (Kalia et al., 1980). Lee et al. (1972) also found some connections with the nucleus ambiguus, suggesting a similarity between the central core circuitry of the BJR reflex and the cardiac baroreflex. After reaching the central nervous system, the cardiopulmonary impulses cause a massive stimulation of PNS and inhibition of the sympathetic activity, producing a profound and simultaneous reduction in arterial BP and HR (Coleridge and Coleridge, 1980; Krayer, 1961).

Until today, the physiological role of the BJR reflex has been hard to define (Verberne and Guyenet, 1992). On one hand, the BJR reflex is activated in specific situations of parameter optimization in the pulmonary circulation, such as pulmonary arterial pressure and pulmonary capillary blood flow, by regulating right and left ventricular outputs to compensate for fluctuations in systemic venous return (Somers and Abboud, 1995). On the other hand, it is activated in specific clinical and pathological conditions, such as ventricular overstretch (Mark, 1983) or myocardial infarction (Anderson et al., 2011), presumed to help reducing the load on the left ventricle. More recently, Aviado and Aviado (2001) hypothesized that cardiopulmonary reflexes are defense mechanisms against chemical inhalants. This way, cardiopulmonary reflexes would reduce BP and HR to reduce the degree of chemical hazards absorbed in the blood, protecting the vital organs from the potential toxicity and, finally, facilitating the elimination and deactivation of the pollutant.

2-5 Myocardial infarction

Myocardial infarction (MI), also known as heart attack, is a condition of heart muscle death due to the sudden blockage of one or more coronary arteries, responsible for supplying oxygen-rich blood to the heart. When a coronary artery is blocked by a sudden rupture of plaques made of fats and cholesterol (coronary artery disease) (Hansson, 2009, 2005), it causes a rapid accumulation of clotting factors at the rupture site, which results in a sudden obstruction of blood flow. This prevents the heart muscle of receiving glucose and oxygen (ischemia), resulting in death if this deprivation is not restored in time. The longer the obstruction persists, the greater the amount of heart muscle dies, which in extreme cases can be permanent (Thygesen et al., 2007).

Identification of MI in a clinical setting can be performed from the patient's history and from ECG. Changes in the ST-T waveforms and Q waves, when present, potentially allow the clinician to time the event, to estimate the amount of myocardial necrosis and at risk, to identify the blocked artery, and to determine a therapeutic strategy. Other ECG signs associated with myocardial infarction include cardiac arrhythmias, atrioventricular and intraventricular conduction delays, and loss of pre-cordial R wave amplitude (Zimetbaum and Josephson, 2003).

[5] Abnormally slow resting HR.
[6] State of no cardiac electrical activity, thus no contractions of the myocardium and no CO.

MI is a major cause of death and disability worldwide, although it may also be a minor event in a lifelong chronic disease or even go undetected (Thygesen et al., 2007). Information on myocardial infarction trends can be used as a proxy of the prevalence of coronary artery disease within and across populations (Thygesen et al., 2012). In 2012, ischemic heart disease was responsible for 7.4 million deaths worldwide (Mendis et al., 2014). In Portugal, cardiovascular diseases were responsible for 30.7% of the approximately 105 000 deaths in 2014, accounting an increase of 2.4% when compared with data from 2013. Heart diseases remain the main underlying cause of death in Portugal, with more deaths in women than in men (Carvalho et al., 2014).

2-6 Summary

This chapter provides an overview of the cardiovascular anatomy and the basic cardiovascular physiology concepts, such as preload, afterload and contractility, stroke work and cardiac work efficiency, were explained. Furthermore, ventricular-arterial coupling was presented, due to its importance when addressing the interaction between heart and arterial system. The chapter further detailed on cardiovascular homeostasis. Finally, the last section provided an overview of myocardial infarction.

The fundamental ideas and concepts described in this chapter are further discussed in the development of the single-beat analysis framework, presented in the next chapter.

CHAPTER 3

Numerical Methods and Implementation

In this chapter, numerical methods for PV data analysis and their computational implementation are fully explained. To begin with, it is enlightened how the physiological data was acquired and converted. Subsequently, a thorough description of the data processing pipeline is presented, from data preparation and systole identification to estimation of cardiovascular properties. In each stage, a detailed overview of the implemented numerical methods is presented, along with a brief literature review and examples from the PV data available. Finally, methods for statistical analysis of computed LV cardiovascular properties are discussed.

3-1 Data acquisition

The data was acquired from controlled experiments in fourteen anesthetized, paralyzed and artificially ventilated New Zealand rabbits ($3.35 \pm 0.85\ kg$) of either sex. The protocol was conformed according to national laws and international guidelines. An intraventricular impedance catheter was used to measure simultaneously LV pressure and volume. The carotid sinus region was exposed to insert a catheter through the external carotid artery into the left carotid bifurcation, allowing to record carotid blood pressure. Four surface-electrodes applied to the limbs were used to record ECG signal and, thus, to derive instantaneous HR. Detailed information on the experimental protocol is presented in Rocha et al. (2003a) and Rosario et al. (2003).

In order to investigate possible changes in LV and arterial physiologic properties evoked on cardiovascular reflexes before and following acute myocardial infarction, arterial chemoreceptors, cardiac chemosensitive fibers and baroreceptors were stimulated. Arterial chemoreflex was evoked by injection of lobeline ($20\ \mu g/kg$, $pH = 7.4 \pm 0.1$) into the carotid sinus, whereas the Bezold-Jarisch reflex was evoked by cardiac injection of ATP ($0.1\ mL$; $20\ mM$, $pH = 5.4 \pm 0.1$). Cardiac baroreflex was assessed

by inflating a Swan-Ganz balloon in the descending aorta, to raise peripheral resistance. Before repetition of the test, 30 minutes were allowed to elapse. Heart ischemia was provoked by ligation of the descending coronary artery.

Data was recorded from $10\ s$ before the beginning of a reflex stimulation until the rabbit returned to baseline conditions, both before and following acute MI. This means all three cardiovascular reflexes were acquired in a *healthy* condition (without acute MI) and in a pathological condition (following acute MI). All recorded signals were digitized at a sampling rate of $100\ Hz$ and 620 different files were stored in `.adicht` (AD Instruments ®) format. Afterwards, each data file was organized in a Matlab ® object structure with raw PV data, in `.mat` format, using Hokanson's ADInstruments-to-Matlab SDK library (MIT open-source license).

3-2 Graphical user interface

In this work, a custom Graphical User Interface (GUI) was designed and implemented in Matlab ® 2014b (The Mathworks; Natick, USA), to provide a powerful, easy-to-use framework for researchers and enthusiasts to manage stored pressure-volume data and to compute single-beat cardiovascular parameters, using the algorithms and methods described throughout this section (see **Figure 3-1**). This software is available for both Windows and Unix users.

The pipeline of the processing stage is depicted in **Figure 3-2**. The aim of the first stage is to select data for analysis and filtering, in order to reduce or smooth noisy data. Data is posteriorly normalized to account typical LV volume and pressure values in rabbits. The second stage consists on using a custom algorithm to automatically identify end-diastole and end-systole points. If it happens to miscalculate any point, it is possible to add a correction by a complementary manual process (optional). Afterwards, systoles are normalized. The third stage estimates the LV elastance and volume-intercept, using a recently proposed single-beat method. The fourth stage consists on a preliminary statistic analysis on the recently computed variables using Peirce's criterion method, in order to account for possible outliers that might influence the estimation results. The LV and arterial physiologic properties are computed on the fifth stage, together with the isovolumic relaxation constant τ. Finally, on the last stage, results can be plotted, compared and saved by the visualization tool.

In the following sections, each stage of the processing pipeline is described with detail.

3-2-1 Pressure-volume data preparation

In the first stage, PV data is selected, filtered and scaled. This is one of the most important phases of the processing pipeline, because a careless selection and filtration of the data will definitely produce less reliable results.

3-2-1-1 Selection

After opening the GUI, the user should inform where the PV data is stored, by specifying the *dataset path* to a directory containing the `.mat` files (**Figure 3-4 [1]**). This directory can be located anywhere

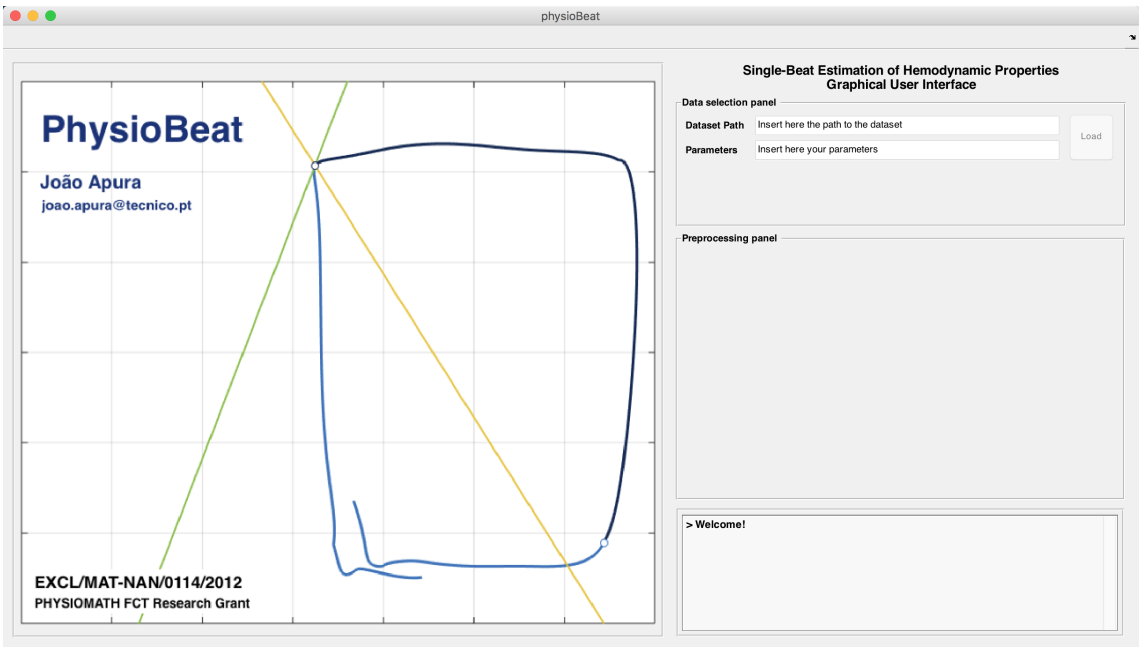

Figure 3-1: Custom GUI for processing of PV data, designed and implemented in Matlab ® 2014b.

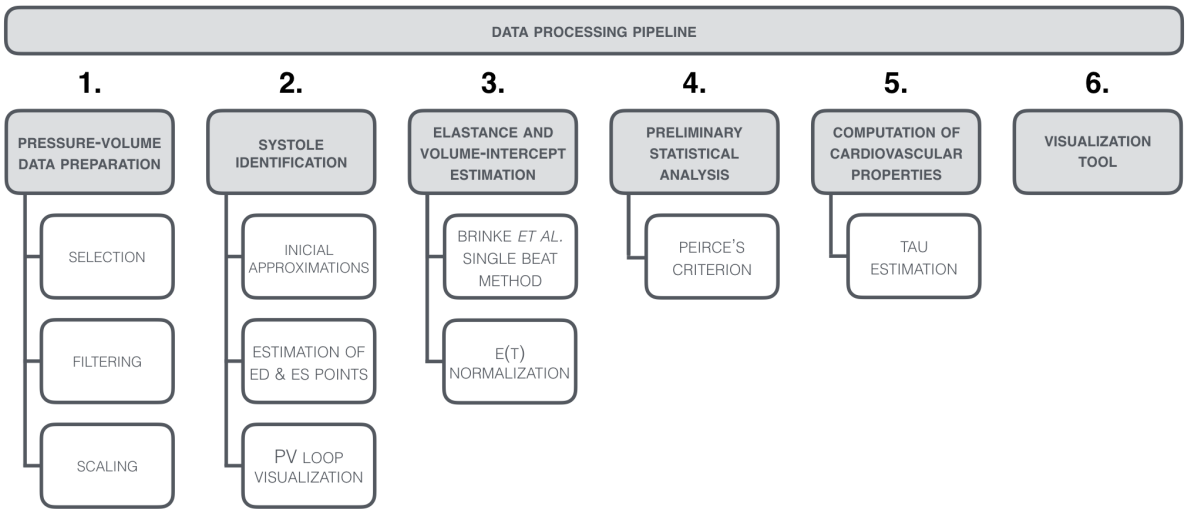

Figure 3-2: Six stages of the pressure-volume data processing pipeline.

in the user's computer, and it does not need to be one of `Matlab`'s search paths. The next step is to select which files the user wants to analyze. The input case-sensitive parameters are summarized in **Table 3-3**. When loading all files of interest into the GUI, the list is sorted alphabetically and each file is accessible by clicking on *back* and *forward* buttons to move upwards and downwards on the list, respectively (**Figure 3-4 [2]**). Every time a new file is selected, the *textbox* field at the bottom of the GUI gets updated with crucial information, such as the file's name and the position of the current file compared to the total number files in the list, and other comments (**Figure 3-4 [3]**).

Once a file is loaded, its first four signal-channels are displayed on the GUI's left-side (**Figure 3-4 [4]**). Each file can have up to eight channels, each one corresponding to a recorded signal. In this PV analysis, only four channels are used for computations: LV pressure, LV volume, arterial blood pressure

Condition	Parameter
Cardiac Baroreflex	`pc`
Arterial Chemoreflex	`ql`
Bezold-Jarisch reflex	`bz`
Healthy heart	`NOR` or `VNOR`
Following acute MI	`EAM` or `VEAM`

Figure 3-3: Input parameters for file selection in the GUI.

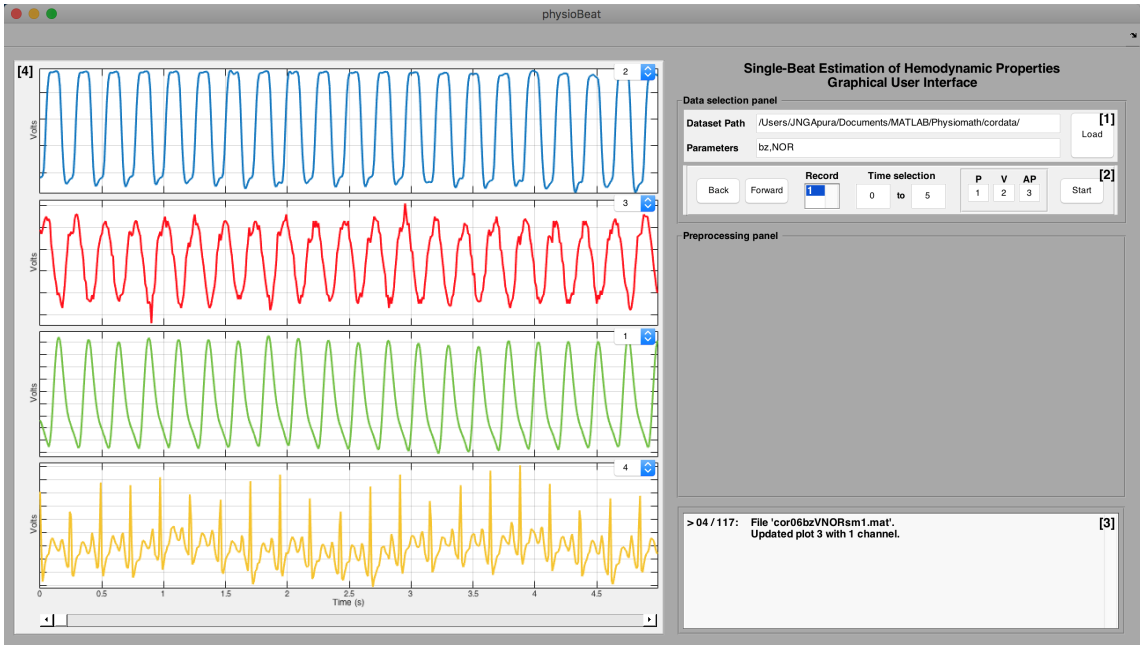

Figure 3-4: In **[1]**, the dataset directory and the input parameters are set. After loading every file from the dataset directory matching the input parameters, it is possible to access them in **[2]**. Furthermore, it is possible to select a time interval to analyze. LV pressure, LV volume and arterial blood pressure channels should be specified in **[2]**. The *textbox* field in **[3]** displays comments which help the user to get more insight about the analysis. The contents of each file's channels are displayed in **[4]**.

and ECG, but not necessarily in this order. Thus, each graphical representation has a *popup-menu*, which allows to select which channel to plot, providing a better user experience. This step is very important, because the user should make sure all relevant data is plotted in the GUI's left-side, as from now on the other channels will be ignored.

The next step is to select a time interval to analyze. For instance, in **Figure 3-4 [3]**, the user selects a time interval of $5\ s$, from $t_i = 0\ s$ to $t_f = 5\ s$, which corresponds to 20 full rabbit beats. Afterwards, it is necessary to inform the GUI which channel corresponds to the LV pressure, LV volume or arterial blood pressure, in order to minimize possible errors in posterior computations. The user should be able to visually match each channel to its correspondent signal type (for knowledge regarding the shape of each signal use, as reference, Wigger's diagram in **Figure 2-1**). LV pressure, LV volume, arterial blood

pressure and ECG signals should look like the signals represented in **Figure 3-4 [4]**, respectively.

By pressing the *start* button, the selection step is completed. A custom object structure, named `DataPhysioBeat`, is created to pro-actively store several important variables, such as sampling frequency and raw PV data, as well as any estimation computed throughout the rest of this chapter. More detail about this structure is provided in the **Appendix A**.

3-2-1-2 Filtering

When acquiring biological signals, these can be contaminated by random and unpredictable noise, which can come from a variety of sources: catheter, combination with unwanted signals, among others. There are several ways to extract the important part of some signal, while eliminating these random contributions or other unwanted features, a process called filtering (Oppenheim et al., 1989). Their respective performance depends on both the characteristics of the signal and the noise, as well as what analysis is to be made of the filtered data. The GUI provides two ways of filtering pressure-volume data: a band-pass filter and a Savitzky-Golay (SG) filter.

Band-pass filter is a frequency-selective filter, intended to select frequencies within a specific range, determined by the lower and upper cutoff frequencies, and attenuate others both higher and lower than the range specified (Oppenheim et al., 1989). It is a combination of both low-pass and high-pass filters, where the cut-off frequency of the low-pass (f_{lp}) is higher than that of the high-pass (f_{hp}).

The band-pass filtering can be used to enhance edges, by suppressing low frequencies, while reducing the noise at the same time, by attenuating high frequencies. However, it should be applied with caution because the high frequency information is very important in systole identification and the low frequency information is important to observe the changes in E_{max}. Sometimes band-pass filtering actually leads to information loss.

In the GUI, the band-pass filter was implemented using Matlab's functions `firpmod`, `firpm` and `filtfilt`. The first two functions apply an iterative algorithm suggested in (Rabiner and Herrmann, 1973) for estimation of an efficient and optimal Chebyshev finite impulse response (FIR) filter that meet the specifications f_{lp} and f_{hp}. This method is very accurate if the band edges are not either zero, nor the Nyquist frequency. The digital filter's magnitude and phase responses for a bandpass with $f_{lp} = 35\ Hz$ and $f_{hp} = 40\ Hz$ is presented in **Figure 3-5**. `filtfilt` applies to the input signal a filter with the coefficients determined previously, both forward and backward in time, squaring the amplitude response of the filter and zeroing the phase response (Oppenheim et al., 1989). This usually improves the response of the band-pass filter, because by squaring the stop-band ripple, the stop-band attenuation is doubled in dB.

Savitzky-Golay filter is a particular type of low-pass filter well-adapted for data smoothing (Savitzky and Golay, 1964). It is derived directly from a particular formulation of the data smoothing problem in the time domain, instead of having their properties defined in the frequency domain. Its premise is that it can sometimes be useful to replace each data point by a local average of surrounding data points, as

this can reduce the level of noise without too much bias. This filtering process can be achieved through a simple and efficient linear time-invariant (LTI) filtering scheme.

Although Savitzky and Golay (1964) was described as one of the top ten papers ever published in the journal *Analytical Chemistry* (Riordon et al., 2000), literature on the SG filter is scarce. There are some papers reporting the utilization of SG filters in chemistry, physics and biomedical engineering (Hofmanis et al., 2013; Molaee-Ardekani et al., 2010), and recently it has attracted significant attention due to the study of Schafer (2011), in which the frequency response of SG filters is studied in detail.

A digital filter is applied to a series of equally spaced data values $f_i \equiv f(t_i)$, in which $t_1 = t_0 + i\Delta$ for some constant sampling interval Δ, and $i = \ldots, -2, -1, 0,\ 1,\ 2, \ldots$. One of its simplest types, for example the finite impulse response filter, replaces each data value f_i by a linear combination g_i of itself and some number of surrounding points:

$$g_i = \sum_{n=n_L}^{n_R} c_n f_{i+n} \tag{3-1}$$

where n_L is the number of points used to the left of a data point i, while n_R is the number of points used to the right.

To derive the SG filter, consider the simplest possible averaging procedure: for some fixed $n_L = n_R = N$, compute each g_i as the average points from f_{i-N} to f_{i+N}. This is called a *moving-window averaging* and corresponds to **Equation (3-1)** with constant $c_n = 1/(2N+1)$. If the underlying function is constant, or is increasing or decreasing with time, then no bias is introduced into the result: higher points at one end are averaged by lower points at the other end. However, if the function has a non-zero second derivative, a bias is introduced due to the behavior of the *moving window averaging*.

The SG filter is designed to find filter coefficients c_n that preserve higher moments. This is accomplished by approximating the underlying function within the moving window by a higher-order polynomial (typically quadratic), instead of a constant. For each point f_i, a polynomial is fitted using the least-squares method (Hayes, 2009) to all unweighted $2N+1$ points in the moving window, and then set g_i to be the value of that polynomial at position i. At any other position, the value of the polynomial is not used. Instead, when the next point f_{i+1} is considered, a new least-squares fit is done using the shifted window. Since the least-squares method involves a linear matrix inversion, the coefficients of a fitted polynomial are themselves linear in the values of the data. That means that it is possible to do all the fitting in advance, and then fit on the real data simply by taking linear combinations, as showed by Savitzky and Golay's original paper. There are particular tables of filter coefficients c_n for which **Equation (3-1)** "automatically" accomplishes the process of polynomial least-squared fitting inside a moving window. Some errors in the tables have been corrected (Steinier et al., 1972), since publication in 1964. In the GUI, the SG filter was applied using Matlab's function `sgolayfilt`.

When compared with moving average (MA) filter, SG filtering has its advantages and disadvantages. On one hand, the MA average filter is the simplest digital filter to understand and use, and it is optimal for reducing random noise while retaining a sharp step response (Smith et al., 1997). In certain occasions, it might be more successful than a SG filter at noise rejection. On the other hand, a simple MA filter

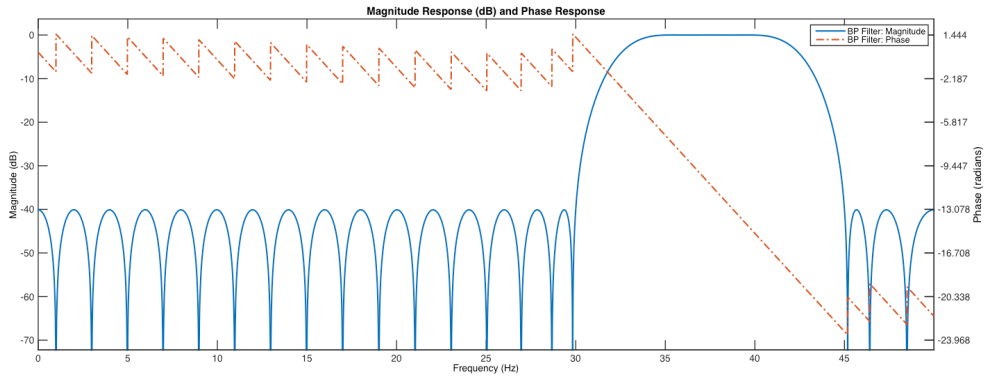

Figure 3-5: Magnitude and phase responses of a digital bandpass filter to be used with signals sampled at $100\ Hz$. The passband spans the frequencies between $35\ Hz$ and $40\ Hz$, with a transition region on either side with $5\ Hz$ of width. Low-frequency and high-frequency stopbands are attenuated equally.

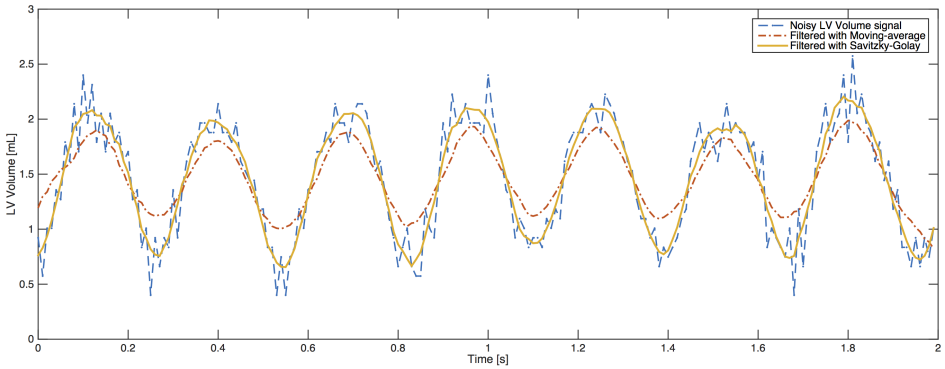

Figure 3-6: Comparison of a 2-second noisy LV volume signal and the results from two filters: moving-average (15 samples) and Savitzky-Golay (window: 15 samples, polynomial order: 3). The signal-to-noise ratio (SNR) is defined as the ratio of signal power to the noise power, expressed in decibels. For the noisy signal, the SNR is $10.28\ dB$, while in the case of the filtered signals is $31.68\ dB$ (moving-average) and $31.91\ dB$ (Savitzky-Golay). A higher SNR corresponds to more signal over noise.

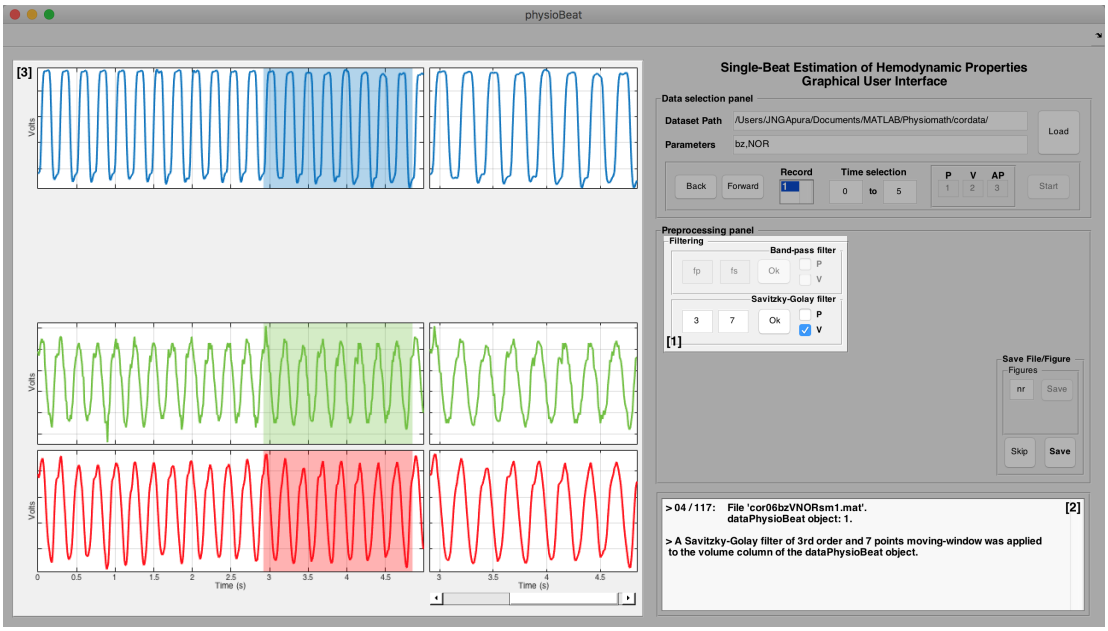

Figure 3-7: The filtering specifications are presented in **[1]**. In this example, there was no need to use a band-pass filter, thus f_{lp} (*fs*) and f_{hp} (*fp*) were not specified. A Savitzky-Golay filter of the third-order and 7-sample point moving-window was applied to the LV volume curve (green line), and the results from the smoothing are presented in **[3]** (red line).

tends to filter out a significant portion of the signal's high-frequency components, produce significant distortions and reduce the signal intensity, with subsequent loss of adjacent small signals. As pointed out by Schafer (2011), the SG filter is better in preserving the width and height of the peaks in the signal waveform, also retaining its pertinent high-frequency components (see **Figure 3-6** for a comparison between these two filters).

In the filtering step, the user is free to use both filters, only one, or none of them (see **Figure 3-7**). For the band-pass filter, the user has to introduce the pass-band and stop-band frequencies (recommended values are $f_{lp} = 35\ Hz$ and $f_{hp} = 40\ Hz$); for the Savitzky-Golay filter, the user has to choose the polynomial's order and the number of points in the moving window. It is recommended to use a SG filter of the third-order and 7-sample point moving-window, following the specifications proposed by Segers et al. (2005). In extremely noisy data, it is recommended to increase the number of points in the moving window.

3-2-1-3 Scaling

A more detailed analysis of **Figure 3-4** and **Figure 3-7** might show the PV signals have arbitrary dimensions. Since the signals were digitized in *volts* using the equipment Instrutech VR100B, Digitimer Ltd., their dimensions are not physiologically correct and cannot be compared with literature. Although their variations throughout time are still accountable and may help get some insight beforehand, a conversion and scaling step is required to correctly estimate the cardiovascular properties of the rabbit's heart in the following stages. This step is performed automatically, after filtering.

For the scaling step, a literature review was needed, in order to find the typical rabbit ranges for the pressure and the volume in normal (non-pathological) conditions. The pressure interval was consistent, with values in the range $[0,\ 100]\ mmHg$ (Abe et al., 1995; Niazmand et al., 2011; Ning et al., 1998; Yamakawa et al., 2014). The volume interval was more difficult to define, due to multiple ranges in literature. In fact, average volume values vary significantly between studies depending on the setup used. Also, some authors prefer to use stroke volume values, instead of a specific volume range (Ning et al., 1998). In this computational framework, the volume range was fixed to $[0.4, 2.4]\ mL$ under normal conditions, based on the studies of Rocha et al. (2009) and Cooper et al. (2012).

3-2-2 Systole identification

The next stage is characterized by the identification of the end-diastolic and end-systolic points of each cardiac cycle in the data. Some initial approximations are considered by fixing pre-determined variables, such as V_0. Although some error is introduced, this is consistent over all systoles and, thus, this scenario is likely to be preferred over an identification where the error is unknown or inconsistent.

3-2-2-1 Initial approximations

The first approximation is assuming that the volume-axis intercept V_0 is zero (Segers et al., 2005; Senzaki et al., 1996). According to **Equation (2-4)**, the time-varying LV elastance would only depend on time-varying pressure ($P(t)$) and volume ($V(t)$) data. Since V_0 directly trades off with $E(t)$, a higher V_0

value produces a higher $E(t)$ value and vice-versa. Therefore, it follows that there is no effect on the systole identification process and this approximation only changes the absolute value of $E(t)$. Further, in the following stages, $E(t)$ is adjusted by correcting V_0 to a more *realistic* value.

The second approximation is to re-sample each cardiac cycle from the PV data ($P(t)$, $V(t)$ and $E(t)$) to $M = 1000$ points, with the missing data points constructed by cubic spline interpolation. This ensures both end-diastolic and end-systolic points are determined with the minimal error possible. A spline allows to draw a smooth curve through a given distribution of points. The most frequently used splines for computational interpolation are cubic splines, which are made of polynomials pieces of third degree at most, twice continuously differentiable. Cubic splines are popular because they are easy to implement and produce a smooth interpolant curve, at a small expense of computational power. Also, when compared to the conventional linear interpolation methods, such as Lagrange interpolation or Newton interpolation, they are more accurate, which is particularly important in the interpolation of physiological signals over wide ranges. Though the interpolation curve of high-degree polynomials can suffer from a oscillating character at the edges of an interpolation interval, cubic splines do not usually suffer from this phenomenon (Cheney and Kincaid, 2012).

Please note that an exact fit is ensured if the given data has a high level of accuracy, so the user must make sure the filtering step rejects the maximum noise possible, without compromising the data.

3-2-2-2 Estimation of end-diastolic and end-systolic points

The beginning and end of diastole and systole of each cardiac cycle are determined using time-varying LV elastance, computed in the previous step. When representing graphically $E(t)$, multiple curves similar to **Figure 2-5 (B)** are plotted continuously against time, each corresponding to a beat. For each beat, elastance increases from EDPVR to ESPVR during systole, reaching its maximum at end-ejection, and decreases during diastole.

Sagawa (1981) defined the point when the active contractile process peaks, identified as the point of maximal $E(t)$, as the end-systolic point. There are some studies which additionally use iterative method of linear regression analysis on the resulting points to estimate E_{max} (Kass et al., 1989; Segers et al., 2005), in order to successively improve end-systolic estimation. However, these improvements were not computationally efficient. They would not only decrease the overall performance of the GUI, but also provide estimations that are not significantly better. In this study, the corner points of the PV loops were detected by an automatic algorithm proposed in Lankhaar et al. (2009). For each cardiac cycle, the distance $d(t_i)$ of each point in the PV loop's upper left part to its center (V_c, P_c) is calculated, and the point with the maximal distance is defined as the end-systolic point. The method is illustrated in **Figure 3-8**.

$$d(t_i) = \sqrt{\left[\frac{V(t_i) - V_c}{\Delta V}\right]^2 + \left[\frac{P(t_i) - P_c}{\Delta P}\right]^2} \tag{3-2}$$

where $\Delta V = V_{max} - V_{min}$, $\Delta P = P_{max} - P_{min}$, $V_c = (V_{max} + V_{min})/2$ and $P_c = (P_{max} + P_{min})/2$. For end-systolic point detection, the interval for t_i only considers points with volume smaller than V_c and pressure larger than P_c.

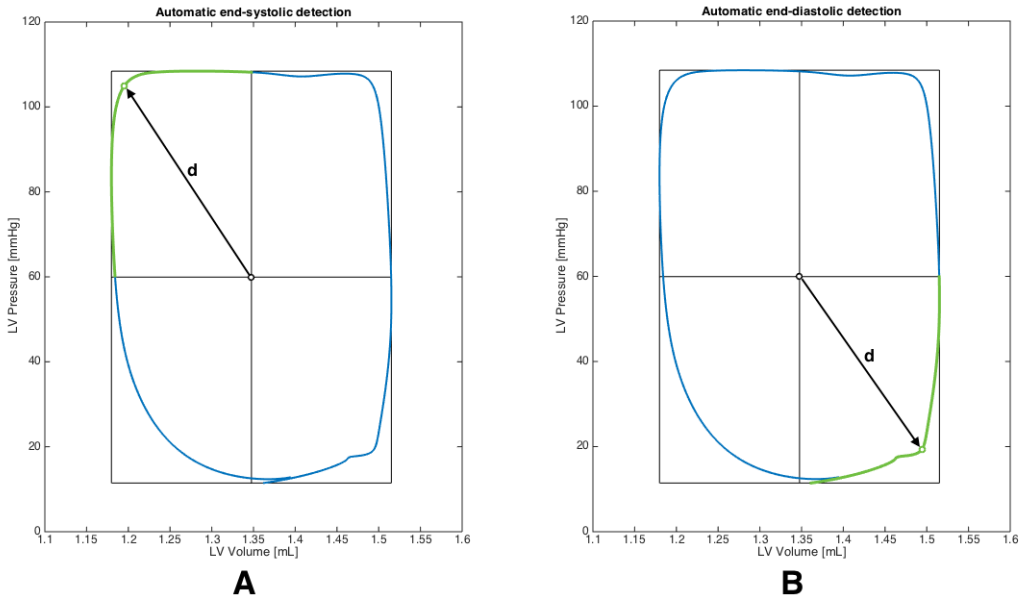

Figure 3-8: Detection of the corner points of a PV loop, using a method proposed by Lankhaar et al. (2009). For each quadrant, corner points are defined as the point where the distance to the center of the circumscribing rectangle is maximal. **(A)** Detection of an end-systolic point, in the upper-left quadrant. **(B)** Detection of an end-diastolic point, in the lower-right quadrant.

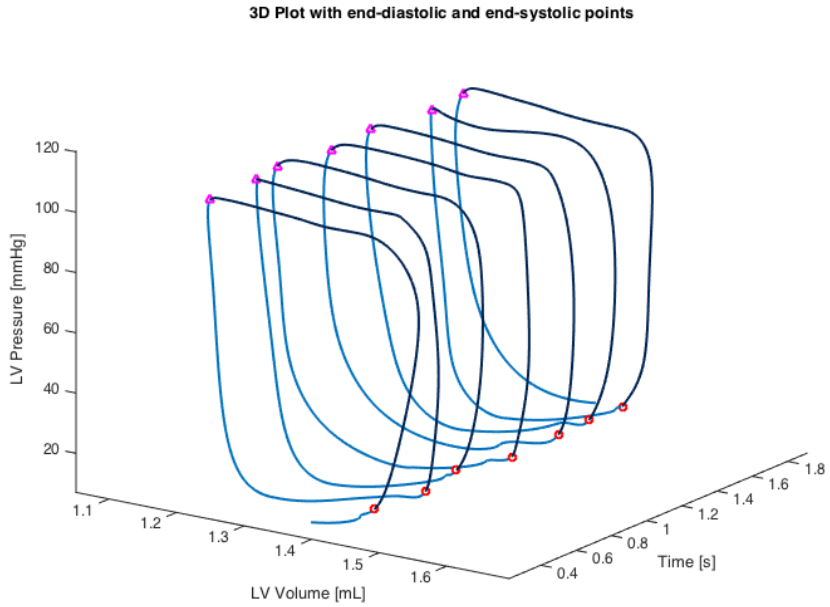

Figure 3-9: Representative example of a series of 7 PV loops under steady-state (baseline conditions), against time. In each cardiac cycle, the darker blue line represent a systole. Red circle and pink triangle represent the onset and end of systole, respectively.

Regarding the end-diastolic points, the first assumption was that, analogously, the point of the minimum LV $E(t)$ would correspond to the end-diastolic point. Since the end-diastolic point occurs immediately before the period of isovolumic contraction, when the ventricular volume is maximal and the pressure starts to increase to match the aorta's pressure, this is fair proposition given **Equation (2-4)**. While in some data this assumption provided a rough approximation of the end-diastolic points location, it was not consistent in other sets of PV data. A literature review revealed there is no consensus regarding the best method to estimate end-diastolic points. Whereas some studies would use the R wave of

the ECG as a maker of end-diastoles (Kind et al., 2011; Regen et al., 1993), others considered the end of a diastole as the time instant in the PV plane where the LV pressure was $4\ mmHg$ higher than the pressure corresponding to a volume of 98% of the maximum LV volume (Claessens et al., 2006). Since Lankhaar et al.'s automatic corner detection algorithm had been proven to be robust enough in end-systolic point estimation, it was also used to compute end-diastolic time instants, based on the distance of the PV loop's lower-right quadrant points to its center (see **Figure 3-8 [B]**). In this case, the interval for t_i considered points with volume larger than V_c and pressure smaller than P_c. Visual control of the obtained time points proved this algorithm to be sufficient robust (**Figure 3-9**), allowing an objective and automated determination of the onset of each systole.

To improve systole identification, a constraint is applied to this method by defining a median value of $E(t)$ above which its maximum values can be located, and below which the minimum values can be estimated. This threshold is estimated using a moving window of $2\ s$, to address possible changes in LV elastance's amplitude. At this point, data is also excluded from analysis if an extra-systole occurred, as a result of an arrhythmia, or if the end-diastolic pressure value prior to the isovolumic contraction differed more than $3\ mmHg$ from the pressure value after the ejecting beat.

3-2-2-3 PV loop visualization

In this step, each cardiac beat from the data is represented in the PV plane, so that the user can visually verify the results and manually correct any possible error. In this step, LV volume is plotted against LV pressure in a PV loop, as displayed in **Figure 3-10 [2]**. The systole is identified by a thicker dark-blue line, constrained by the end-diastolic (in red) and end-systolic (in pink) points. Additionally, $P(t)$, $V(t)$ and $E(t)$ are displayed as auxiliary plots, against an time interval containing the previous, current and following cardiac cycles, which might come in hand during any decision-making in the PV loop analysis.

Every systole must be confirmed by the user, to reduce any possible misestimation that might influence the final results. If the user notices the systole was poorly identified, either by a miscalculation of one of the points, or both, it is possible to add a correction by a complementary manual process (**Figure 3-10 [3]**). For example, the end-diastolic point in **Figure 3-10 [2]** was miscalculated: instead of being located prior to the isovolumic contraction phase, it is located in the diastasis phase. The user should add a correction, otherwise it will produce less reliable results. By clicking on the *start* button, a data cursor in enabled on the figure where the PV loop is displayed, enabling the user to interactively select a position on a graph or line. In addition to the data cursor, which is a small black square with a white border, a small text box with pressure and volume values is also displayed. This way, the user gets all the information needed to decide where to set the end-diastolic point. After selecting its new location, the user has to confirm the decision by clicking *ok*. This updates the PV loop in the figure, with the new end-diastolic location. In addition to end-diastolic or end-systolic correction, the user may also skip the entire systole by clicking in the *skip systole* button.

Once all the systoles are confirmed by the user, it is necessary to inform the GUI no more corrections will be added. To save the systole map, containing the location of the end-diastolic and end-systolic

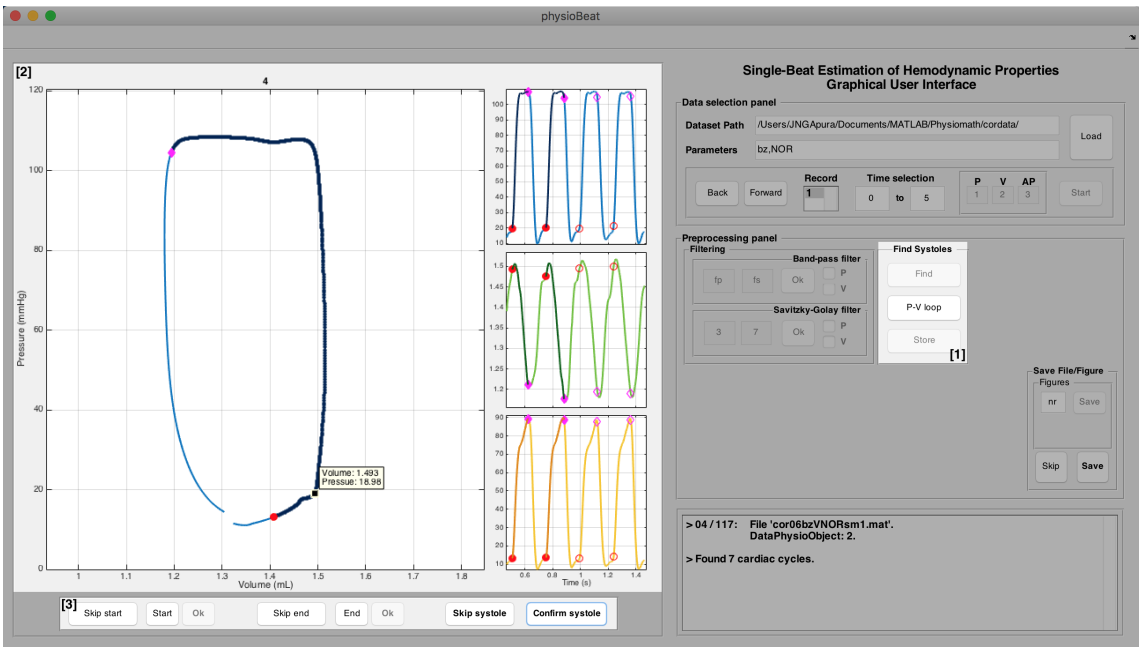

Figure 3-10: Each cardiac beat is represented in the PV plane **[2]** for visual verification of current results and manual correction of possible errors, using the menu in **[3]**. Red circle and pink triangle represent the onset and end of systole, respectively. The systole is represented by the darker blue line.

points, in the `dataPhyioBeat` object, the user needs to press the *store* button (see **Figure 3-10 [1]**).

3-2-3 LV elastance and volume-intercept estimation

In the previous stage, a time-varying LV elastance was computed with the assumption that the volume-axis intercept V_0 is negligible. Since information from the end-systolic points is now available, it is possible to calculate an approximated E_{es} value for each cardiac cycle. However, since V_0 directly trades off with E_{es}, a second approach was implemented to improve the initial E_{es} parameter value estimate. This approach estimates E_{es} based on a previously published single-beat estimation method, which is described below after a literature review on single-beat methods.

3-2-3-1 Single-beat method

The ESPVR of the LV is a comprehensive index of the heart's pumping function. The conventional procedure, however, is difficult and invasive, since it requires computing several PV loops while gradually decreasing cardiac preload, for example using a balloon occlusion of the inferior vena cava (Gupta et al., 1989). This assessment limits clinical applications and, thus, has motivated several authors to propose other approaches for computing the ESPVR for a single PV loop.

One of the first non-invasive methods, proposed by Takeuchi et al. (1991), consisted on estimating ESPVR by drawing a line from the maximal isovolumic pressure (P_{MAX}) and the end-systolic pressure-volume point of a single ejecting beat. Theoretically, P_{MAX} is the maximum pressure reached by LV if ejection did not take place. This method was based on three assumptions: 1) an isovolumic pressure wave could be modeled by an inverted cosine with offset, 2) the cosine wave was fitted through both isovolumic contraction and relaxations phases of a beat, and 3) the systolic duration of an isovolumic

beat was similar to that of an ejecting beat (Sunagawa et al., 1980). P_{MAX} was taken as the maximum of this fitted cosine, allowing to compute E_{es} as the slope of the line connecting the point defined by (V_{ed}, P_{MAX}) and (V_{es}, P_{es}).

$$Ees = \frac{P_{MAX} - P_{es}}{V_{ed} - V_{es}} \tag{3-3}$$

Later, some authors proposed alternative methods to estimate E_{es} (Kjørstad et al., 2002; Senzaki et al., 1996; Shishido et al., 2000; Ten Brinke et al., 2010). With the exception of Senzaki et al. and Shishido et al., whose methods relied on a time-varying elastance model, all of these methods were based on simplified wave shapes of isovolumic pressure, fitted through both isovolumic contraction and relaxation phases of an ejecting beat. Senzaki et al. (1996) calculated V_0 and then defined the ESPVR by connecting the volume-intercept point with the end-systolic point of the single loop. Shishido et al. (2000) refuted some of Senzaki et al.'s assumptions and provided a bi-linear fitting of an approximated time-varying elastance curve to derive E_{es}. Chen et al. (2001) used a simplified version of Senzaki et al.'s method, coupled with systolic and diastolic arterial pressure measurements, and validated the results against an invasive measurement of E_{es}. Later, Rocha et al. (2009) took into consideration two conditions of equal elastance, one in the diastolic and other in the systolic phase of the same cardiac cycle, to compute an estimated value for V_0 and, consequently, calculate E_{es}.

Although published results were generally promising, some authors have doubts about single-beat estimation methods accuracy and their capabilities to assess ventricular contractility (Kjørstad et al., 2002). Recently, Ten Brinke et al. (2010) using Takeuchi et al.'s technique with a modified fitting scheme (fifth order polynomial), proved that it is possible to achieve a good estimation of V_0 in heart failure patients. They argued that, even through the single-beat method might underestimate E_{es} and disagrees with the VCO technique estimation, it is still a reasonable approach.

In this study, E_{es} was improved following the method proposed by Ten Brinke et al. (2010). Maximal pressure of an isovolumetric beat, P_{MAX}, is determined by fitting a fifth-order polynomial to the LV pressure curve, excluding all data points that lie after $\mathrm{d}P/\mathrm{d}t_{max}$ and before $\mathrm{d}P/\mathrm{d}t_{min}$ and those after the time-point when $\mathrm{d}P/\mathrm{d}t$ increased above 15% of $\mathrm{d}P/\mathrm{d}t_{min}$ (see **Figure 3-11 [3]**). The fifth-order polynomial was chosen instead of the original cosine function described by Takeuchi et al. (1991), because it offers a more accurate approximation in case of an asymmetrical LV pressure curve (Ten Brinke et al., 2010). Curve-fitting was performed with Matlab's `fit` function, with the options *poly5*, *bisquare* weights and *Levenberg-Marquardt* algorithm. These options ensure the weighted sum of squares is minimized, reducing the effect of outliers and thus optimizing the solution in a nonlinear least-squares sense. P_{MAX} is obtained as the maximum of the fitted pressure curve, mathematically represented by the following equation:

$$P(t) = c_1 \cdot t^5 + c_2 \cdot t^4 + c_3 \cdot t^3 + c_4 \cdot t^2 + c_5 \cdot t + c_6 \tag{3-4}$$

where t corresponds to time and c_i are constants. Although these constants are optimized until the difference between consecutive iterations is smaller than 10^{-6}, it is not possible to know if this solution is local or global, due to the limited options of Matlab's function `fit`.

Although studies have proposed various models to represent the instantaneous PV relation of the

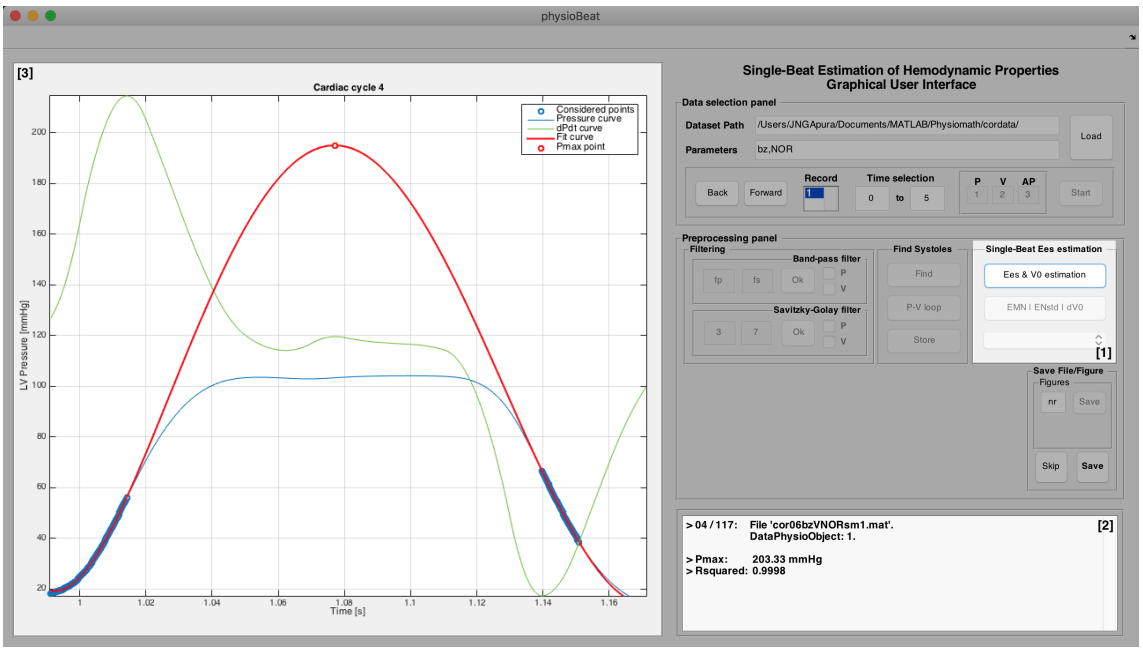

Figure 3-11: Representation of Ten Brinke et al.'s single-beat method used to estimate the isovolumic pressure curve and its maximum, P_{MAX}, from a single ejecting beat (**[3]**). The isovolumetric pressure curve (in red) is fitted through the isovolumic contraction and relaxation periods. The pressure curve is represented in blue and $\mathrm{d}P/\mathrm{d}t$ is represented in green. P_{MAX} and the fitting curve's R^2 (coefficient of determination) are presented in **[2]**.

LV since it is unknown whether a linear model is accurate enough for simulations (Burkhoff et al., 2005; Lankhaar et al., 2009), for simplicity this computational framework considers the classical model of Suga et al. (1973), in which each beat has a single ESPVR straight line with a fixed volume intercept, connecting the points (V_{ed}, P_{MAX}) and $(V_0,\ 0)$, through the end-systolic point of the single loop. For each beat, E_{es} is estimated by solving **Equation (3-3)**, representing the slope of the ESPVR. V_0 is estimated by solving **Equation (2-4)** for P_{es}, V_{es} and E_{es}.

3-2-3-2 Validation with multiple-beat analysis

To validate this thesis' single-beat approach for ESPVR estimation, it was necessary to compare its results with the measurements obtained by constructing the ESPVR from multiple beats at different loading conditions. The gold-standard method uses a balloon occlusion of the inferior vena cava, a method which enables a rapid mechanical reduction in preload, that prevents cardiovascular reflex mechanisms and is easily reversed by deflation of the balloon. The procedure is described in detail in various publications (Gupta et al., 1989; Kass, 1992).

PV loops were measured at steady state, followed by gradual preload reduction induced by inferior VCO. The duration of VCO was kept limited to several seconds and the pressure drop remained within physiological ranges, which effectively guarantees minimized reflex changes and limited signal artifacts. During offline analysis, PV loops acquired during preload reduction were used to construct the ESPVR from VCO, using an iterative method of linear regression analysis on the estimated end-systolic points (Gupta et al., 1989). The slope of the fitted line was defined as VCO end-systolic elastance (E_{es}). The

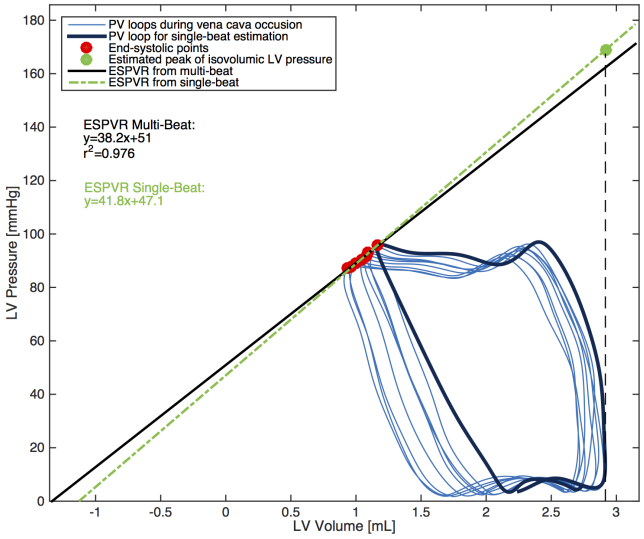

Figure 3-12: The end-systolic PV relationships are derived by multiple-beat analysis (black solid line), through linear regression ($R^2 = 0.976$), and single-beat analysis (green dashed line), using the estimated peak isovolumic LV pressure (P_{MAX}). As expected, the slope and volume-intercept of both lines are similar.

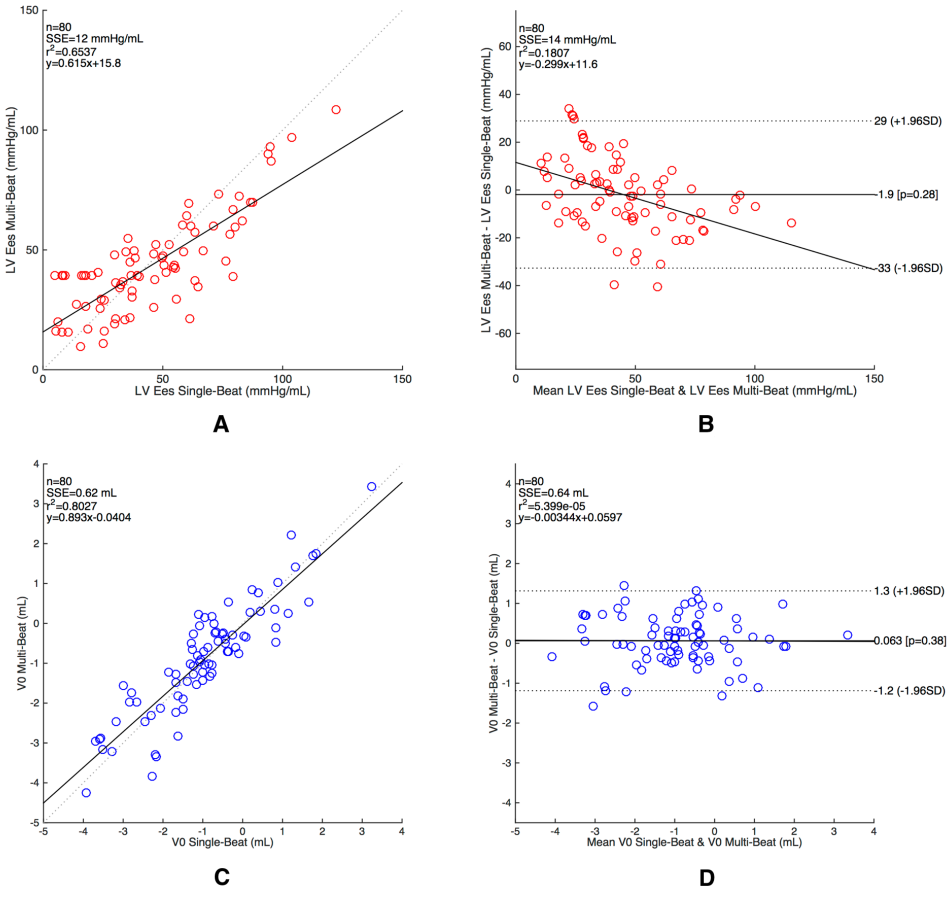

Figure 3-13: **(A)** Scatterplot comparing E_{es} measurements obtained by multiple-beat and single-beat analysis. **(B)** Bland-Altman analysis, in which the difference between the E_{es} estimations from both methods are plotted against their average. **(C)** Scatterplot comparing V_0 measurements obtained by multiple-beat and single-beat analysis. **(D)** The difference between the V_0 estimations from both methods are plotted against their average. Solid lines represent the *bias* line and linear regression; dashed lines define the limits of agreement, corresponding to 95% confidence interval.

ESPVR estimated by the single-beat method was based on the first, steady-state, PV loop of the VCO procedure (see **Figure 3-12**).

Correlation between multiple-beat and single-beat analysis, for E_{es} and V_0, were established by linear regression (see **Figures 3-13 (A)** and **(B)**). The degree of agreement between these two methods is illustrated by Bland-Altman analysis (Bland and Altman, 1986). This method plots the difference between the results of the two methods against their average, as shown in **Figure 3-13 (B)** and **(D)**. In this case, numerical differences were used to accurately portray observed disparities, though it is also possible to use average percentages, or ratios. A solid line is drawn at the mean difference (also designated as *bias*) and two dotted lines represent the limits of agreement, which represent the 95% confidence interval of the mean difference (*bias* $\pm$ two standard deviations). This type of statistics is useful in revealing a relationship between the differences and the averages, systemic *bias*, and also possible outliers (Bland and Altman, 1986).

Both methods for elastance estimation are correlated, with regression given by $E_{es}(MB) = 0.615 \cdot E_{es}(SB) + 15.2$, $R^2 = 0.6537$. From Bland-Altman analysis, E_{es} showed a mean *bias* of $1.9\ mmHg/mL$, with fairly wide limits of agreement ($[-33,\ +29]\ mmHg/mL$), indicating underestimation by the single-beat. An unpaired t-test was performed to compare both sets of data, and the differences in E_{es} did not reach statistical significance ($p = 0.28$).

In the case of V_0, single-beat calculations yielded virtually the same results as multiple-beat estimations, with regression $V_0(MB) = 0.893 \cdot V_0(SB) - 0.040$, $R^2 = 0.8027$. V_0 registered a mean *bias* of $0.063\ mL$, with small limits of agreement ($[-1.2,\ +1.3]\ mL$). According to the unpaired t-test, the differences in V_0 were not statistically significant ($p = 0.38$). Therefore, multiple-beat and single-beat methods can be used interchangeably (Bland and Altman, 1986).

3-2-3-3 Normalization of LV $E(t)$

It has been shown that the normalized elastance curve $E_N(t_N)$, which corresponds to $E(t)$ normalized both by its peak amplitude, E_{max}, and the time to peak elastance, t_{max}, in normal isolated canine hearts was fairly independent of loading conditions, contractile state, and heart rate (Suga and Sagawa, 1974; Suga et al., 1973). Furthermore, Senzaki found a remarkable similarity in the shape of the $E_N(t_N)$ curves between groups with various cardiac disease conditions (Senzaki et al., 1996). Also, the shape of the normalized time-varying elastance curve has been shown to be similar in different animal species (Georgakopoulos et al., 1998). Recently, Jegger et al. (2007) compared $E_N(t_N)$ in healthy and diseased hearts and, despite the general similarity in shape of its waveform, quantitative differences may be found at the ejection phase and during diastole. Since $E(t)$ reflects the time course of the intrinsic contractile properties of the myocardium, these results are not surprising as acute MI involves myocyte hyperthophy and alterations in LV architecture due to an oddly distributed wall tension (see **Figure 3-14**).

Senzaki et al. (1996) noticed the $E_N(t_N)$ curve obtained from measured data would display physiological and statistical deviation that varied with the cardiac cycle phase. Their motivation was that choices of $E_N(t_N)$ at times with least variance would likely yield more reliable and accurate estimates in their proposed single-beat method. In this study, $E_N(t_N)$'s physiological and mathematical deviations

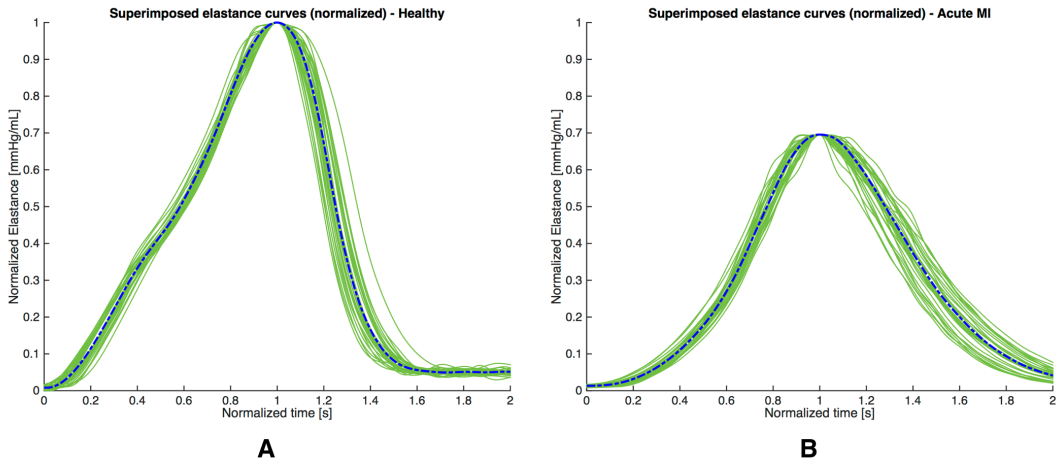

Figure 3-14: (A) Superimposed normalized elastance curves from a rabbit, representing a series of 31 cardiac cycles. The dashed blue line represents the time- and amplitude-normalized LV elastance ($E_N(t_N)$) curve, describing the temporal course of ventricular contractility throughout a cardiac cycle. **(B)** 31 superimposed normalized elastance curves from the same rabbit, following acute MI. These curves are normalized regarding the elastance curves of the healthy heart. By visual inspection, the shape of $E_N(t_N)$ in pathological heart is altered significantly, especially during the ejection period (before E_{max}) and diastolic phase, which is in accordance with a previous study (Jegger et al., 2007).

were also computed, in order to understand if there are quantitative differences when comparing healthy and post-acute MI hearts.

Physiological variance of $E_N(t_N)$ ($\mathrm{d}E_N(t_N)$) is the standard deviation of the measured pooled $E_N(t_N)$ curve. This variance shows the sensitivity of V_0 to changes in normalized elastance, as function of the time point t_N (Senzaki et al., 1996). Mathematical deviation is computed by differentiating Senzaki et al.'s V_0 single-beat equation with respect to $E_N(t_N)$. This variance shows the sensitivity of V_0 estimate, as function of the value of $E_N(t_N)$. Although the explanation behind this mathematical variance is outlined in Senzaki et al. (1996), the expression for the derivative is simplified in Kjørstad et al. (2002).

$$\frac{\mathrm{d}V_0}{\mathrm{d}E_N(t_N)} = \frac{P_N(t_N)\left(V_{es} - V(t_N)\right)}{\left(E_N(t_N) - P_N(t_N)\right)^2} \tag{3-5}$$

where $P_N(t_N) = P(t_N)/P_{es}$.

The result of multiplying both physiological and mathematical variances yields $\mathrm{d}V_0$, which corresponds to the variance about the V_0 estimate, as a function of t_N.

$$\mathrm{d}V_0 = \frac{\mathrm{d}V_0}{\mathrm{d}E_N(t_N)} \cdot \mathrm{d}E_N(t_N) \tag{3-6}$$

3-2-4 Preliminary statistical analysis

In data sets containing large real-numbered measurements, occasional erroneous results my be produced. An outlier is an observation which appears to lie outside the cluster of most of the other observations. In this particular study, any miscalculation of P_{MAX} due to bad fitting of the polynomial to the LV pressure curve would be a potential cause of an outlier and, thus, may contribute to wrong

conclusions. Having this in mind, a preliminary statistical analysis of E_{es} and V_0 was added to the processing pipeline. This stage is optional.

After estimating E_{es} for each cardiac cycle, the user may press the *start* button to access the preliminary statistical analysis. Although the GUI presents by default the results for E_{es}, it is also possible to present the results for V_0 using the *popup-menu* in **Figure 3-15 [1]**. Four plots are presented in the GUI's left-side (see **Figure 3-15 [3]**): **(a)** estimated results, in function of the number of cardiac beats; **(b)** histogram of the estimated results; **(c)** estimated results with mean and standard deviation curves (it is expected approximately 68% of the data lie between one standard deviation); **(d)** estimated results with estimated regression line of type $y = m \cdot x + b$. It is possible to change the contents of each plot with the < and > buttons. This not only enhances data readability, but also has a positive impact on user experience, pro-actively providing the user with robust statistical information that potentially can help making better decisions. Once the preliminary statistical analysis is complete, the user has to press *confirm* to store the results. The user is able to undo any outlier removal by clicking on the *reset* button (see **Figure 3-15 [1]**).

Peirce's criterion, devised by Peirce (1852), was used as a statistical procedure for outlier rejection. Although it is the first method developed for the exclusion of outliers, presented over 170 years ago, a recent study from Ross (2003) provided a simple, but practical, technique for applying this method, and compared his results with those of Chauvenet's criterion, another method for outlier rejection which, contrarily, has been intensively used in many education institutions and laboratories. In (Ross, 2003), the author recommended the use of Peirce's criterion because its formulation was more rigorous, it did not make an arbitrary assumption concerning the rejection of data (Chauvenet's criterion does) and, theoretically, it was able to remove several outliers at once (Chauvenet's criterion does not).

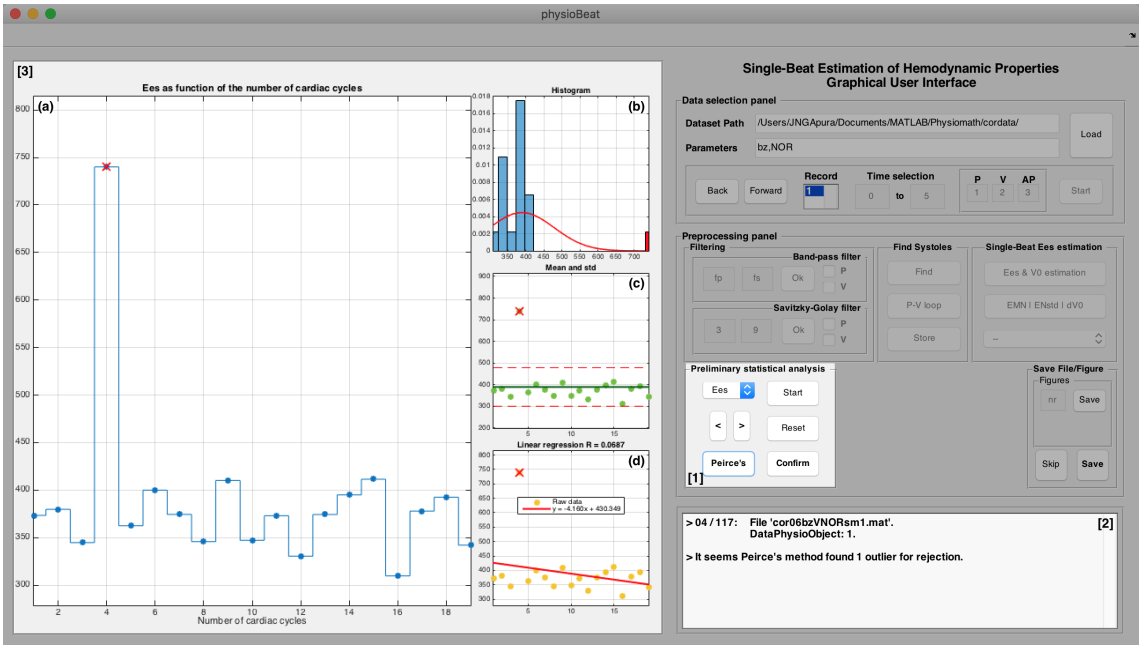

Figure 3-15: An outlier is identified by Peirce's criterion. In **(a)**, **(c)** and **(d)**, the outlier is displayed with a red cross superimposed on the original data point. In **(b)**, the outlier is identified by a red bar.

3-2-4-1 Peirce's method for outlier rejection

In Peirce's method, the idea is to statistically identify what constitutes an error as *too large* and, therefore, identify the corresponding observation as an outlier, whose removal would improve the fit between the observations and a curve. As simple as it may seem, Peirce's formulation proved to be mathematically cumbersome to replicate (the author himself later wrote he was aware of the difficulties in interpreting his original paper), which might have had some influence in the adoption of other methods by the scientific community, such as Chauvenet's criterion. Some years after, Gould (1855) was crucial to clarify Peirce's method, by creating tables of values representing values from Pierce's equations. Unfortunately, there was still a disconnect between Gould's algorithm and the practical application of Peirce's criterion. Recently, Ross (2003) presented a practical technique for Peirce's method, by relying on an updated look-up table.

This study uses Ross's technique. Considering the number of observation pairs (N) and the number of outliers to be removed (n), the aim of the technique is to calculate a threshold value of squared error, and compare it with each observation's squared error. Observations with a squared error smaller than the threshold should be kept and observations with a larger squared error should be removed (i.e., as an outlier). Based on N and n, the algorithm searches the look-up table for the corresponding R value, which is the ratio of the absolute error of one suspicious measurement to the sample standard deviation. x_i is the suspicious observation value, μ_x is the sample's mean, and σ_x is the sample's standard deviation.

$$R = \frac{|x_i - \mu_x|}{\sigma_x} \tag{3-7}$$

Multiplying R by σ_x corresponds to the maximum allowable deviation (threshold) for a value to be kept. For a suspicious measurement x_i, if the difference between x_i and the sample's mean ($|x_i - \mu_x|$) is larger than maximum allowable deviation, then x_i is an outlier and should be removed. Whenever a measurement is rejected, the algorithm sequentially increases the number of suspicious observations, keeping the original values of μ_x, σ_x and N, until no more data measurements need to be eliminated.

Since the Pierce's criteria does not depend on observation data, but instead on characteristics of the observation data (mean and standard deviation), it is a highly repeatable process (Ross, 2003) and, thus, ideal for use in computational applications.

3-2-5 Computation of cardiovascular properties

For each cardiac cycle, the GUI automatically computes LV cardiovascular parameters which can be derived directly from E_{es}. Most of these properties had already been introduced in **Section 2-2**, so **Table 3-1** summarizes the mathematical equations used to compute each cardiovascular property. Please note HR is computed as the inverse of the time span between two consecutive R peaks (known as RR interval). Since the R peaks occur at the end of a diastole (see **Figure 2-1**), in this study the RR interval is estimated as the time span between two consecutive end-diastolic points.

Cardiovascular Property	Equation
Stroke Volume	**Equation (2-1)**
Ejection Fraction	**Equation (2-2)**
Cardiac Output	**Equation (2-3)**
Effective Arterial Elastance	**Equation (2-5)**
Stroke Work	**Equation (2-6)**
Stroke Work to its maximum	$Q_{load} = 4\frac{E_a \cdot E_{es}}{(E_{es}+E_a)^2}$
Pressure-Volume Area	$PVA = SW + P_{es}\frac{V_{es}-V_0}{2} - P_{ed}\frac{V_{ed}-V_0}{4}$
Cardiac Work Efficiency	**Equation (2-9)**
Maximum and minimum rates of pressure change	$max\left(\frac{\mathrm{d}P}{\mathrm{d}t}\right)$ and $min\left(\frac{\mathrm{d}P}{\mathrm{d}t}\right)$
Maximum and minimum rates of volume change	$max\left(\frac{\mathrm{d}V}{\mathrm{d}t}\right)$ and $min\left(\frac{\mathrm{d}V}{\mathrm{d}t}\right)$

Table 3-1: Mathematical equations derived for each cardiovascular property. These properties are computed automatically once the user confirms or skips the results from the preliminary statistical analysis. For an explanation on the origin and mathematical derivation of Q_{load}, which represents the optimality of the afterload, please refer to Sugimachi and Sunagawa (1997).

3-2-5-1 Tau estimation

The LV isovolumic relaxation constant has been formally introduced in **Section 2-2-8**. In the GUI, τ is computed using five different methods: half-pressure (Mirsky, 1984), Weiss (Weiss et al., 1976), Raff & Glantz (Raff and Glantz, 1981), Levenberg-Marquardt (Martin et al., 1984) and Logistic (Matsubara et al., 1995). τ is computed on the LV pressure segment after $\mathrm{d}P/\mathrm{d}t_{min}$ and before the filling phase, τ end-point, defined as the pressure $5\ mmHg$ above the end-diastolic pressure of the next cardiac cycle (see **Figure 3-16**).

Each τ estimation method is briefly described below:

(a) Half-pressure: $T_{50\%}$ is the time required for the pressure to decline to 50% of the value recorded at $\mathrm{d}P/\mathrm{d}t_{min}$ (Mirsky, 1984).

(b) Weiss: τ_W is the time constant of the monoexponential model of isovolumic pressure fall, as expressed in **Equation (2-10)**. Since the equation approximates the pressure signal between $\mathrm{d}P/\mathrm{d}t_{min}$ and τ end-point, P_0 is the pressure at $\mathrm{d}P/\mathrm{d}t_{min}$ ($t = 0\ ms$). τ_W is estimated from the slope of the natural logarithm of the pressure curve against time, using a least-square fit algorithm (Weiss et al., 1976).

(c) Raff & Glantz: τ_{RG} is the time constant of the monoexponential model of isovolumic pressure fall, as expressed in **Equation (2-11)**. τ_{RG}, P_0 and P_∞ are estimated by considering three points equally spaced in time on the pressure time curve, between the time points of $\mathrm{d}P/\mathrm{d}t_{min}$ and τ end-point (Raff and Glantz, 1981).

(d) Levenberg-Marquardt: τ is the time constant of the monoexponential model of isovolumic

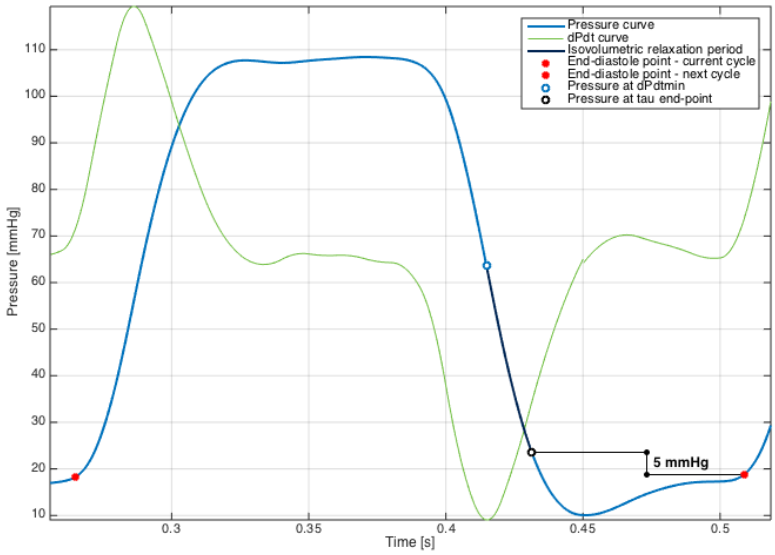

Figure 3-16: LV pressure curve (thick blue line) is represented in function of time, with $\mathrm{d}P/\mathrm{d}t$ (green narrow line) and end-diastolic points (red) from both current and following cardiac cycle. The isovolumetric relaxation period, used for τ estimation, is represented in darker blue, between the $\mathrm{d}P/\mathrm{d}t_{min}$'s pressure point and τ end-point.

pressure fall. The output of Raff's method is used as the initial conditions of this method. τ is optimized by successive iterations, using Matlab's `fit` function with *bisquare* weights and *Levenberg-Marquardt* algorithm, as proposed in Martin et al. (1984). Estimation ends after 400 iterations or when the difference between two consecutive values is smaller than 10^{-6}.

(e) Logistic: τ_L is the time constant of a logistic model of isovolumic pressure fall (Matsubara et al., 1995), as expressed in **Equation (2-12)**. Similarly as the other methods, the equation approximates the pressure signal between $\mathrm{d}P/\mathrm{d}t_{min}$ and τ end-point. τ_L, P_A and P_B are calculated by least-square fitting.

3-2-6 Visualization tool

Since it is very difficult to make sense of raw data in its natural form, in the last stage of the pipeline the user is presented with various options to interactively visualize the processed data, each one with access to unique visual information regarding the recently computed results. This allows the user to make sense of conclusions faster and observe possible interesting patterns and stunning observations that would not be apparent from looking only at numbers and columns of data. The aim of the visualization tool is to present data in such a way that even someone without any background in PV data analysis is able to digest the results, and easily uncover specific trends or make data-driven conclusions. All built-in visualization possibilities are enumerated below.

Normalized $E(t)$ analysis: mean normalized elastance curve, $E_N(t_N)$'s physiological and mathematical deviations, and variance about the V_0 estimate can be plotted against a normalized time vector. Additionally, it is also possible to visualize graphically the normalized elastance curves for all cardiac cycles in analysis.

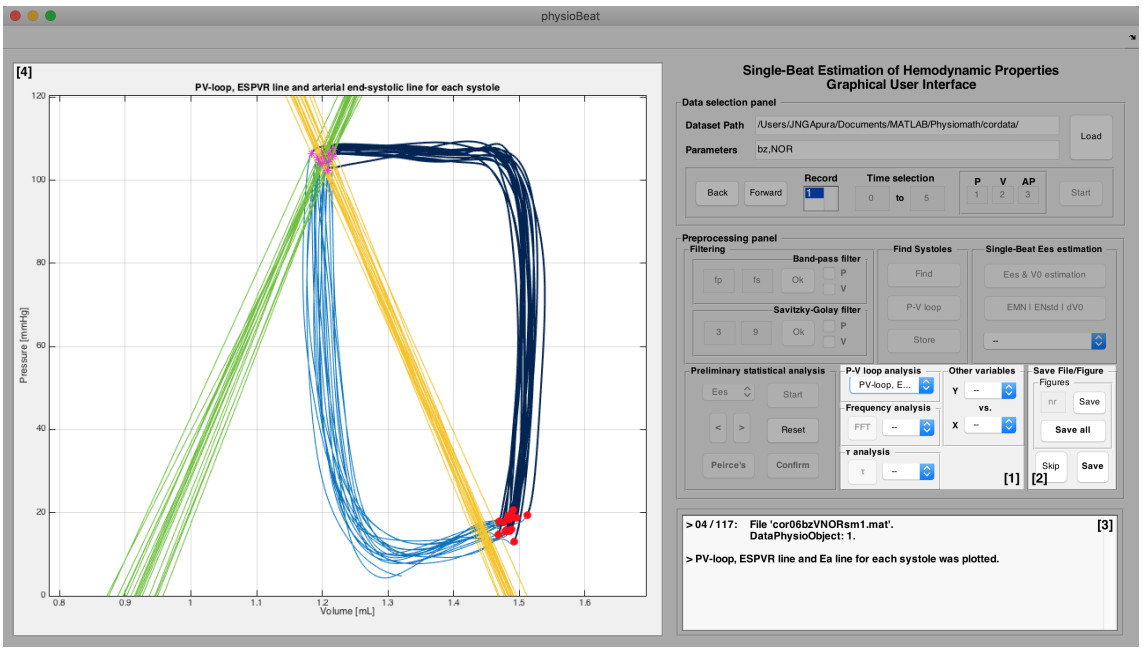

Figure 3-17: The user can visualize the results using various types of graphical representations **[1]**. The GUI allows to save any plot in a directory the user may choose by pressing the *save* button in **[2]**. All plots are displayed in **[4]**.

PV loop analysis: The LV volume is plotted against LV pressure in the PV plane, without any constriction in time (all cardiac beats in analysis are displayed simultaneously). End-systole and end-diastole points are identified, to help the user identify the systole phase. The user can choose to simultaneously plot the ESPVR lines, the E_a lines or both (see **Figure 3-17 [4]**). Furthermore, there is also the possibility to plot all the PV loops in function of time, i.e. in the PV 3D space (pressure *vs.* volume *vs.* time), similarly as in **Figure 3-9**.

FFT analysis: Volume, pressure and elastance from the LV are represented with respect to the frequency, after conversion using the Fast-Fourier Transform algorithm from Matlab's function `fft`. By looking at the whole spectrum of frequencies of the signal, it allows to identify and isolate certain features and frequency components of interest. Furthermore, since the frequency-domain representation of a signal carries information about the signal's magnitude and phase at each frequency, the user might choose to plot each signal in polar coordinates.

Cardiovascular properties analysis: It was developed a fast, flexible and highly customizable visualization tool which allows to plot any cardiovascular property in function of another. This allows the user to compare LV properties that researchers may have never tried before, spot new interesting patterns, and make more insightful conclusions regarding the data in analysis.

τ **analysis**: Behaves similar to the previous analysis, allowing to plot τ and the asymptotes from all five estimation methods against any cardiovascular property of interest. However, the GUI does not allow to display a method's τ values against another's. Furthermore, it is possible to display, for each cardiac beat, the isovolumetric relaxation period with the fitting curves (monoexponential and logistic) from all the methods used. The user can choose which cardiac cycle to visualize.

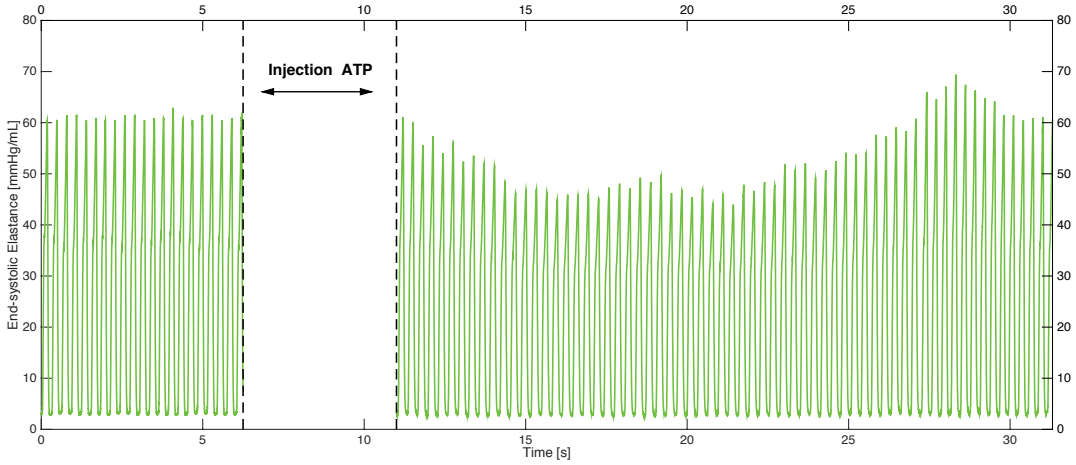

Figure 3-18: Effect of stimulating cardiopulmonary afferent fibers by cardiac injection of ATP on time-varying LV elastance ($E(t)$), in a healthy rabbit heart. Dashed vertical line denote the time interval when ATP was injected.

Other plots: There are two experimental plots in the GUI. An E_{es} value can be plotted against its succeeding E_{es} value in a Poincaré plot, a standard visualizing technique to detect the presence of oscillations in non-linear dynamic systems. Poincaré plots are often used in electrocardiography to assess heart functionality (Kleiger et al., 2005). The second experimental plot displays, for each cardiac cycle, the time interval when volume change is negative, i.e. when the blood is pumped out of the heart. The user can choose which cardiac cycle to visualize.

With such intuitive visualization tools, it is now easier for the researcher to explore PV data in acutely altered hemodynamic states, including short term reflexes (mechano- and chemoreflexes) and diseases (myocadial infarction), and analyze how the cardiovascular system instantly compensates for these homeostatic perturbations. For example, it is possible to capture time-continuous changes in cardiac contractility throughout a full reflex, from prior stimulation to its after-effects (see **Figure 3-18** for an example of von Bezold-Jarisch reflex, under normal conditions), providing a refreshed and powerful framework for cardiovascular study.

After the visualization stage is complete, the user has two options: *skip* or *save* the analysis (see **Figure 3-17 [2]**). The first option erases the analysis and returns to the first stage of the processing analysis, allowing the user to analyze other PV data files. In the second option, before returning to the first stage of the data processing pipeline, the user is asked to choose a directory in which the `dataPhysioBeat` object will be saved. The following data objects will be saved in the chosen directory by default.

3-3 Statistical methods

This section describes briefly the statistical methods used to evaluate the statistical significance between baseline and after reflex stimulation, in healthy and pathological hearts. It begins with an overview of the general features of longitudinal data, and a description of common approaches to analysis.

Longitudinal study is ubiquitous in the biomedical sciences. It refers to a study in which measurements are collected repeatedly at multiple follow-up times (repeated measures) on each subject, with the aim of characterizing changes in the response of interest over time (Fitzmaurice and Ravichandran, 2008). Although longitudinal studies involve a great effort in data acquisition, its benefits add richness to the types of analysis that can be undertaken. Some of those benefits include:

(a) Correlation of measures within subjects: Since most biological processes are not completely random, the assumption of independence of repeated measures on the same subject cannot be assumed. In fact, sequential observations of the same individual tend to be closer in value to one another than the same number of observations collected from different individuals would be (Gueorguieva and Krystal, 2004);

(b) Measurement of individual change: The opportunity to observe individual patterns of change is one of the key strengths of the longitudinal design. However, average profile of change over time for a population can be complex, and individuals may exhibit considerable variability which may change over the duration of the study. This violate the fundamental assumption of homogeneity of variance, which is the basis of many transversal statistical methods, such as t-test or one-way analysis of variance (ANOVA) (Fitzmaurice and Ravichandran, 2008);

(c) Separation of time-effects: Longitudinal studies allow to separate time-trends processes within individuals from cross-sectional effects between subjects (cohort effects), whereas in transversal analyses these are often combined (Diggle, 2002).

By allowing to assess the influence of covariates on both average responses, and rates of change of response over time in subjects, a longitudinal approach allows to explore average differences in outcomes and to model time-trends between groups of individuals (Diggle, 2002). However, one must use appropriate statistical methods to adjust for this.

The most common approaches for analyzing longitudinal data are analysis of variance (ANOVA), ANOVA for repeated measures and derived methods[1], and are technically simple to apply. However, since longitudinal data may lead to multiple inferences over that are not independent, repeated-measures ANOVA cannot be used, despite its strengths (Diggle, 2002). The method treats time as a categorical factor and assumes a constant correlation between repeated measures on an individual (*sphericity*), regardless of the time-interval between observations. This assumption is infrequently justified, since consecutive observations on the same subject tend to be correlated more highly than observations on the same subject in the future (Gueorguieva and Krystal, 2004). Thus, it is not suited to assessing the effect of multiple covariates on outcomes, nor can provide information about individual level trends over time (Fitzmaurice and Ravichandran, 2008; Twisk, 2013).

Mixed-effects regression models (LMM), or multilevel models, provide a general framework for the analysis of longitudinal data, as they permit make specific assumptions about the response trajectory

[1] These methods are mentioned here briefly, since they are not used in this thesis.

over time for each individual (within-subject variation) and how it varies with the individual's characteristics (between-subject variation) (Diggle, 2002). Also, they do not require balanced data across different recordings of data, which provides researchers a more flexible and powerful approach when handling missing data, "drop-out" of study participants, or other forms of missing measurements within individuals (Shek and Ma, 2011). This overcomes the limitations of other conventional statistical techniques, such as multivariate ANOVA. Furthermore, mixed-effect models allows the researcher to specify several different patterns with varying complexity and to select best-fitting one using indices of relative goodness of fit, or how well each model agrees with the data, such as Akaike Information Criterion (AIC). For a detailed description of different indices, please refer to the tutorial by Littell et al. (2000).

These models focus on the regression relationship between outcomes and covariates for an individual, by incorporating two distinct components: a **fixed-effect** component, which describes covariate effects that are assumed to be identical across the population; and a **random-effects** component, that allows each individual to vary from the population average in a prescribed manner. This between-subject heterogeneity reflects natural variability due to unmeasured factors that are not captured in the fixed-effects. The fixed-effects in the model are estimated as discrete parameters, which can change over time (e.g. current medication) or can be time-independent (e.g. genre), whereas the random-effects are drawn from a probability distribution, estimated in the model (Diggle, 2002; Twisk, 2013). Also, in the random-effects approach, the covariance structure in the model can be directly specified and can use data to estimate its parameters, varying in complexity from a compoud symmetry (equal variances at all time points and equal correlations between measurements on the same subject) to no restrictions at all (Brown and Prescott, 2014). Two of the most common structures are the unstructured covariance, which allows every term to be different and often offers the best fit, and the autoregressive covariance, which has homogeneous variances and correlations that decline exponentially as measurements get further and further apart (Kincaid, 2005).

Mathematically, linear mixed-effects model is represented as straight lines:

$$Y_i = X_i\beta + Z_i\gamma_i + \epsilon_i \tag{3-8}$$

where Y_i is the dependent variable, X_i and Z_i are the fixed and random design matrices, respectively, β is a vector of unknown fixed effects (parameters that are the same for all subjects), γ_i is a vector of unknown random effects (parameters that are allowed to vary over subjects) and ϵ_i is the unknown random error normally distributed with mean zero and variance σ_e^2.

LMM supports different approaches to fit longitudinal data, depending how parameters are modeled as fixed or random. The simplest model assumes that repeated measures on individual subjects are fixed within and between subjects, i.e. slopes and intercepts are fixed, resulting in a simple linear regression of the data. Often, this does not provide a good fit. In order to achieve better results, slope and intercepts should be allowed to change within and between subjects. Random-intercept-and-slope model assumes that repeated measures on individuals vary independently around a subject-specific linear-trend, that itself varies randomly between subjects (Laird and Ware, 1982). This model

decomposes the overall random variation in the data into three components: between subjects; between times within subjects; and measurement error.

As final note, in model parameter estimation a popular approach is maximum likelihood (ML). ML estimates converge on the true value as the sample size, are asymptotically normal distributed with variance estimated from the model, and generate standard errors that are smaller than those obtained through other methods of parameter estimation (Singer and Willett, 2003).

3-3-1 Custom statistical analysis procedure

Aiming to make a comparison between results, a custom statistical analysis procedure was created (see **Figure 3-19**). The procedure provides three different methods, which allow not only to pool data for a certain reflex response, but also to decide which statistical methods would be more appropriate to test the significance between different groups.

In the first step, data is organized according to the group of analysis. Results from healthy hearts (`NOR` group) are separated from those from pathological hearts (`AMI` group) and, in each group, data is arranged by type of reflex: cardiac baroreflex (BR), arterial chemoreflex (CR) and von Bezold-Jarisch reflex (BJR). In total, there are six different *groups-reflex* combinations (thereafter, designated by *dataset*), each one stored in a tensor represented in **Figure 3-20**. Each *dataset* comprises data from at least 20 beats before reflex stimulation, until at least 20 beats after PV curves have returned to baseline conditions.

Each *dataset* is divided in three different *measurements*: at baseline conditions, before reflex stimulation (`M1`, or *pre-test*), immediately after reflex stimulation (`M2`, or *post-test*), and when the reflex response reaches its maximum, before returning to the initial baseline conditions (`M3`, or *follow-up*). The last measurement is determined by visual inspection of changes in arterial pressure, LV pressure and LV volume, for each rabbit. In order to reduce the effect of the artificial respiration (a rabbit has a respiration rate of 30-60 cycles per minute), 20 consecutive cardiac beats are selected for each measurement, which corresponds to approximately $5 - 7\ s$.

After this, it depends on the approach chosen. Approach **(A)** aims to analyze temporal patterns between different measurements of a specified cardiovascular property, during a reflex stimulation, for a group of rabbits. To accomplish this, a second custom GUI was designed and implemented in Matlab ® 2014b (see **Figure 3-21 [1]**), to help organizing longitudinal data. For a measurement, the results of a chosen cardiovascular property for each cardiac beat are plotted for all rabbits that belong to that *dataset*. Although this beat-to-beat analysis might be helpful to spot possible overall trends and patterns, it can also be difficult to analyze due to the quantity of the data. When the interest is in the mean response over time, estimation of beat-to-beat means and standard deviations can reveal whether groups are changing in a similar or different fashion. This 'simple' approach to longitudinal data analysis allows to visually compare possible differences between and within measurements.

However, approach **(A)** is not informative about individual level change. Using LMM for analysis of repeated measurements over time, approach **B** seeks to discover patterns of systematic variation across groups of rabbits, as well as aspects of random variation that can distinguish between individual rabbits.

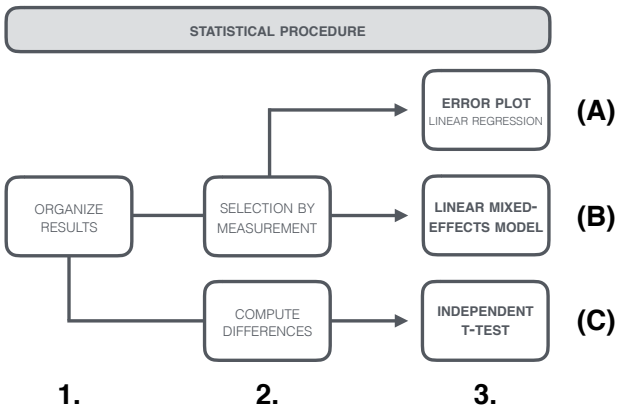

Figure 3-19: Statistical analysis procedure.

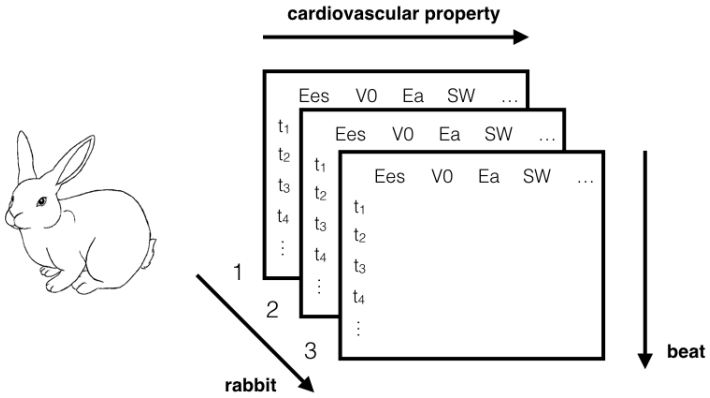

Figure 3-20: Structure of the data in a *dataset*. The tensor is composed of various matrices, each one representing a rabbit. In a matrix, each cardiac cycle has information regarding all cardiovascular properties in analysis.

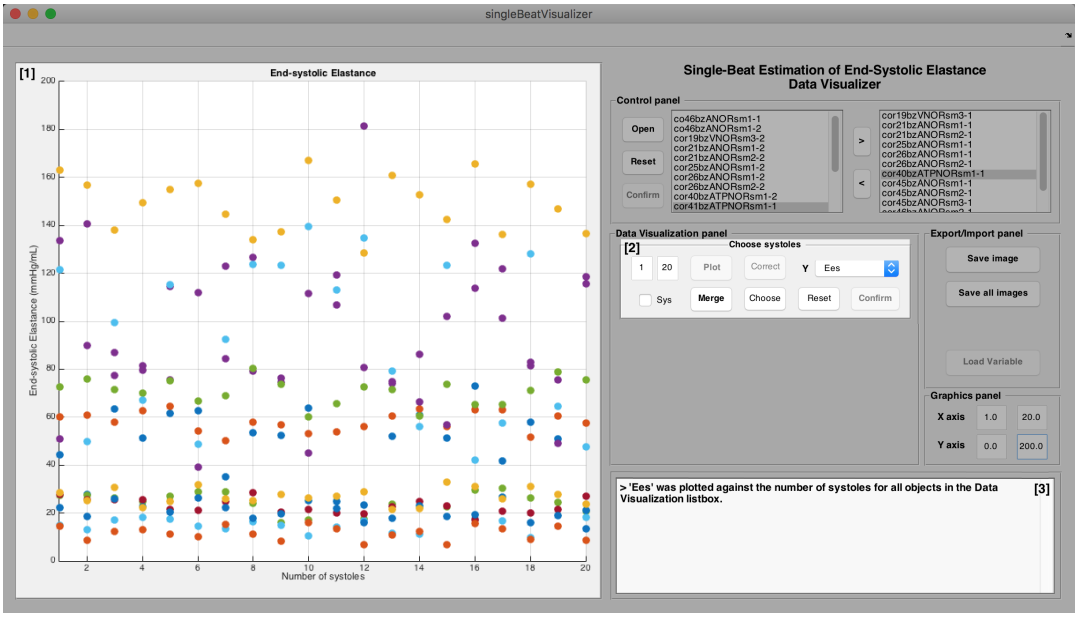

Figure 3-21: Custom GUI for comparison and analysis of a dataset. In **[1]**, E_{es} values from all rabbits in that dataset are plotted in function of the corresponding cardiac cycle. **[2]** enables to select how many consecutive beats for each *measurement*, to choose which cardiovascular property to display, and to merge data for each cardiac beat.

This approach follows a number of steps. Firstly, cardiac beats in each measurement were used as predictors; cardiovascular properties were referred as dependent variables; measurement, condition and combinations of these were defined as fixed and/or random parameters, depending on the model used. Then, all model parameters were computed by ML estimation and, in the case of a random-effects model, various covariance structures were used. AIC was used to test the goodness of model parameters. It is recommended to start with a simpler model, with fixed slopes and intercepts, and gradually increase the complexity of the model, adding variability to the model (Tabachnick and Fidell, 2007). There is no way to know, prior to testing, which model and correlation structure will provide the best fitting to the longitudinal data in analysis.

Finally, approach **(C)** focus on testing whether there are significant differences between groups `NOR` and `AMI`, when comparing the difference of mean in both `M2` and `M3` relatively to `M1`. Differences between beat-to-beat means in both groups are estimated for `M1`, together with two additional metrics: mean (μ) and standard error of the mean (SEM), which are plotted in a bar graph for each reflex stimulation. This provides a simple way to compare baselines for populations with different conditions, and thus examine unbiased effect of myocardial infarction on the cardiovascular properties in study, since baseline data was acquired before reflex stimulations. Consequently, estimated metrics should be similar, with main differences possibly being related to different sample sizes in each population. Furthermore, for each group, these metrics are also computed, but instead of comparing difference values from the same measurement, beat-to-beat means of `M1` (baseline) are subtracted from both `M2` and `M3`. This provides a bigger picture on how coronary ligation might compromise the heart's response to the reflex stimulations, when compared to normal conditions. Statistical differences between groups were estimated by independent, or unpaired-samples, t-test.

Statistical tests were performed in SPSS Statistics 12.0 (Chicago, Illinois, USA). All p-values are specified in **Chapter 4**, unless $p < 0.001$.

3-4 Summary

This chapter provided an overview of this study's numerical methods and their computational implementation. First, the physiological data acquisition was explained. Afterwards, the chapter presented a thorough description of the custom easy-to-use framework, used for PV data analysis and interpretation of results. The PV data processing pipeline was divided in six major stages: data preparation, systole identification, elastance and volume-intercept estimation, preliminary statistical analysis, computational of cardiovascular properties, and visualization tool. In each stage, a detailed overview of the implemented numerical methods is presented, along with a brief literature review and examples. In the last section, the statistical methods t-test and linear mixed effects model were discussed, and a custom statistical analysis procedure was presented.

CHAPTER 4

Results

In this chapter, results obtained after data processing and statistical analysis are presented in detail. Focus is given to ventricular-arterial coupling, cardiac energetic efficiency and cardiac contraction efficiency during reflex stimulation, in both healthy and pathological groups.

4-1 Data size

Recorded PV signals from the controlled experiments in rabbits were processed with the custom GUI presented in the previous chapter, and were organized by *dataset*. **Table 4-1** summarizes the data size available, along with the number of rejected files.

The elevated exclusion rate is due to the high contamination of the signals by unpredictable and unavoidable noise, which can be expected when acquiring biological signals, and may lead to an erroneous interpretation of the signal. Although cable motion artifacts, clogged catheter interference, and combination with respiratory signals or other unwanted signals can be almost totally eliminated with digital filtering, in certain cases these contaminations were so severe that it was very troublesome to retrieve a signal with elevated SNR. Even when filtering the maximum amount of noise while retaining as much of the desired signal frequency spectrum as possible, this produced variations in the physiological signals

	Healthy heart (NOR)			**After acute MI (AMI)**			
	BR	CR	BJR	BR	CR	BJR	
Accepted	42	26	23	27	11	13	141
Rejected	191	79	47	79	42	40	479
Total	233	105	70	106	53	53	$\sum = 620$

Table 4-1: Size of physiological PV data available for analysis, divided by group and reflex stimulation.

which had great consequences in the PV loop shape. A PV loop with a rounded or ellipsoid shape, instead of rectangular, influences the systole identification process and, thus, results into a bad estimation of LV elastance. In most cases, it was found a middle ground between no-filtering and high rejection of noise, to avoid deep changes in the physiological signals.

Additionally, data was also excluded if an arrhythmia was encountered during normal systole identification, or if volume changes during isovolumic cardiac phases were significant. A tolerance of $3\ mmHg$ between the end-diastolic pressure prior to isovolumic contraction and the pressure value after the ejecting beat was given before rejection.

Finally, results were also excluded during the custom statistical analysis. If the LV end-systolic elastance of a specific rabbit differed significantly (two standard errors) from those of all rabbits in that *dataset*, in more than 50% of the cardiac beats of measurement `M1`, all the results from that rabbit would be rejected for all measurements.

4-2 Statistical analysis with LMM

In the following sections, LMM was used to test for significant differences in slopes between and within measurements, for each group. For most of the cases, smallest AIC was achieved from a random-slope-and-intercept model, which included the group and measurement as predictors. Cardiac beat was defined as covariate, since the main focus of the analysis is to compare changes in the dependent variable during the 20-beats of each measurement. Interaction terms for group *times* cardiac beat, measurement *times* cardiac beat, and group *times* measurement *times* cardiac beat were also included. Variance components were used as unstructured or auto-regressive AR(1).

Please note that the fit coefficients a, b in the following tables correspond to the intercept and slope parameters, respectively, estimated using LMM. The coefficient of determination R^2 measures how well the estimated straight line can replicate the data it corresponds to.

4-3 Heart Rate during reflex activation

The main goal of analyzing heart rate (HR) variations during the physiological perturbations evoked in this study is to validate the results as a whole. Until today, only blood pressure and heart rate had been studied (Rocha et al., 2003a; Rosario et al., 2003) and, therefore, this section provides a starting point for the description of the results. In order to analyze the temporal patterns between different measurements in HR, mean values were plotted against time with one standard deviation (see **Figure 4-1**). This analysis allows to compare possible differences between and within measurements by visual inspection and, consequently, reveal trends in the results. Simultaneously, LMM was used to test for significant differences in slopes. No suspicious outliers were identified for HR.

Visual inspection of **Figure 4-1** indicates that, under normal conditions (`NOR`) during `M1`, HR was similar in the baseline: $243\ \pm\ 1.010\ bpm$ before unloading of the baroreceptors ($n = 42$), $243\ \pm\ 0.923\ bpm$ before activation of the chemoreceptors with lobeline ($n = 26$), and $243\ \pm\ 1.224\ bpm$ before activation

of the cardiopulmonary afferent fibers by injection of ATP ($n = 23$).

During M2, HR decreased in accordance with time. Cardiac baroreflex decreased the mean HR (mHR) to $236 \pm 3.958\ bpm$ (difference in slope against M1, $-0.474\ bpm$ per cardiac beat; $p < 0.001$); arterial chemoreflex resulted in bradycardia with mHR of $235 \pm 4.528\ bpm$ (slope, $-0.665\ bpm$ per cardiac beat; $p < 0.001$); and activation of the von Bezold-Jarisch reflex decreased mHR to values similar to those of chemoreflex: $235 \pm 4.921\ bpm$ (slope, $-0.772\ bpm$ per cardiac beat; $p < 0.001$). Detailed examination of measurement M2 indicated that, during the baroreflex stimulation, HR stabilized at $233 \pm 1.122\ bpm$ after 10 beats ($2 - 3$ seconds). This was faster than in the case of both chemical reflexes, which according to **Figure 4-1** did not stabilized during the first 20 beats after the reflex stimulation. Fit analysis of the baroreflex results in M2 also indicated these were not well represented by a monotonically decrescent line ($R^2 = 0.765$), contrarily to results from the other reflexes ($R^2 = 0.918$ and $R^2 = 0.948$ for CR and BJR reflexes, respectively).

The monotonically decrescent lines in M3 imply that HR started to return to baseline conditions even before the end of the reflex response. HR presented approximately the rate per cardiac beat for all reflexes, with difference in slope against M2 of $0.949\ bpm/beat$ for baroreflex ($p < 0.001$), $1.261\ bpm/beat$ for chemoreflex ($p < 0.001$), and $1.242\ bpm/beat$ for von Bezold-Jarisch reflex ($p < 0.001$), which might suggest the heart's recovery is similar in all three. Difference in slope between M1 and M3 was statistically significant for all reflexes ($p < 0.001$). Furthermore, pairwise comparison between all measurements, based on estimated marginal means, revealed significant difference ($p < 0.001$) when Bonferroni correction for multiple comparisons was performed.

After coronary ligation and stabilization for 30 minutes (AMI), during M1, between-group difference in slope was not found significant ($p = 0.17$): $243 \pm 1.469\ bpm$ before baroreflex stimulation ($n = 27$), $243 \pm 1.430\ bpm$ before stimulation of the arterial chemoreceptors ($n = 11$) and $243 \pm 1.470\ bpm$ before activation of the cardiopulmonary afferent fibers ($n = 13$).

Equivalently to normal conditions, the values of mHR were reduced in M2 (see **Figure 4-2**). Vena cava occlusion during cardiac ischemia decreased lightly the mHR to $239 \pm 2.301\ bpm$ (difference in slope against M1, $-0.256\ bpm$ per cardiac beat; $p < 0.001$), whereas chemical stimulation of the carotid chemoreceptors and the chemosensitive cardiac fibers caused a significant decrease of the mHR, to $229 \pm 9.276\ bpm$ (slope, $-1.597\ bpm$ per cardiac beat; $p < 0.001$) and $228 \pm 8.443\ bpm$ (slope, $-1.477\ bpm$ per cardiac beat; $p < 0.001$) respectively. Also, visual inspection of **Figure 4-2** revealed that, after inflating a balloon in the descending aorta, HR reduction was rapidly controlled at a higher mHR, than when under normal conditions, resulting in a low fitting of the data by the fit analysis ($R^2 = 0.403$). During M2, between-group difference in slope was statistically significant ($p < 0.001$) for all reflexes.

During M3, HR had already stated to recover. mHR for the baroreflex increased to $240 \pm 2.043\ bpm$, whereas it was slightly reduced in the case of the chemoreflex and von Bezold-Jarisch reflex, $226 \pm 6.470\ bpm$ and $226 \pm 6.278\ bpm$ respectively. Again, the chemical reflexes seemed to walk hand-in-hand regarding HR, with similar fit coefficients from LMM (see **Table 4-3** for intercept and slope). Differences in rate of change between M2 and M3, and M1 and M3, were statistically significant ($p = 0.01$ for the baroreflex between M2 and M3; $p < 0.001$ for the rest). Between-group difference in slope was statistically significant

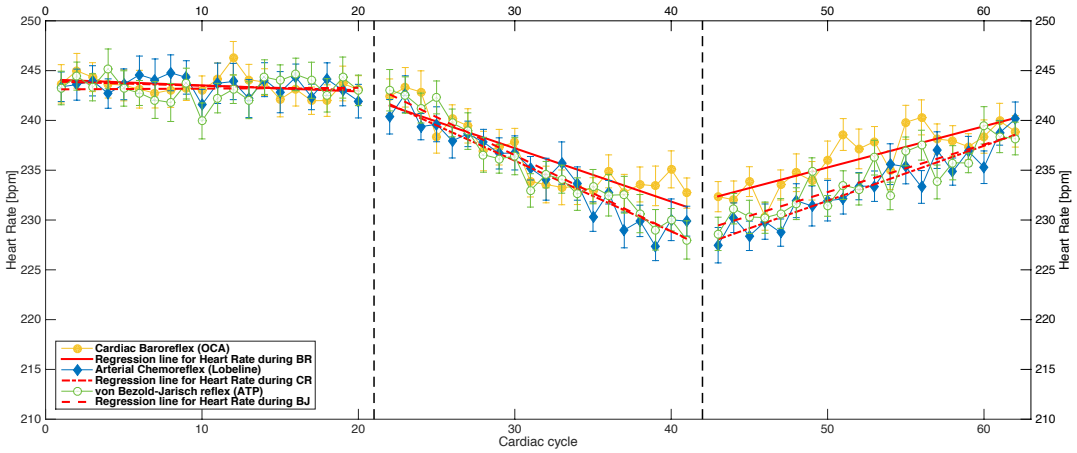

Figure 4-1: Mean heart rate (HR) during three 20-beat measurements, under normal conditions (`NOR`), according to type of reflex. Bars denote standard deviation. Y-axis limits were set to $[210;\ 250]\ bpm$.

	Measurement M1					Measurement M2					Measurement M3				
	μ	SEM	a	b	R^2	μ	σ	a	b	R^2	μ	σ	a	b	R^2
BR	243	1.010	-0.061	244.125	0.126	236	3.958	-0.535	254.068	0.765	236	2.910	0.414	214.582	0.708
CR	243	0.923	-0.044	243.924	0.080	235	4.528	-0.709	257.224	0.918	233	3.465	0.552	204.305	0.890
BJR	243	1.224	0.008	243.112	0.002	235	4.921	-0.764	259.427	0.948	234	3.174	0.478	208.909	0.793

Table 4-2: Mean (μ), standard error of mean (SEM) and fit coefficients (a, b and R^2) of heart rate during the three 20-beat measurements, for all reflexes, under normal conditions (`NOR`).

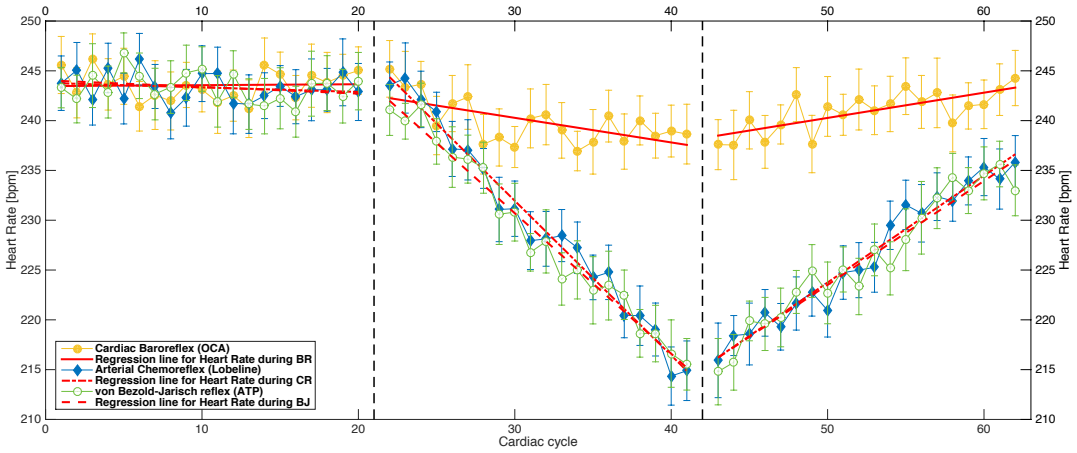

Figure 4-2: Mean heart rate (HR) during three 20-beat measurements, after myocardial infarction (`AMI`), according to type of reflex. Bars denote standard deviation. Y-axis limits were set to $[210;\ 250]\ bpm$.

	Measurement M1					Measurement M2					Measurement M3				
	μ	SEM	a	b	R^2	μ	σ	a	b	R^2	μ	σ	a	b	R^2
BR	243	1.469	0.009	243.466	0.001	239	2.301	-0.247	247.692	0.403	240	2.043	0.254	227.595	0.539
CR	243	1.430	-0.045	243.790	0.035	229	9.276	-1.552	278.501	0.979	226	6.470	1.073	170.077	0.963
BJR	243	1.470	-0.067	244.047	0.072	228	8.443	-1.410	273.017	0.977	226	6.278	1.030	172.117	0.941

Table 4-3: Mean (μ), standard error of mean (SEM) and fit coefficients (a, b and R^2) of heart rate during the three 20-beat measurements, for all reflexes, after coronary ligation (`AMI`).

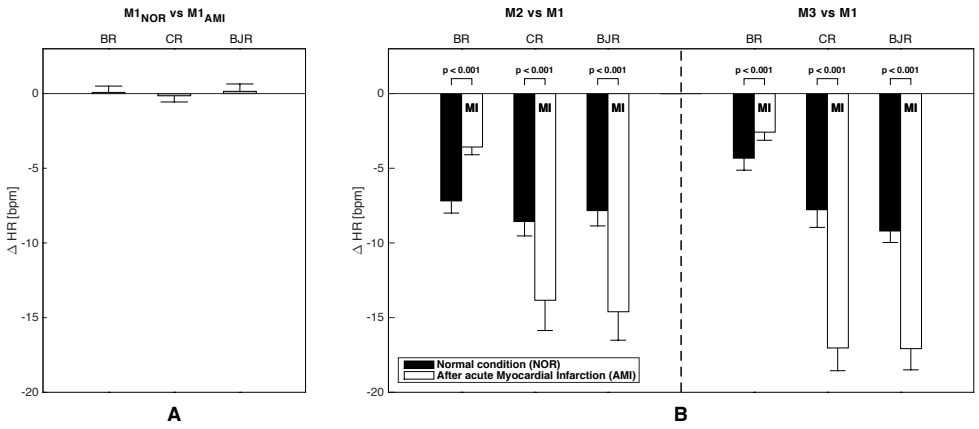

Figure 4-3: Bar graph showing changes in heart rate, evoked on the unloading of baroreceptors and chemical stimulation of the arterial chemoreceptors and the chemosensitive cardiac fibers. **(A)** represents the difference in mean between groups, for `M1`. **(B)** shows the each group's difference in mean in both `M2` and `M3` relatively to `M1`. Bars denote standard error of mean (SEM).

($p < 0.001$) for all reflexes. Again, pairwise comparison between all measurements revealed significant difference ($p < 0.001$) when Bonferroni correction for multiple comparisons was performed.

Figure 4-3 displays a complementary analysis of the HR, focusing on between-group differences in mean. Visual inspection of graph **(A)** indicates that both groups have similar mean HR values during `M1`, a conclusion that has been confirmed statistically above. In graph **(B)**, differences in mean relatively to each group's baseline (`M1`) are presented. It is interesting to notice that the HR's behavior in both **Figure 4-1** and **Figure 4-2** is well represented in **(B)**, even when only considering differences in mean. Between-group differences revealed statistically significant ($p < 0.001$) for all reflexes when an independent t-test was performed.

4-4 The BR dataset

In this section, results from cardiac baroreflex, before ($n = 42$) and after acute MI ($n = 27$), are presented. Single-beat LV end-systolic elastance (E_{es}), arterial elastance (E_a) and their ratio (E_a/E_{es}) were estimated as metrics to evaluate ventriculo-arterial coupling. LV stroke work (SW), total energy expenditure (PVA), ratio of the SW to its theoretical maximum (Q_{load}) and energetic efficiency (CWE) were also calculated to evaluate cardiac energetic and contraction efficiencies. In order to analyze the temporal patterns between different measurements, mean values were plotted against time with one standard deviation. Simultaneously, LMM was used to test for significant differences in slopes. No suspicious outliers were identified for all these cardiovascular indexes.

Note that each graph has y-axes on the left and right sides, allowing to display multiple plots of interest in the same graph. Depending of the cardiovascular properties in analysis, the left y-axis can represent elastance ($mmHg/mL$) or energy ($mmHg \cdot mL$). The right y-axis always represents ratio (unit-less).

Visual inspection of **Figure 4-4** indicates that E_{es} and E_a followed the same pattern throughout measurements `M1-3`, which resulted in a constant E_a/E_{es} ratio. Mean E_{es} and E_a indexes started at 59.936

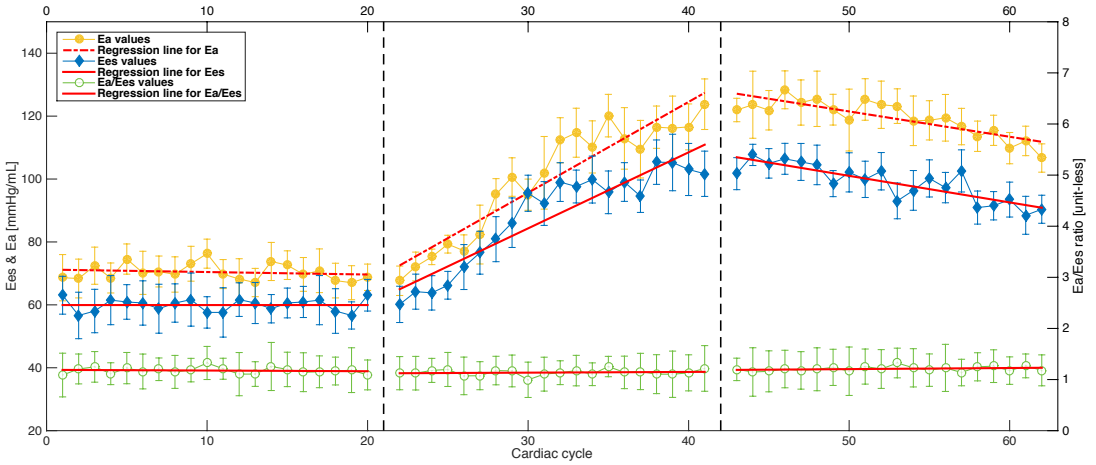

Figure 4-4: Beat-to-beat mean E_{es}, E_a and E_a/E_{es}, evoked during occlusion of the descending aorta ($n = 42$) under normal conditions (NOR), for measurements M1-3. Bars denote standard deviation. Left y-axis limits were set to $[0;\ 140]\ mmHg/mL$ and right y-axis limits to $[0; 9]$ (unit-less), for better readability and comparison.

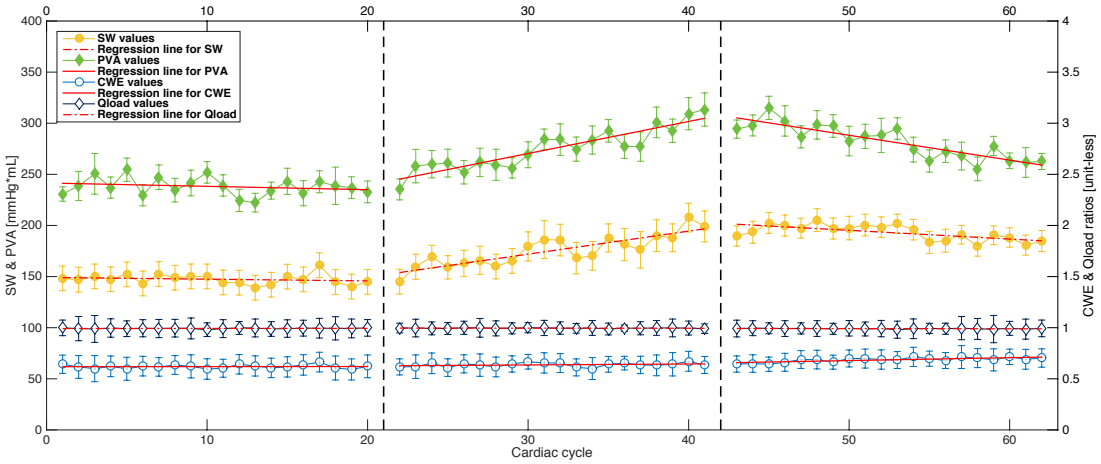

Figure 4-5: Beat-to-beat mean SW, PVA, Q_{load} and CWE during three 20-beat measurements, evoked on the unloading of baroreceptors ($n = 42$) under normal conditions (NOR). Bars denote standard deviation. Left y-axis limits were set to $[0;\ 380]\ mmHg \cdot mL$ and right y-axis limits to $[0; 4]$ (unit-less), for better readability and comparison.

	Measurement M1					Measurement M2					Measurement M3				
	μ	σ	a	b	R^2	μ	σ	a	b	R^2	μ	σ	a	b	R^2
E_a	70.394	2.605	-0.079	71.220	0.032	99.979	18.146	2.888	8.992	0.887	119.481	5.669	-0.805	161.734	0.705
E_{es}	59.936	2.010	0.000	59.936	-0.000	87.944	15.403	2.418	11.778	0.863	98.902	5.913	-0.845	143.247	0.714
E_a/E_{es}	1.176	0.061	-0.001	1.190	0.017	1.137	0.078	0.001	1.093	0.021	1.160	0.067	0.002	1.096	0.075
SW	147.380	4.967	-0.169	149.150	0.040	175.342	15.465	2.251	104.436	0.741	193.099	7.646	-0.854	237.914	0.436
PVA	238.127	8.639	-0.327	241.557	0.050	275.121	20.267	3.132	176.462	0.836	282.153	16.595	-2.430	409.749	0.751
Q_{load}	0.993	0.004	0.000	0.993	0.019	0.994	0.003	-0.000	0.995	0.023	0.993	0.005	-0.000	0.994	0.075
CWE	0.619	0.018	0.000	0.618	0.001	0.627	0.020	0.001	0.597	0.080	0.645	0.022	0.003	0.557	0.555

Table 4-4: Mean (μ), standard deviation (σ) and fit coefficients (a, b and R^2) of E_{es}, E_a, E_a/E_{es}, SW, PVA, Q_{load} and CWE in baroreflex *stimulation* of group NOR ($n = 42$), discriminated by measurement.

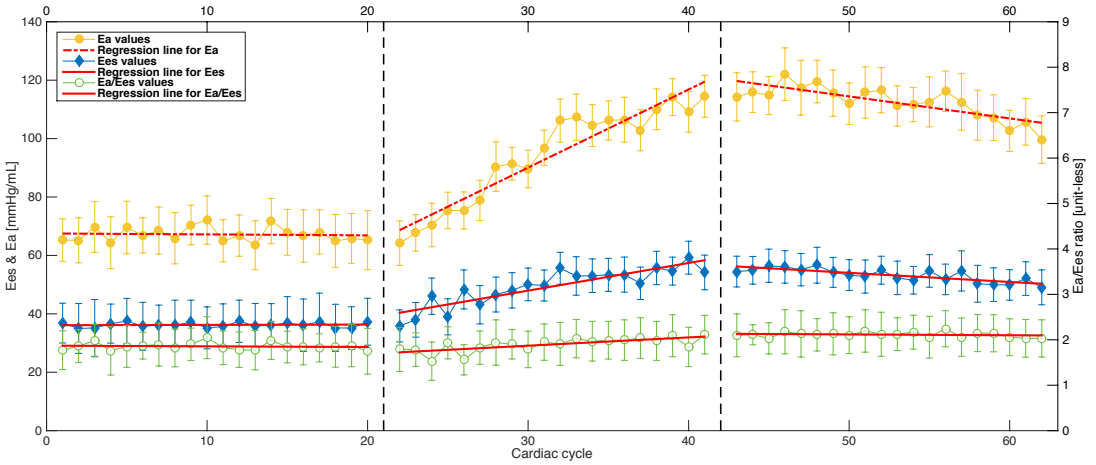

Figure 4-6: Beat-to-beat mean E_{es}, E_a and E_a/E_{es}, due to aorta occlusion ($n = 27$) after acute myocardial infarction (`AMI`), for measurements `M1-3`. Bars denote standard deviation. Left y-axis limits were set to $[0;\ 140]\ mmHg/mL$ and right y-axis limits to $[0; 9]$ (unit-less), for better readability and comparison.

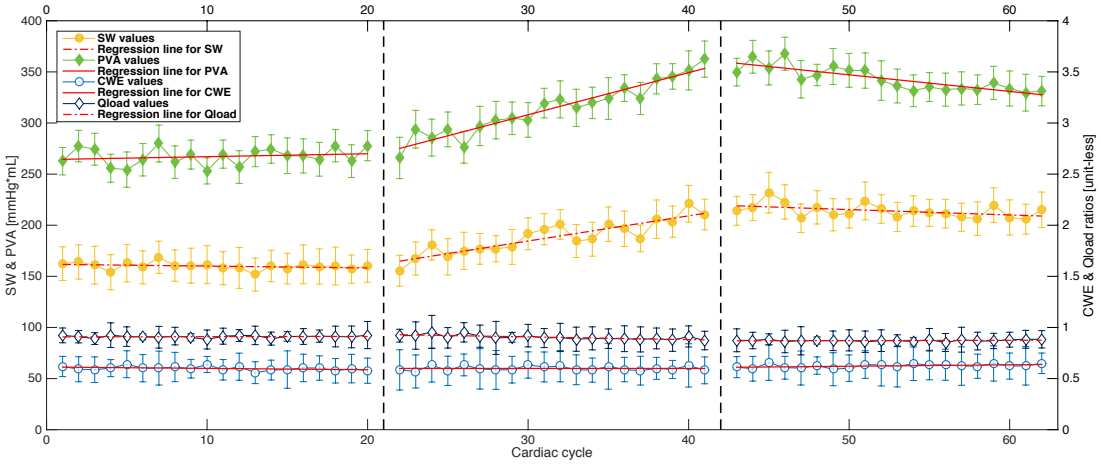

Figure 4-7: Beat-to-beat mean SW, PVA, Q_{load} and CWE during three 20-beat measurements, caused by inflation of a balloon in the descending aorta ($n = 27$) after acute myocardial infarction (`AMI`). Bars denote standard deviation. Left y-axis limits were set to $[0;\ 380]\ mmHg \cdot mL$ and right y-axis limits to $[0; 4]$ (unit-less), for better readability and comparison.

	Measurement M1					**Measurement M2**					**Measurement M3**				
	μ	σ	a	b	R^2	μ	σ	a	b	R^2	μ	σ	a	b	R^2
E_a	67.178	2.490	-0.032	67.516	0.006	94.077	16.605	2.675	9.829	0.908	112.561	5.594	-0.753	152.117	0.635
E_{es}	36.221	0.854	0.011	36.106	0.006	49.367	6.359	0.946	19.560	0.775	53.257	2.308	-0.312	69.662	0.641
E_a/E_{es}	1.856	0.079	-0.001	1.871	0.012	1.898	0.154	0.018	1.324	0.492	2.104	0.058	-0.002	2.201	0.036
SW	159.944	3.546	-0.179	161.823	0.089	188.270	16.291	2.461	110.738	0.799	213.988	6.784	-0.526	241.585	0.210
PVA	267.218	8.326	0.286	264.212	0.041	314.260	25.478	4.117	184.560	0.914	343.077	11.511	-1.622	428.253	0.695
Q_{load}	0.910	0.012	0.000	0.908	0.012	0.904	0.022	-0.003	0.987	0.498	0.897	0.019	0.000	0.898	0.037
CWE	0.599	0.020	-0.001	0.613	0.151	0.598	0.022	0.000	0.599	0.000	0.604	0.038	0.001	0.544	0.206

Table 4-5: Mean (μ), standard deviation (σ) and fit coefficients (a, b and R^2) of E_{es}, E_a, E_a/E_{es}, SW, PVA, Q_{load} and CWE in baroreflex *stimulation*, after acute myocardial infarction (`AMI`, $n = 27$), discriminated by measurement.

$\pm 2.010\ mmHg/mL$ and $70.394 \pm 2.605\ mmHg/mL$ before reflex stimulation, respectively, and increased to $87.944 \pm 15.403\ mmHg/mL$ (difference in slope against M1, $2.418\ mmHg/mL$ per cardiac beat; $p < 0.001$) and $99.979 \pm 18.146\ mmHg/mL$ (slope, $2.967\ mmHg/mL$ per beat ; $p < 0.001$) after unloading of the baroreceptors (measurement M2). During M3, which corresponds to when the reflex response reaches its maximum before returning to the initial baseline conditions, E_{es} and E_a had already started to recover, with a statistically significant between-measurement slope difference relatively to M2 of $-3.693\ mmHg/mL$ per cardiac beat ($p < 0.001$) and $-3.263\ mmHg/mL$ per beat ($p < 0.001$), respectively. Ventriculo-arterial coupling, represented by the ratio E_a/E_{es}, was not statistically significant between-measurements, with difference in slope of 0.002 per beat ($p = 0.14$) between M1 and M2, and 0.003 per beat ($p = 0.18$) between M2 and M3. Pairwise comparisons between measurements did not reveal any significant difference in E_a/E_{es} ratio when Bonferroni correction was performed.

Regarding cardiac performance, SW decreased slightly throughout measurements when compared to PVA, which resulted in an almost imperceptible increase in cardiac work efficiency (see **Figure 4-5**). Q_{load} also changed very lightly. During M1, mean SW and PVA indexes registered $147.380 \pm 4.967\ mmHg{\cdot}mL$ and $238.127 \pm 8.639\ mmHg{\cdot}mL$ respectively, and increased to $175.342 \pm 15.465\ mmHg{\cdot}mL$ (slope, $2.420\ mmHg{\cdot}mL$ per beat; $p < 0.001$) and $275.121 \pm 20.267\ mmHg{\cdot}mL$ (slope, $3.459\ mmHg{\cdot}mL$ per beat; $p < 0.001$) after baroreflex stimulation. In M3, differences in slope against M2 were statistically different for SW ($3.105\ mmHg \cdot mL$ per beat; $p < 0.001$) and PVA ($5.562\ mmHg \cdot mL$ per beat; $p < 0.001$). Both stroke work to its maximum (Q_{load}) and cardiac work efficiency (CWE) were not found statistically significant in between-measurements using LMM, with difference in slope of < 0.001 per beat ($p = 0.46$) and 0.001 per beat ($p = 0.31$), respectively, between M1 and M2, and < 0.001 per beat ($p = 0.42$) and 0.002 per beat ($p = 0.22$) between M2 and M3. This was also confirmed by pairwise comparisons between measurements, with Bonferroni correction.

After heart ischemia, it is noticeable that there was no change in pattern regarding E_a when compared to normal conditions, but the same could not be concluded regarding E_{es}. Results from **Figure 4-6** show that E_{es} values in pathological hearts were roughly $60\ \%$ smaller than E_{es} values for normal hearts. This major difference is behind the great increase of E_a/E_{es} ratio in hearts with coronary ligation. Furthermore, in M2, E_a and E_{es} did not increase at the same pace, which resulted in a slight increase of E_a/E_{es} during baroreflex stimulation. According to **Table 4-5**, mean E_{es} and E_a indexes started at $36.221 \pm 0.854\ mmHg/mL$ and $67.178 \pm 2.490\ mmHg/mL$ in M1, respectively, and increased to $49.367 \pm 6.359\ mmHg/mL$ (difference in slope regarding M1, $0.935\ mmHg/mL$ per cardiac beat; $p < 0.001$) and $94.077 \pm 16.605\ mmHg/mL$ (slope, $2.707\ mmHg/mL$ per beat ; $p < 0.001$) after unloading of the baroreceptors. During M3, heart and arterial system's contractile properties had already started to recover, with a statistically significant between-measurement slope difference relatively to M2 of $-1.258\ mmHg/mL$ per beat ($p < 0.001$) and $-3.428\ mmHg/mL$ per beat ($p < 0.001$), respectively. Although ventriculo-arterial coupling increases slightly in M2, the transition between M1 and M2 was not found statistically significant, with an increase in slope of 0.019 per beat ($p = 0.19$). However, the transition between M2 and M3 yielded a p-value of 0.003, with a difference in slope of -0.020. Pairwise comparisons between measurements, with Bonferroni correction, revealed the same results.

Finally, visual inspection of **Figure 4-7** reveals a considerable baseline increase in PVA, while left-ventricle SW kept approximately the same baseline values as when in normal conditions, resulting in a overall decrease of the cardiac work efficiency throughout all measurements. Q_{load} also suffered a slight decrease in baseline in M1-3. According to **Table 4-5**, during M1, mean SW and PVA indexes registered $159.944 \pm 3.546\ mmHg \cdot mL$ and $267.218 \pm 8.326\ mmHg \cdot mL$ respectively, and increased to $188.270 \pm 16.291\ mmHg \cdot mL$ (slope, $2.460\ mmHg \cdot mL$ per beat; $p < 0.001$) and $314.260 \pm 25.478\ mmHg \cdot mL$ (slope, $4.403\ mmHg \cdot mL$ per beat; $p < 0.001$) after baroreflex stimulation. During M3, differences in slope relatively to M2 were also statistically different for SW ($2.987\ mmHg \cdot mL$ per beat; $p < 0.001$) and for the PVA index ($5.739\ mmHg \cdot mL$ per beat; $p < 0.001$). Both stroke work to its maximum (Q_{load}) and cardiac work efficiency (CWE) were not found statistically significant in between-measurements using LMM, with difference in slope of -0.004 per beat ($p = 0.26$) and 0.001 per beat ($p = 0.90$), respectively, between M1 and M2, and 0.004 per beat ($p = 0.22$) and 0.001 per beat ($p = 0.36$) between M2 and M3. As before, this was also confirmed by pairwise comparisons between measurements, with Bonferroni correction.

4-5 The CR dataset

This section presents the results obtained for arterial chemoreflex, before ($n = 26$) and after coronary ligation ($n = 11$). Ventriculo-arterial coupling was characterized by the behavior of single-beat LV end-systolic elastance (E_{es}), arterial elastance (E_a) and their ratio (E_a/E_{es}). Cardiac effeciencies were quantified by LV stroke work (SW), total energy expenditure (PVA), ratio of the SW to its theoretical maximum (Q_{load}) and energetic efficiency (CWE). In order to analyze the temporal patterns between different measurements, mean values were plotted against time with one standard deviation. Simultaneously, LMM was used to test for significant differences in slopes. No suspicious outliers were identified for all these cardiovascular indexes.

Each of the following graphs have y-axes on the left and right sides, allowing to display together multiple plots of interest. The left y-axis can either represent elastance ($mmHg/mL$) or energy ($mmHg \cdot mL$), depending of the cardiovascular index in analysis. The right y-axis represents ratio (unit-less).

Visual inspection of **Figure 4-8** reveals that, similarly to the baroreflex stimulation, E_{es} and E_a followed the same pattern throughout measurements M1-3, resulting in a constant E_a/E_{es} ratio. Chemical stimulation of the carotid chemoreceptors caused a considerable increase in both mean E_{es} and E_a indexes, from $59.736 \pm 1.990\ mmHg/mL$ (M1) to $71.000 \pm 6.423\ mmHg/mL$ (difference in slope, $1.204\ mmHg/mL$ per cardiac beat; $p < 0.001$) and $71.143 \pm 3.085\ mmHg/mL$ to $79.450 \pm 6.195\ mmHg/mL$ (slope, $0.849\ mmHg/mL$ per beat ; $p < 0.001$), respectively. During follow-up, E_{es} and E_a had already started to recover, with a statistically significant between-measurement slope difference relatively to M2 of $-1.577\ mmHg/mL$ per cardiac beat ($p < 0.001$) and $-1.556\ mmHg/mL$ per beat ($p < 0.001$), respectively. Ventriculo-arterial coupling, represented by the ratio E_a/E_{es}, was not statistically significant between-measurements, with difference in slope of 0.004 per beat ($p = 0.23$) between M1 and M2, and 0.003 per beat ($p = 0.84$) between M2 and M3. These results were corroborated by pairwise comparisons

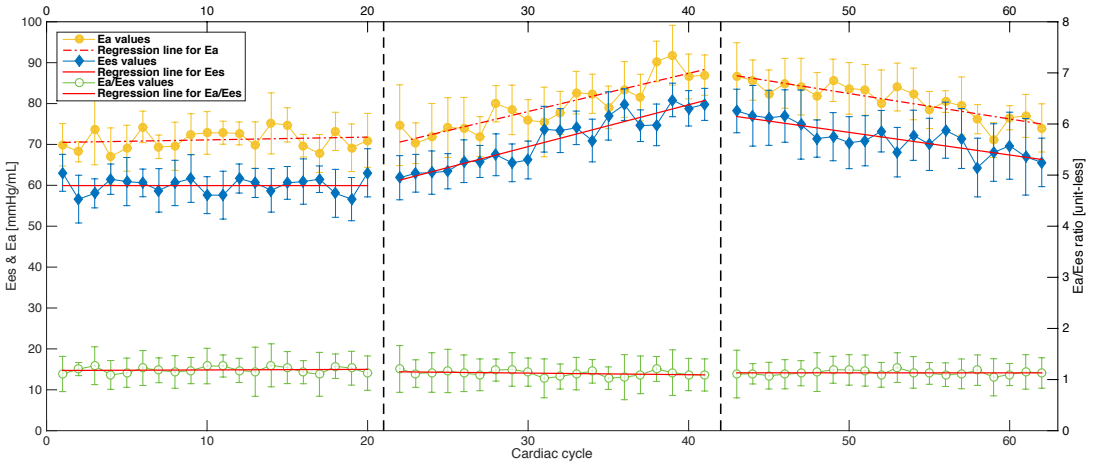

Figure 4-8: Beat-to-beat mean E_{es}, E_a and E_a/E_{es}, evoked on the stimulation of the carotid chemoreceptors ($n = 26$) under normal conditions (NOR), for measurements M1-3. Bars denote standard deviation. Left y-axis limits were set to $[0;\ 100]$ $mmHg/mL$ and right y-axis limits to $[0; 8]$ (unit-less), for better readability and comparison.

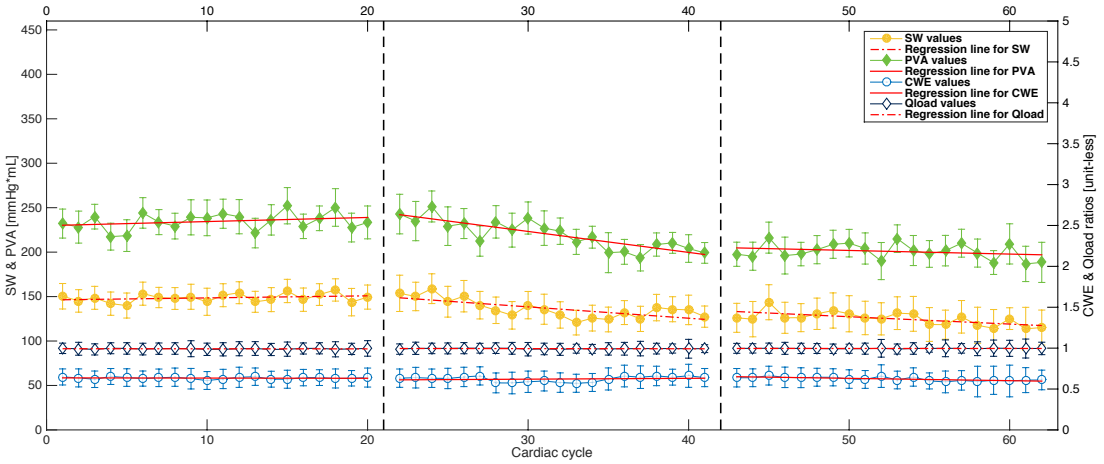

Figure 4-9: Beat-to-beat mean SW, PVA, Q_{load} and CWE during three 20-beat measurements, as response to the activation of the chemoreceptors with lobeline ($n = 26$) under normal conditions (NOR). Bars denote standard deviation. Left y-axis limits were set to $[0;\ 470]$ $mmHg \cdot mL$ and right y-axis limits to $[0; 4]$ (unit-less), for better readability and comparison.

	Measurement M1					Measurement M2					Measurement M3				
	μ	σ	a	b	R^2	μ	σ	a	b	R^2	μ	σ	a	b	R^2
E_a	71.143	3.085	0.085	70.251	0.027	79.450	6.195	0.934	50.036	0.795	80.894	4.259	-0.622	113.538	0.746
E_{es}	59.736	1.990	0.000	59.736	-0.000	71.000	6.423	1.024	38.735	0.890	71.568	3.876	-0.553	100.604	0.71
E_a/E_{es}	1.188	0.062	0.001	1.142	0.097	1.132	0.097	-0.002	1.220	0.108	1.141	0.046	-0.000	1.141	0.000
SW	148.621	4.717	0.233	146.172	0.086	136.506	10.595	-1.276	176.700	0.508	125.280	7.457	-0.828	168.740	0.43
PVA	234.629	9.483	0.460	229.798	0.082	219.733	16.439	-2.358	294.024	0.720	200.878	8.814	-0.409	222.337	0.075
Q_{load}	0.992	0.005	-0.000	0.993	0.012	0.994	0.004	-0.000	0.994	0.065	0.995	0.003	-0.000	0.996	0.000
CWE	0.634	0.012	-0.000	0.636	0.015	0.622	0.033	0.001	0.590	0.033	0.624	0.023	-0.001	0.773	0.541

Table 4-6: Mean (μ), standard deviation (σ) and fit coefficients (a, b and R^2) of E_{es}, E_a, E_a/E_{es}, SW, PVA, Q_{load} and CWE in chemoreflex *stimulation*, under normal conditions (NOR, $n = 26$), discriminated by measurement.

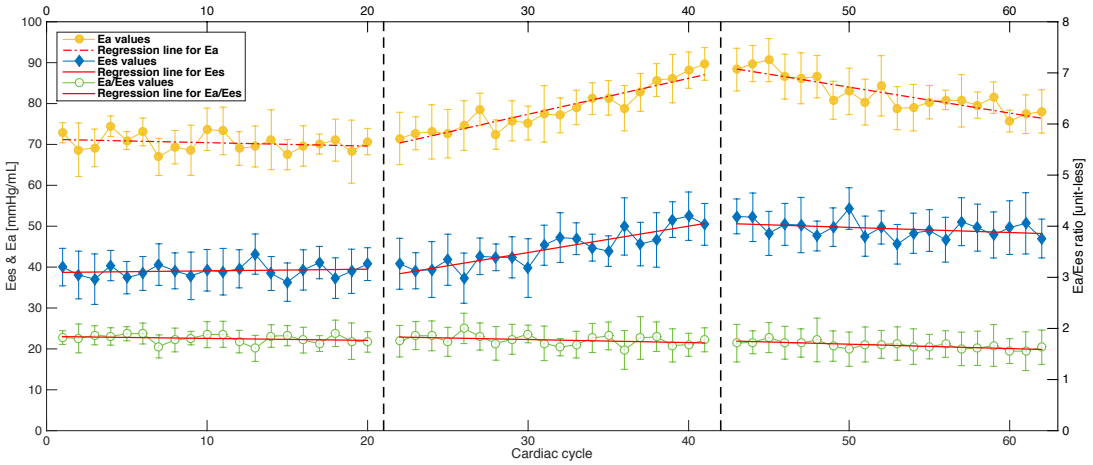

Figure 4-10: Beat-to-beat mean E_{es}, E_a and E_a/E_{es}, caused by stimulation of the carotid chemoreceptors ($n = 11$) after acute myocardial infarction (`AMI`), for measurements `M1-3`. Bars denote standard deviation. Left y-axis limits were set to $[0;\ 100]\ mmHg/mL$ and right y-axis limits to $[0; 8]$ (unit-less), for better readability and comparison.

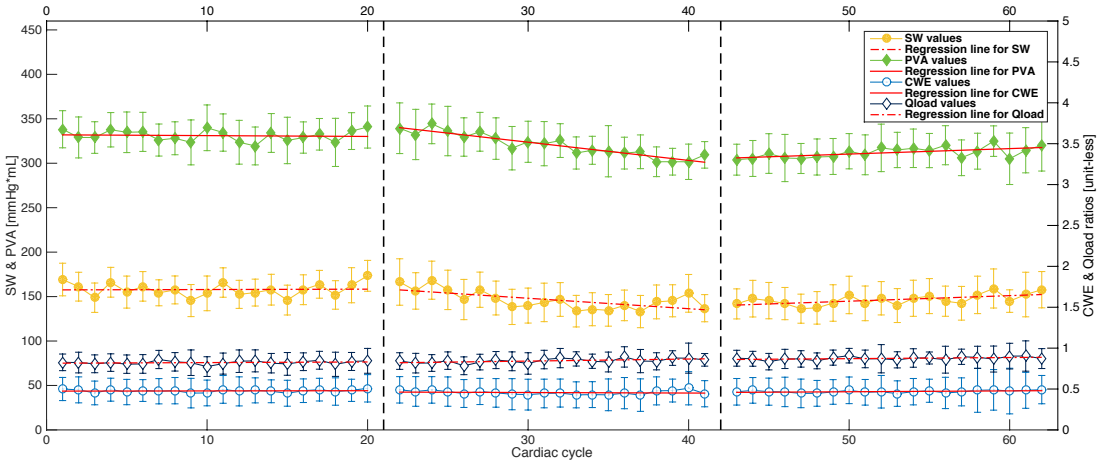

Figure 4-11: Beat-to-beat mean SW, PVA, Q_{load} and CWE during three 20-beat measurements, as response to the activation of the chemoreceptors with lobeline ($n = 11$) after myocardial infarction (`AMI`). Bars denote standard deviation. Left y-axis limits were set to $[0;\ 470]\ mmHg \cdot mL$ and right y-axis limits to $[0; 4]$ (unit-less), for better readability and comparison.

	Measurement M1					**Measurement M2**					**Measurement M3**				
	μ	σ	a	b	R^2	μ	σ	a	b	R^2	μ	σ	a	b	R^2
E_a	70.393	2.147	-0.083	71.269	0.053	78.700	5.532	0.877	51.062	0.881	82.428	4.278	-0.634	115.694	0.768
E_{es}	39.099	1.620	0.041	38.670	0.022	44.527	4.364	0.646	24.170	0.767	49.402	2.143	-0.125	55.969	0.119
E_a/E_{es}	1.803	0.085	-0.004	1.844	0.073	1.774	0.101	-0.006	1.964	0.125	1.670	0.069	-0.009	2.121	0.548
SW	157.940	7.516	0.042	157.495	0.001	146.349	10.611	-1.175	183.355	0.429	146.380	6.175	0.623	113.651	0.357
PVA	331.037	6.199	-0.093	332.013	0.008	320.598	12.995	-2.048	385.098	0.869	311.862	6.071	0.614	279.647	0.358
Q_{load}	0.824	0.021	0.001	0.816	0.048	0.831	0.037	0.003	0.766	0.313	0.835	0.049	0.001	0.802	0.191
CWE	0.477	0.017	0.000	0.474	0.007	0.471	0.034	-0.001	0.477	0.024	0.469	0.015	0.001	0.413	0.185

Table 4-7: Mean (μ), standard deviation (σ) and fit coefficients (a, b and R^2) of E_{es}, E_a, E_a/E_{es}, SW, PVA, Q_{load} and CWE in chemoreflex *stimulation* in group `AMI` ($n = 11$), discriminated by measurement.

between measurements, with Bonferroni correction for multiple comparisons

Regarding cardiac performance and efficiency, the chemoreflex reduced both SW and PVA indexes in a similar pace, which resulted in an almost imperceptible decrease in CWE (see **Figure 4-9**). Q_{load} did not change. During M1, mean SW and PVA indexes registered $148.621 \pm 4.717\ mmHg \cdot mL$ and $234.629 \pm 9.483\ mmHg \cdot mL$ respectively, and decreased to $136.506 \pm 10.595\ mmHg \cdot mL$ (slope, $1.509\ mmHg \cdot mL$ per beat; $p < 0.001$) and $219.733 \pm 16.439\ mmHg \cdot mL$ (slope, $2.818\ mmHg \cdot mL$ per beat; $p < 0.001$) after activation of the chemoreceptors. In M3, differences in slope against M2 were statistically different for both SW ($0.448\ mmHg \cdot mL$ per beat; $p < 0.001$) and PVA indexes ($1.949\ mmHg \cdot mL$ per beat; $p < 0.001$). Both stroke work to its maximum (Q_{load}) and cardiac work efficiency (CWE) were not found statistically significant in between-measurements using LMM, with difference in slope of < 0.001 per beat ($p = 0.20$) and 0.001 per beat ($p = 0.15$), respectively, between M1 and M2, and < 0.001 per beat ($p = 0.34$) and -0.002 per beat ($p = 0.86$), respectively, between M2 and M3. This was also confirmed by pairwise comparisons between measurements, with Bonferroni correction.

After coronary ligation, it is noticeable that there was no change in pattern over time for both E_{es} and E_a when compared to normal conditions. However, similarly as in the baroreflex stimulation, E_{es} values in pathological hearts were roughly $60\ \%$ smaller than those for normal hearts, which caused a great increase of E_a/E_{es} ratio in hearts with heart ischemia. In M2, E_{es} and E_a indexes had dissimilar growths, which resulted in a slight decrease of E_a/E_{es} during chemoreflex stimulation. According to **Table 4-7**, mean values started at $39.099 \pm 1.620\ mmHg/mL$ and $70.393 \pm 2.147\ mmHg/mL$ in M1, respectively, and increased to $44.527 \pm 4.364\ mmHg/mL$ (slope, $0.605\ mmHg/mL$ per cardiac beat; $p < 0.001$) and $78.700 \pm 5.532\ mmHg/mL$ (slope, $0.794\ mmHg/mL$ per beat ; $p < 0.001$) after chemoreceptor activation in the carotid sinus. During follow-up, heart and arterial system's contractile properties had already started to recover, with a statistically significant between-measurement slope difference relatively to M2 of $-0.771\ mmHg/mL$ per beat ($p < 0.001$) and $-1.511\ mmHg/mL$ per beat ($p < 0.001$), respectively. Although ventriculo-arterial coupling decreases slightly in M2, it was not found statistically significant in between-measurements using LMM, with difference in slope of -0.002 per beat ($p = 0.33$) between M1 and M2, and -0.003 per beat ($p = 0.28$) between M2 and M3. Pairwise comparisons between measurements, with Bonferroni correction, revealed the same results.

Finally, visual inspection of **Figure 4-11** reveals a considerable baseline increase in PVA, while left-ventricle SW maintained approximately the same baseline values as when in normal conditions, resulting in a overall decrease of the cardiac work efficiency throughout M1-3. Q_{load} also suffered a slight decrease in baseline throughout all measurements. According to **Table 4-5**, both SW and PVA indexes decreased during post-test, from $157.940 \pm 7.516\ mmHg \cdot mL$ and $331.037 \pm 6.199\ mmHg \cdot mL$ to $146.349 \pm 10.611\ mmHg \cdot mL$ (slope, $1.217\ mmHg \cdot mL$ per beat; $p < 0.001$) and $320.598 \pm 12.995\ mmHg \cdot mL$ (slope, $-2.141\ mmHg \cdot mL$ per beat; $p < 0.001$), respectively. During M3, differences in slope relatively to M2 were statistically different for SW ($1.798\ mmHg \cdot mL$ per beat; $p < 0.001$) and for PVA ($-2.662\ mmHg \cdot mL$ per beat; $p < 0.001$). Both Q_{load} and CWE were not found statistical significant in between-measurements, with difference in slope of 0.002 per beat ($p = 0.37$) and -0.001 per beat ($p = 0.46$), respectively, between M1 and M2, and -0.002 per beat ($p = 0.44$) and 0.002 per beat ($p = 0.35$) between M2 and M3. As before,

this was also confirmed by pairwise comparisons between measurements, with Bonferroni correction.

4-6 The BJR dataset

In this section, results from cardiopulmunary reflex, before ($n = 23$) and after coronary ligation ($n = 13$), are presented. Single-beat LV end-systolic elastance (E_{es}), arterial elastance (E_a) and the coupling ratio (E_a/E_{es}) were estimated as metrics to characterize ventriculo-arterial coupling. LV stroke work (SW), total energy expenditure (PVA), ratio of the SW to its theoretical maximum (Q_{load}) and energetic efficiency (CWE) were also calculated to evaluate cardiac energetic and mechanical efficiencies. In order to analyze the temporal patterns between different measurements, mean values were plotted against time with one standard deviation. Simultaneously, LMM was used to test for significant differences in slopes. No suspicious outliers were identified for all these cardiovascular indexes.

Note that each graph has y-axes on the left and right sides, allowing to display multiple plots of interest in the same graph. Depending of the cardiovascular properties in analysis, the left y-axis can represent elastance ($mmHg/mL$) or energy ($mmHg \cdot mL$). The right y-axis always represents ratio (unit-less).

Visual inspection of **Figure 4-12** reveals that E_{es} and E_a evolved similarly during measurements `M1-3`, without compromising E_a/E_{es} coupling ratio. Chemical stimulation of chemosensitive cardiac fibers caused a significant decrease of mean E_a from $69.998 \pm 1.901\ mmHg/mL$ (`M1`) to $59.726 \pm 7.542\ mmHg/mL$ (difference in slope, $-1.375\ mmHg/mL$ per cardiac beat; $p < 0.001$), whereas mean E_{es} decreased from $62.480 \pm 2.074\ mmHg/mL$ to $50.650 \pm 8.131\ mmHg/mL$ (slope, $-1.362\ mmHg/mL$ per beat ; $p < 0.001$). Comparing slope differences between `M2` and `M3`, LMM analysis found differences were statistically significant between these measurements for both E_{es} ($1.433\ mmHg/mL$ per cardiac beat; $p < 0.001$) and E_a ($1.292\ mmHg/mL$ per cardiac beat; $p < 0.001$). Ventriculo-arterial coupling was not statistically significant between-measurements, with difference in slope of 0.005 per beat ($p = 0.26$) between `M1` and `M2`, and -0.008 per beat ($p = 0.37$) between `M2` and `M3`. These results were corroborated by pairwise comparisons between measurements, with Bonferroni correction for multiple comparisons.

Figure 4-13 displays the results for cardiac performance and efficiency. The heart's total energy expenditure and stroke work decreased considerably after activation of the von Bezold-Jarisch reflex, with such a balance that Q_{load} and cardiac work efficiency remained unchanged. During `M1`, mean SW and PVA indexes registered $149.492 \pm 1.476\ mmHg \cdot mL$ and $235.308 \pm 4.356\ mmHg \cdot mL$ respectively, and decreased to $130.325 \pm 9.349\ mmHg \cdot mL$ (slope, $-1.461\ mmHg \cdot mL$ per beat; $p < 0.001$) and $199.943 \pm 18.541\ mmHg \cdot mL$ (slope, $-3.025\ mmHg \cdot mL$ per beat; $p < 0.001$) after chemical activation of cadiopulmunary afferent fibers. In `M3`, differences in slope against `M2` were statistically different for both SW ($1.254\ mmHg \cdot mL$ per beat; $p < 0.001$) and PVA ($3.268\ mmHg \cdot mL$ per beat; $p < 0.001$). Both stroke work to its maximum (Q_{load}) and cardiac work efficiency (CWE) were not found statistically significant in between-measurements using LMM, with difference in slope of -0.002 per beat ($p = 0.15$) and 0.002 per beat ($p = 0.17$), respectively, between `M1` and `M2`. However, between `M2` and `M3`, only Q_{load} was not found significant ($p = 0.56$), with a difference in slope of 0.002 per beat. For CWE, the tran-

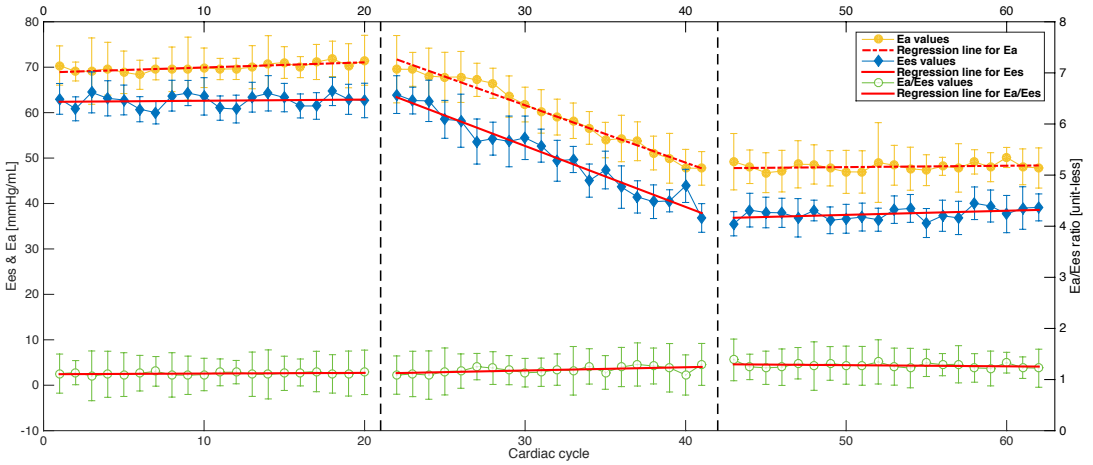

Figure 4-12: Beat-to-beat mean E_{es}, E_a and E_a/E_{es}, evoked on the stimulation of the pulmonary afferent fibers ($n = 23$) under normal conditions (NOR), for measurements M1-3. Bars denote standard deviation. Left y-axis limits were set to $[0;\ 80]$ $mmHg/mL$ and right y-axis limits to $[0; 8]$ (unit-less), for better readability and comparison.

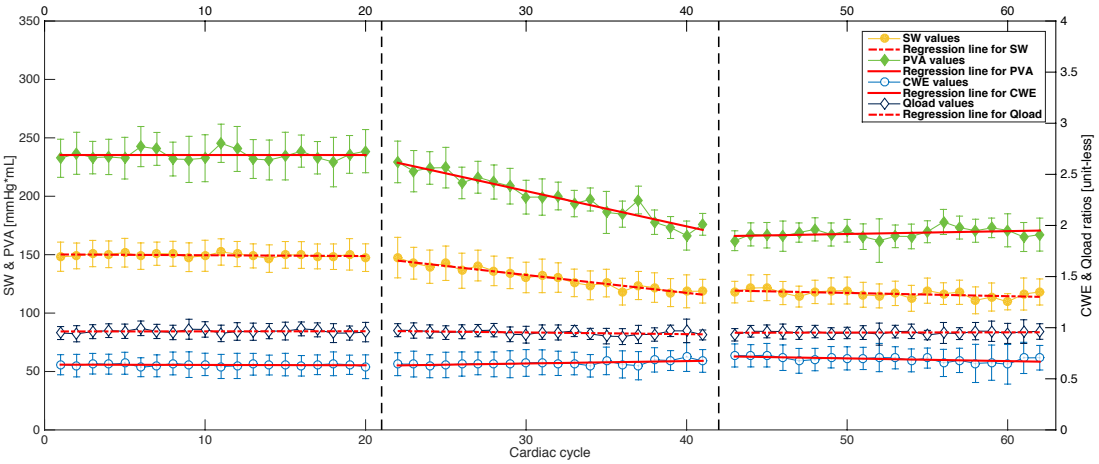

Figure 4-13: Beat-to-beat mean SW, PVA, Q_{load} and CWE during three 20-beat measurements, as response to activation of the von Bezold-Jarisch reflex with ATP ($n = 23$) under normal conditions (NOR). Bars denote standard deviation. Left y-axis limits were set to $[0;\ 350]$ $mmHg \cdot mL$ and right y-axis limits to $[0; 4]$ (unit-less), for better readability and comparison.

	Measurement M1					**Measurement M2**					**Measurement M3**				
	μ	σ	a	b	R^2	μ	σ	a	b	R^2	μ	σ	a	b	R^2
E_a	69.998	1.901	0.113	68.816	0.546	59.726	7.542	-1.262	99.476	0.980	48.085	0.868	0.030	46.493	0.043
E_{es}	62.630	1.436	0.025	62.364	0.011	50.650	8.131	-1.342	92.920	0.953	37.724	1.290	0.091	32.937	0.175
E_a/E_{es}	1.118	0.025	0.001	1.104	0.102	1.137	0.089	0.006	0.976	0.300	1.146	0.048	-0.002	1.336	0.078
SW	149.492	1.476	-0.072	150.247	0.083	130.325	9.349	-1.533	178.621	0.941	116.560	3.179	-0.279	131.218	0.270
PVA	235.308	4.356	0.000	235.308	0.000	199.943	18.541	-3.025	295.236	0.932	168.319	3.933	0.243	155.554	0.134
Q_{load}	0.964	0.015	0.000	0.963	0.002	0.956	0.020	-0.002	1.003	0.236	0.953	0.012	0.000	0.941	0.013
CWE	0.635	0.011	-0.000	0.639	0.028	0.643	0.022	0.002	0.569	0.386	0.657	0.026	-0.003	0.802	0.365

Table 4-8: Mean (μ), standard deviation (σ) and fit coefficients (a, b and R^2) of E_{es}, E_a, E_a/E_{es}, SW, PVA, Q_{load} and CWE in von Bezold-Jarisch reflex *stimulation*, under normal conditions (NOR, $n = 23$), discriminated by measurement.

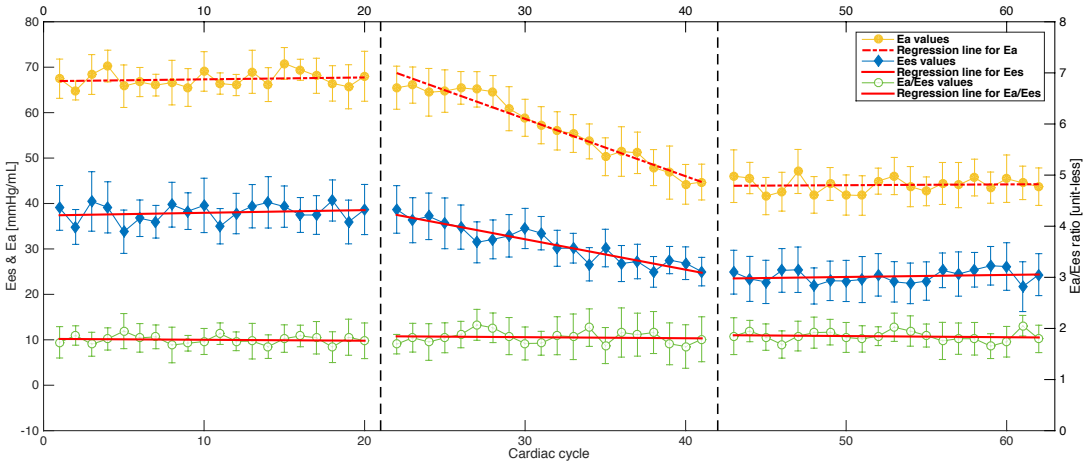

Figure 4-14: Beat-to-beat mean E_{es}, E_a and E_a/E_{es}, caused by activation of the cardiopulmonary reflex ($n = 13$) after acute myocardial infarction (`AMI`), for measurements `M1-3`. Bars denote standard deviation. Left y-axis limits were set to $[0;\ 80]\ mmHg/mL$ and right y-axis limits to $[0; 8]$ (unit-less), for better readability and comparison.

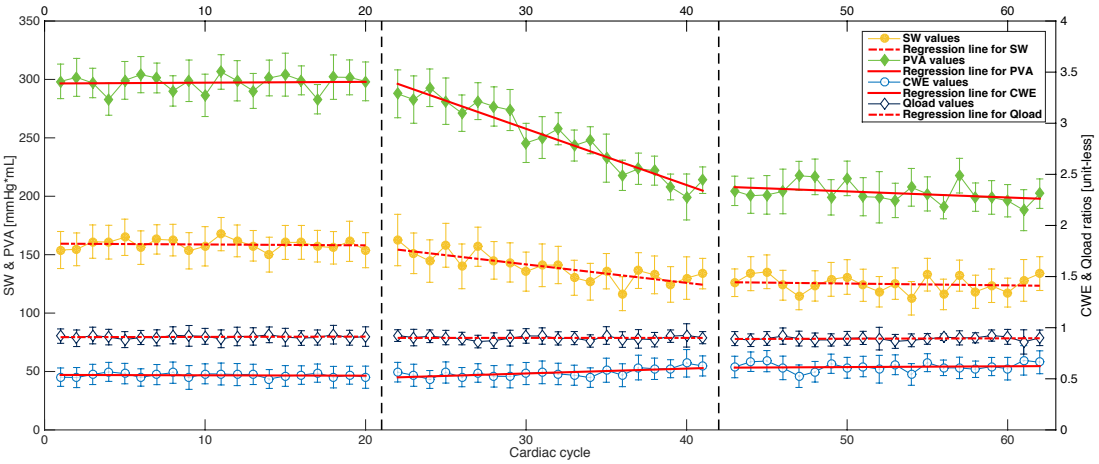

Figure 4-15: Beat-to-beat mean SW, PVA, Q_{load} and CWE during three 20-beat measurements, as response to the activation of the von Bezold-Jarisch reflex ($n = 13$) after myocardial infarction (`AMI`). Bars denote standard deviation. Left y-axis limits were set to $[0;\ 350]\ mmHg \cdot mL$ and right y-axis limits to $[0; 4]$ (unit-less), for better readability and comparison.

	Measurement M1					**Measurement M2**					**Measurement M3**				
	μ	σ	a	b	R^2	μ	σ	a	b	R^2	μ	σ	a	b	R^2
E_a	67.348	1.695	0.042	66.910	0.021	56.726	7.637	-1.262	96.476	0.956	44.073	1.626	0.018	43.139	0.004
E_{es}	37.980	2.021	0.059	37.359	0.030	31.128	4.226	-0.670	52.219	0.878	23.942	1.414	0.045	21.556	0.036
E_a/E_{es}	1.777	0.083	-0.002	1.796	0.017	1.826	0.123	-0.002	1.891	0.010	1.845	0.103	-0.002	1.965	0.017
SW	158.694	4.424	-0.074	159.469	0.010	139.302	11.674	-1.579	189.053	0.641	124.902	7.017	-0.155	133.048	0.017
PVA	297.260	6.911	0.071	296.510	0.004	250.505	29.574	-4.813	402.108	0.927	202.853	8.366	-0.520	230.161	0.135
Q_{load}	0.910	0.013	0.000	0.907	0.018	0.905	0.021	-0.000	0.900	0.000	0.898	0.019	0.000	0.874	0.019
CWE	0.534	0.019	-0.000	0.538	0.014	0.559	0.041	0.005	0.410	0.467	0.617	0.041	0.001	0.576	0.012

Table 4-9: Mean (μ), standard deviation (σ) and fit coefficients (a, b and R^2) of E_{es}, E_a, E_a/E_{es}, SW, PVA, Q_{load} and CWE in von Bezold-Jarisch reflex *stimulation* in group `AMI` ($n = 13$), discriminated by measurement.

sition yielded a p-value of $p < 0.002$ (slope, -0.005 per beat). This was also confirmed by pairwise comparisons between measurements, with Bonferroni correction.

After coronary ligation, it is noticeable that there was no change in pattern regarding E_a and E_{es} when compared to normal conditions. Again, results show that E_{es} values in pathological hearts are smaller than E_{es} values for normal hearts. This major difference is behind the great increase of E_a/E_{es} ratio in hearts with acute myocardial infarction.

Furthermore, in M2, E_a and E_{es} did not decrease at the same pace, which resulted in a slight decrease of E_a/E_{es} during stimulation of chemosensitive cardiac fibers. According to **Table 4-9**, mean E_{es} and E_a indexes started at $37.980 \pm 2.021\ mmHg/mL$ and $67.348 \pm 1.695\ mmHg/mL$ in M1, respectively, and increased to $31.128 \pm 4.226\ mmHg/mL$ (difference in slope regarding M1, $-0.729\ mmHg/mL$ per cardiac beat; $p < 0.001$) and $56.726 \pm 7.637\ mmHg/mL$ (slope, $-1.304\ mmHg/mL$ per beat ; $p < 0.001$) after cardiac injection of ATP. During M3, heart and arterial system's contractile properties had already started to recover, with a statistically significant between-measurement slope difference relatively to M2 of $0.715\ mmHg/mL$ per beat ($p < 0.001$) and $1.280\ mmHg/mL$ per beat ($p < 0.001$), respectively. Although ventriculo-arterial coupling decreased slightly in M2, the transition between M1 and M2 was not found statistically significant, with an increase in slope of < 0.001 per beat ($p = 0.14$). The transition between M2 and M3 yielded a p-value of 0.59, with a difference in slope of -0.020. Pairwise comparisons between measurements, with Bonferroni correction, revealed the same results.

Finally, visual inspection of **Figure 4-15** revealed that a considerable baseline decrease in both SW and PVA, without any major change in work efficiency. Q_{load} also remained unchanged throughout measurements M1-3. According to **Table 4-9**, during M1, mean SW and PVA indexes registered $149.492 \pm 1.476\ mmHg \cdot mL$ and $235.308 \pm 4.356\ mmHg \cdot mL$ respectively, and decreased to $130.325 \pm 9.349\ mmHg{\cdot}mL$ (slope, $-1.461\ mmHg{\cdot}mL$ per beat; $p < 0.001$) and $199.943 \pm 18.541\ mmHg{\cdot}mL$ (slope, $-3.025\ mmHg{\cdot}mL$ per beat; $p < 0.001$) after chemical stimulation of chemosensitive cardiac fibers. During M3, differences in slope relatively to M2 were also statistically different for SW ($1.254\ mmHg \cdot mL$ per beat; $p < 0.001$) and for the PVA index ($3.268\ mmHg \cdot mL$ per beat; $p < 0.001$). Both cardiac efficiency indexes, Q_{load} and CWE were not found statistically significant between M1 and M2, yielding a difference in slope of -0.002 per beat ($p = 0.59$) and 0.002 per beat ($p = 0.11$), respectively. Between M2 and M3, Q_{load} was not found statistically significant (0.002 per beat, with $p = 0.21$), whereas CWE was (-0.005 per beat, $p < 0.001$). As before, this was also confirmed by pairwise comparisons between measurements, with Bonferroni correction as a post-hoc test.

4-7 Differences between groups NOR and AMI

This section aims at analyzing each cardiovascular property independently, in order to examine: **(a)** the effect of heart ischemia on baseline values; **(b)** how acute myocardial infarction might compromise the cardiovascular property response to the reflex stimulation, when compared to an intact cardiovascular system. To accomplish this, two metrics were computed for measurements M1-3 of each dataset: mean (μ) and standard error of the mean (SEM).

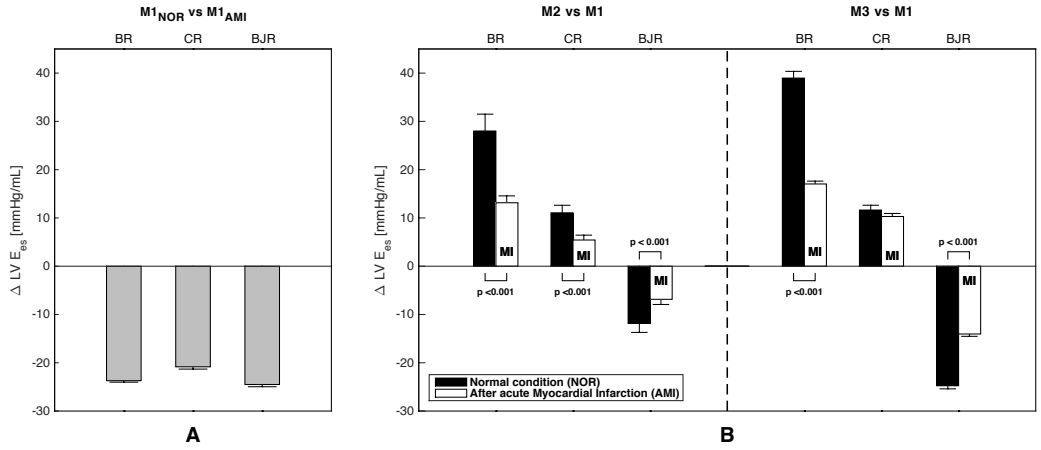

Figure 4-16: Bar graph showing changes in left-ventricle end-systolic elastance (E_{es}), according to type of reflex. **(A)** represents the difference in mean between groups, for M1. **(B)** shows the each group's difference in mean in both M2 and M3 relatively to M1. Bars denote standard error of mean (SEM).

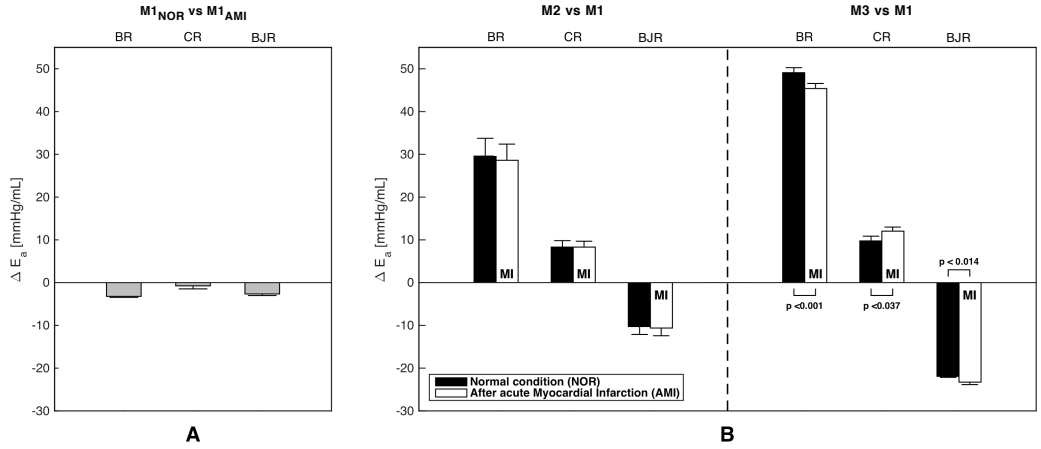

Figure 4-17: Bar graph showing changes in arterial elastance (E_a), according to type of reflex. **(A)** represents the difference in mean between groups, for M1. **(B)** shows the each group's difference in mean in both M2 and M3 relatively to M1. Bars denote standard error of mean (SEM).

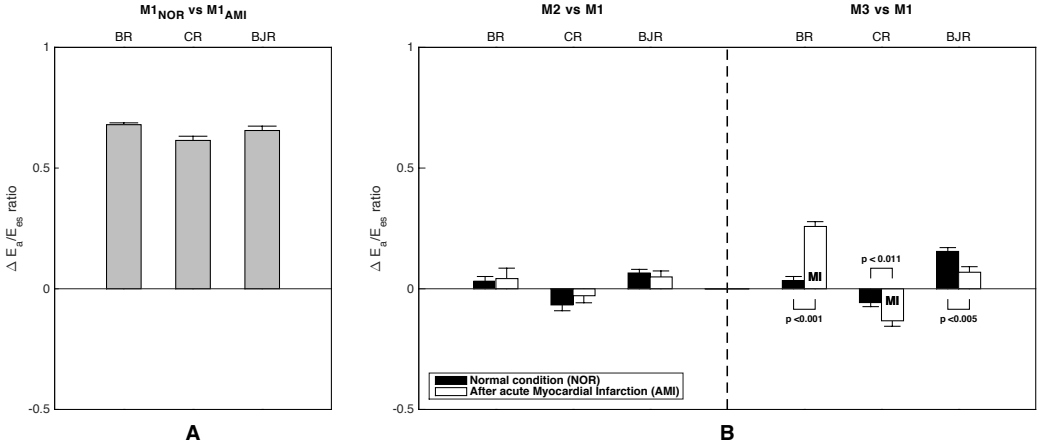

Figure 4-18: Bar graph showing changes in ventriculo-arterial coupling (E_a/E_{es}), according to type of reflex. **(A)** represents the difference in mean between groups, for M1. **(B)** shows the each group's difference in mean in both M2 and M3 relatively to M1. Bars denote standard error of mean (SEM).

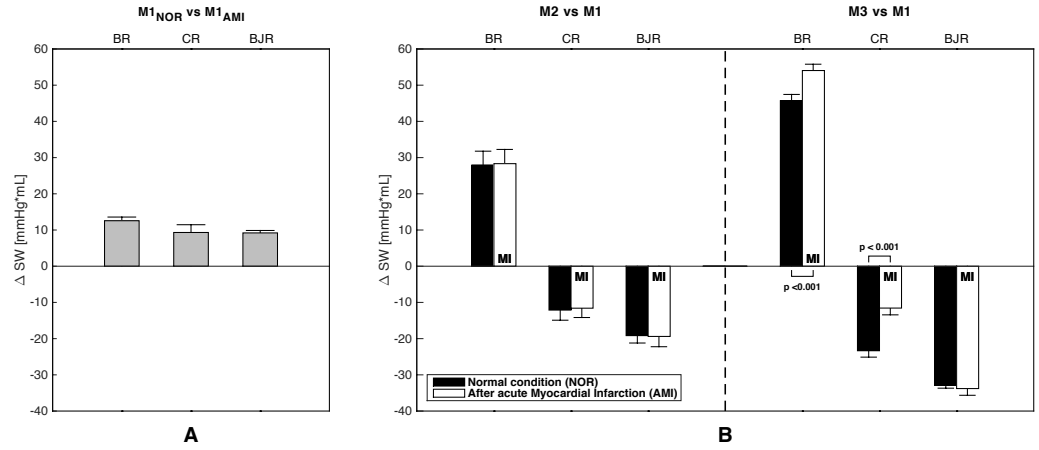

Figure 4-19: Bar graph showing changes in stroke work (SW), according to type of reflex. **(A)** represents the difference in mean between groups, for `M1`. **(B)** shows the each group's difference in mean in both `M2` and `M3` relatively to `M1`. Bars denote standard error of mean (SEM).

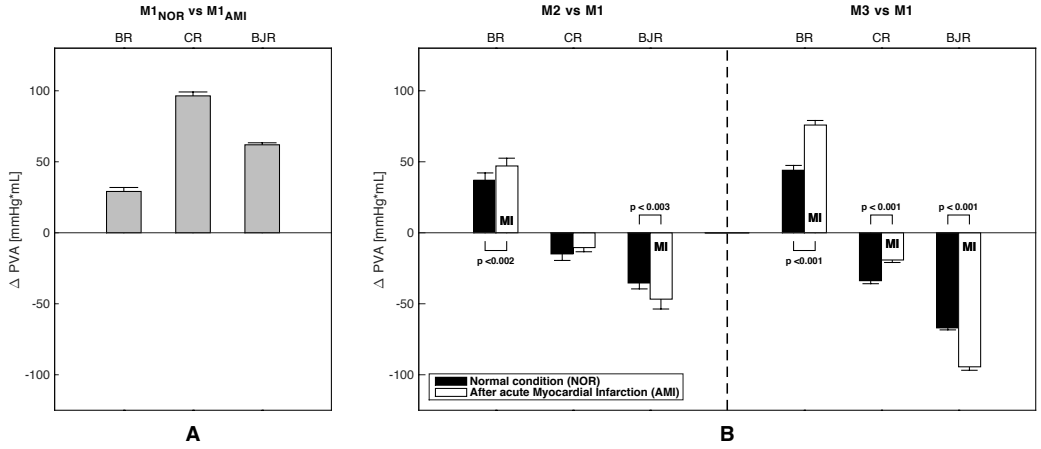

Figure 4-20: Bar graph showing changes in total energy expenditure (PVA), according to type of reflex. **(A)** represents the difference in mean between groups, for `M1`. **(B)** shows the each group's difference in mean in both `M2` and `M3` relatively to `M1`. Bars denote standard error of mean (SEM).

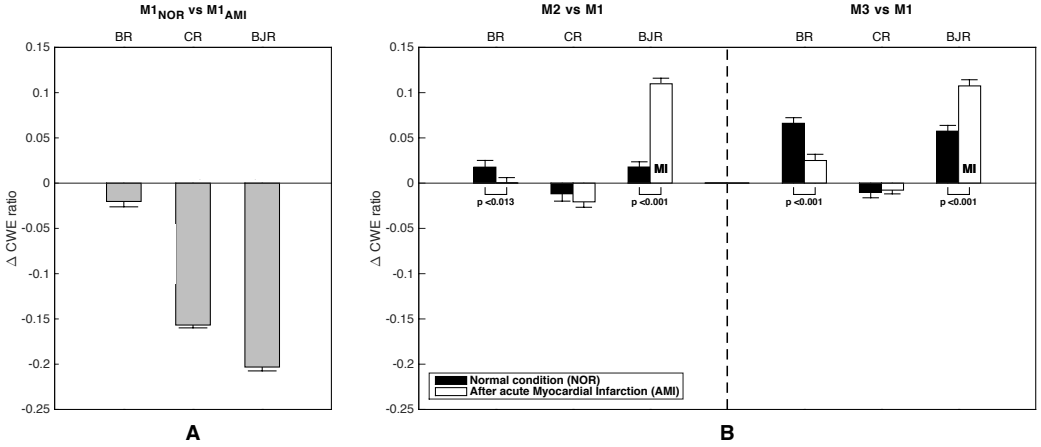

Figure 4-21: Bar graph showing changes in cardiac work efficiency (CWE), according to type of reflex. **(A)** represents the difference in mean between groups, for `M1`. **(B)** shows the each group's difference in mean in both `M2` and `M3` relatively to `M1`. Bars denote standard error of mean (SEM).

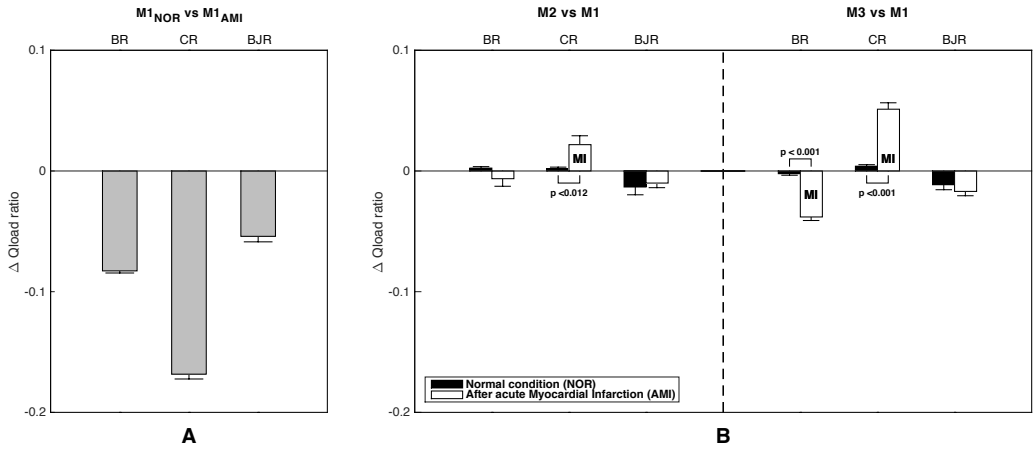

Figure 4-22: Bar graph showing changes in stroke work to its maximum (Q_{load}) according to type of reflex. **(A)** represents the difference in mean between groups, for `M1`. **(B)** shows the each group's difference in mean in both `M2` and `M3` relatively to `M1`. Bars denote standard error of mean (SEM).

For **(a)**, differences in baseline means between groups were plotted in a bar graph (see **Figure 4-16-22 - A**). During `M1` the reflex has not been evoked yet, so these observations are free from any reflex influence. Thus, this provides a simple and straight-forward way to examine the effect of myocardial infarction on the cardiovascular properties in study. For example, visual inspection of **Figure 4-16 - A** revealed an impairment in myocardial contractility for all cardiovascular reflexes evoked after acute myocardial infarction. However, for the case of arterial input impedance, demonstrated by E_a, coronary ligation did not seem to have a direct influence, since the baseline means between groups `NOR` and `AMI` were very similar among all reflexes (see **Figure 4-17 - A**).

For **(b)**, instead of comparing difference in means from the same measurement, `M1` mean was subtracted from both `M2` and `M3` means (see **Figure 4-16-7 - B**). This allowed to quantitatively examine how coronary ligation might have compromised heart's response to the altered hemodynamic profiles in study, when compared to an intact cardiovascular system. For instance, in the case of the ATP-induced von Bezold-Jarisch reflex, the infarcted heart's stroke work was not compromised, even though it was augmented for the diseased group (see **Figure 4-19 - B**). Conversely, regarding total energy consumption, results presented a higher decrease in oxygen intake for the diseased group (see **Figure 4-19 - B**), in both measurements `M2` and `M3`, when compared to the control group.

Statistical differences between groups were estimated by independent t-test. A detailed analysis of these following plots was performed in **Chapter 5**.

4-8 Summary

This chapter presents the results obtained after processing and statistical analysis of rabbit physiological PV data during three different cardiovascular reflex responses, in both intact and pathological cardiovascular systems. Special attention was given to cardiovascular performance (PVA, Q_{load} and CWE) and ventriculo-arterial coupling (E_a, E_{es} and E_a/E_{es}), throughout the dynamic changes during autonomic reflexes and during acute myocardial infarction.

CHAPTER 5

Discussion

In this chapter, all results are discussed in an integrated manner, in order to identify and compare differences between normal and pathological conditions in rabbits. As a starting point, heart rate results during reflex activation are briefly discussed and compared to literature. Then, ventriculo-arterial coupling and cardiac performance are analyzed in detail for each cardiovascular reflex, evoked under normal conditions, in order to capture and further understand how heart's mechanical properties change during these short-term reflexes. This is followed by a thorough description and analysis of the major hemodynamic changes in a pathological cardiovascular system, according to the results presented in this study. It should be emphasized that these results were made 30 minutes after coronary occlusion. Finally, in order to capture how acute interventions might compromise the heart's response during reflex activation, cardiovascular coupling, performance and efficiency are addressed for each reflex, once more.

Changes in heart rate during cardiovascular reflexes - Groups `NOR` and `AMI`

The effect of cardiovascular reflexes on heart rate and arterial blood pressure has been extensively evaluated over the past years, given the advantages of experimental acquisition. Although these have been investigated before using this study's physiological data (Rocha et al., 2003a), the main goal of analyzing HR variations during reflex cardiovascular responses is to confirm previous observations and to validate the results are a whole, thus providing a starting for discussion. As expected, results are in line with literature: elevated BP by inflation of a balloon in the descending aorta was sensed by baroreceptor afferents, which induced the heart to slow down (Spyer, 1981), mostly justified by cardiac parasympathetic activation; lobeline activated chemoreceptors by mimicking an increase in arterial pressure of O_2, which resulted in bradycardia (Daly, 1997); and activation of cardiac chemosensitive receptors by injection of ATP provoked the von Bezold-Jarisch reflex, involving a decrease in HR (Dawes and Comroe, 1954; Verberne and Guyenet, 1992) by triggering parasympathetic activity and inhibiting sympathetic activity.

In the acute phase of MI, the present data confirm an enhancement of HR variations in chemical

evoked reflexes as compared to the changes measured prior to ligation, which is accordance with Rocha et al. (2003a) and Rosario et al. (2003). Moreover, there is a noticeable decrease in the baroreflex activity, which had likewise been described by other authors (Krüger et al., 1997; Schwartz et al., 1988). These results strongly suggest the cardiovascular system facilitates responses to chemosensitive-reflexes rather than mechanosensitive-reflexes, a pattern of response that has direct consequences in the continuous balance of sympathetic-parasympathetic outflow during the acute phase of MI.

Since cardiac output is mediated by heart rate and stroke volume (SV), it is hypothesized that evoked cardiovascular reflexes must influence how heart and arterial systems work together to optimize cardiovascular energy consumption and efficiency. Due to the rise of single-beat methods, it is now possible to assess left ventricular and arterial physiologic properties, including chamber contractility, performance and oxygen consumption. Therefore, in order to study and further characterize cardiovascular function, beat-by-beat LV end-systolic elastance (E_{es}), arterial elastance (E_a) and their coupling ratio (E_a/E_{es}) were computed as metrics to quantify ventriculo-arterial coupling. From these, LV stroke work (SW), total energy expenditure (PVA), ratio of the SW to its theoretical maximum (Q_{load}) and energetic efficiency (CWE) were estimated to evaluate cardiac performance and efficiency.

Cardiac baroreflex - Group `NOR`

In the intact cardiovascular system, the systemic pressure increase is sensed by the baroreceptors, mainly located in the transverse aortic and carotid arteries wall. This results in a stimulation of the baroreflex, with a significant increase in both left ventricle E_{es} and E_a, in a parallel manner such that the coupling between ventricular and arterial systems was maintained in the interval of optimal cardiac efficiency. A ratio spanning $0.3 - 1.3$ is considered optimal, according to a study on the dependency of ventricular work and cardiac efficiency on ventriculo-arterial coupling in dogs (De Tombe et al., 1993). Also, Kubota et al. (1992) evaluated the open loop transfer function from ventricular and arterial properties in canine hearts and reported compatible results. Visual inspection of **Figures C-1** and **C-2** shows that there is an increase in LV pressure (both P_{ed} and P_{es}) during baroreflex stimulation, while maintaining SV practically unchanged, despite a noticeable increase in end-systolic and end-diastolic LV volumes. A constant SV together with a decrease in HR resulted into a decrease of the cardiac output.

Moreover, an enhancement in myocardial contractility resulted in an increase of LV stroke work, obtained at a higher oxygen cost, without sacrificing Q_{load} and CWE. Since Q_{load}, an index of optimal afterload, remained close to unity during the reflex stimulation, this shows that the arterial system was able to extract maximal energy from the left ventricle (Burkhoff and Sagawa, 1986; Glower et al., 1985). Comparing Q_{load} and CWE indexes, it seems the energy transmission was more optimized than was oxygen consumption.

Results indicate that the cardiac baroreflex exerts a feedback modulation on the increased arterial pressure through a balanced augmentation of left ventricle contractility and arterial input impedance, with a subsequent improvement of the stroke work and decrease in cardiac flow to peripheral organs, obtained without compromising the energy efficiency of ventricular coupling with the arterial system.

Arterial chemoreflex - Group NOR

Similar to the cardiac baroreflex, injection of lobeline in the left-carotid sinus, under normal conditions, revealed a statistically significant increase in both E_{es} and E_a, without any noticeable change in their coupling ratio (E_a/E_a), which was maintained in the interval of optimal cardiac efficiency. One might conclude that simultaneous activation of cardiovascular mechanoreceptors could also be claimed to contribute to the chemoreflex response, which would explain the similarity between ventricular and arterial properties' responses. However, some characteristics of the response appear to negate a role for the mechanoreceptors' influence. First, results showed that activation of baroreceptors produces HR variations of lower magnitude than those observed with lobeline. Second, according to **Figures C-5** and **C-6**, pressure and volume did not change in a similar fashion in both reflexes. Although it was noticeable an increase in both end-systolic and end-diastolic volumes, it was higher for V_{es}, which resulted in a decrease in stroke volume. A decrease in cardiac output during the lobeline-induced carotid chemoreflex is related to a combined decrease in HR and SV. Regardless of some methodological differences, the present results are compatible with those reported by Franchini et al. (1997), who studied the chemoreflex activation by intravenous KCN[1] on unanesthetized rats and demonstrated a marked decrease in cardiac output, due to an decrease in stroke work, and increase in total peripheral resistance.

Regarding cardiovascular performance and energetics, results show a noticeable decrease in both SW and PVA, achieved without sacrifice of the mechanical and energetic efficiencies of the heart. Q_{load} remained close to unity throughout the lobeline-induced reflex, which indicates that the arterial system was able to extract maximal energy from the left ventricle. However, a decrease in SW also implicated a loss in energy transmitted to the arterial system, thus influencing total peripheral resistance. Comparing Q_{load} and CWE indexes, oxygen consumption was not optimized.

These results suggest that, for an intact cardiovascular system, the arterial chemoreflex controls an increase of arterial pressure of O_2 through an increase in both cardiac contractility and arterial input impedance, while decreasing cardiac output and heart's oxygen intake, in such a balance that ventriculo-arterial coupling, mechanical and energetic efficiency are maintained between optimal values. By evoking adjustments in the central drive for ventilation and cardiovascular function, the chemoreflex attempts to maintain chemical composition of blood at optimal levels, as well as adequate perfusion of vital organs (Mifflin, 1992).

von Bezold-Jarisch reflex - Group NOR

The activation of cardiac chemosensitive receptors by injection of ATP, under normal conditions, resulted in a significant decrease in both E_{es} and E_a, without any major change in the ventricular coupling with the arterial system, which again was maintained in the interval of optimal cardiac efficiency. **Figures C-9** and **C-10** show a noticeable decrease in end-systolic pressure (P_{es}) and volume (V_{es}), and simultaneous increase in stroke volume. Despite an increase in SV, the bradycardia was superior in magnitude, which resulted in a decreased cardiac output during the ATP-inducing von Bezold-Jarisch reflex.

Moreover, the increase in SV was not sufficient to counteract the decrease in arterial input impedance,

[1] KCN, or potassium cyanide, induces similar cardiovascular responses as lobeline.

which resulted in a significant fall of cardiac stroke work and total energy consumption, in such a balance that Q_{load} and CWE remained unchanged. Q_{load} remained close to unity. Although CWE was not optimized, results between activation of the reflex (measurement `M2`) and follow-up (measurement `M3`) were found statistically significant, which indicates that the cardiovascular system might have attempted to increase cardiac work efficiency during the ATP-induced von Bezold-Jarisch reflex.

Overall results provide more evidence to the assumption that the von Bezold-Jarisch reflex is a cardioprotective reflex (Somers and Abboud, 1995) that focus on defending the heart during severe hypovolemia and from chemical agents, by regulating cardiac contractility, SW and PVA in a way that reduces workload and oxygen demand, without sacrificing ventriculo-arterial coupling, Q_{load} and CWE.

Effect of acute myocardial infarction in heart's mechanical properties

Coronary ligation contributed to considerable changes in heart's mechanical properties. Results showed an impairment in myocardial contractility throughout all cardiovascular reflexes in analysis (for difference in mean between `NOR` and `AMI` groups, see **Figure 4-16 - A**), as a consequence of myocyte hyperthophy and alterations in LV architecture due to an oddly distributed wall tension (Jegger et al., 2007).

Arterial input impedance did not seem to be affected by the acute nature of the myocardial infarction (see **Figure 4-17 - A**), unlike reports of increased sympathetic tone in other study (Chantler and Lakatta, 2012). Since results reported E_a almost twice as large as E_{es}, there is evidence of an uncoupled cooperation between ventricle and arterial systems, with the E_a/E_{es} ratio spanning far from the optimal conditions (see **Figure 4-18 - A**). These results suggest that arterial tone is maintained within the physiological range at the expense of the deterioration of the energy transfer from the left ventricle to the arterial system (Asanoi et al., 1995). Some observations in clinical studies support these conclusions. Treatment of acute heart failure, a direct consequence of acute MI, is often to increase E_{es} by positive inotropic agents, whereas E_a is decreased using vasodilators. Positive inotropic agents with minimum chronotropic effects would improve myocardial contractility and, consequently, the optimality by decreasing the coupling ratio (Majure and Teerlink, 2011). In the case of pure vasodilators, the decrease in E_a would improve optimality, as well as reduce systemic vascular resistance, with direct improvements on cardiac output and reduction on oxygen consumption. In recent years, the therapeutic use of levosimendan, a novel calcium sensitizer, has been progressively emphasized because of its inotropic and vasodilator properties (Toller and Stranz, 2006). Levosimendan impacts both E_{es} and E_a, improving ventriculo-arterial coupling (Guarracino et al., 2007).

In order to maintain adequate perfusion of vital organs, the failing heart must generate sufficient blood pressure and flow to overcome the peripheral resistance. The infarted heart's response is to dilate its left ventricle, in order to maintain an adequate blood pressure and, thus, compensate for the depressed contractility. The pathological ventricular enlargement, as confirmed by the increased values in V_{ed} and V_{es} in the `AMI` group (see **Figures C-3**, **C-7** and **C-11**), seemed to be a consequence of compensation and not a limiting factor to depressed hemodynamics and energetics. Also, it is interesting to point out

that this heart's dilation was achieved without a significant change in SV, when compared to the control group, which clearly confirms SV as a poor indicator of heart failure or cardiac dysfunction (Maeder and Kaye, 2009).

Results also showed a depression in both Q_{load} and CWE values. Since the heart is no longer able to contract at its full potential due to myocardial necrosis, cardiac work increased as an effort to maintain the arterial tone within the physiological range. Interestingly, visual inspection of **Figure 4-19** suggests that impairment in myocardial contractility did not necessarily result in a deterioration of cardiac work performance between groups. A possible explanation for the improved left ventricle performance lies on increased wall tension. Increased end-systolic pressure could act on mechanical stretch-activated channels, creating a transmembrane pressure gradient that could be sufficient to increase calcium release (Morris, 1990).

Moreover, the overall augmentation of LV stroke work was obtained at a higher oxygen cost. Stahl et al. (1988) also found a significant increase in mean oxygen consumption in dog hearts with impairment of contractile function. Unbalanced increase in SW and PVA indexes resulted in an overall decrease in cardiac work efficiency (see **Figure 4-21**), as it would be expected from a failing heart.

Cardiac baroreflex - Group `AMI`

Upon the unloading of the baroreceptors in an ischemic heart, the baroreflex continues to participate in the regulation of the cardiac contractility indexes. Reflex activation show an increase in both impaired E_{es} and unaltered E_a, without any significant change in their mismatched coupling ratio. It is noticeable an attenuation of myocardial contractility's increase in the baroreflex (see **Figure 4-16 - B**), whereas arterial input impedance remained similar to under normal conditions (see **Figure 4-17 - B**). According to **Figure 4-18 - B**, although differences in E_a/E_{es} mean between `M2` and `M1` were similar between control and disease groups, it was higher between `M3` and `M1`, which might suggest an increase in deterioration of ventriculo-arterial coupling as the baroreflex is stimulated.

Stroke volume remained unchanged throughout the reflex (see **Figure C-3**), despite enlargement of the left ventricle. Cardiac stroke work and total energy consumption, which were already enhanced as a result of heart's dilation to maintain an adequate blood pressure, continued to increase during reflex stimulation, at a constant Q_{load} and CWE. Visual inspection of **Figure 4-19 - B** shows that acute MI did not seem to compromise how SW is affected by the reflex. Surprisingly, there seems to be a statistically significant improvement of SW for the infarcted heart, when comparing mean differences in `M3` relatively to `M1` between groups. Regarding total energy expenditure, mean differences between measurements were found statistically significant between groups (see **Figure 4-20 - B**), suggesting an abnormal oxygen intake by the ischemic heart. Moreover, both optimality indexes behaved differently. Moreover, visual inspection of **Figure 4-21** suggests there is an attenuation of CWE change in ischemic hearts.

Overall, these observations allow to conclude that, after acute MI, the cardiac baroreflex continues to exert the same feedback modulation on the increased arterial pressure as in normal conditions, represented by an augmentation of cardiac contractility and arterial input impedance, improvement of stroke work and increased oxygen consumption. However, since the cardiovascular system is impaired due

to muscle death, ventriculo-arterial coupling, ratio of the SW to its theoretical maximum and energetic efficiency are compromised.

Arterial chemoreflex - Group `AMI`

Application of the lobeline-induced arterial chemoreflex in ischemic hearts elicited similar changes in the mechanical properties of the heart as under normal conditions. Similarly to the cardiac baroreflex, both impaired E_{es} and unaltered E_a increased, in such a balance the uncoupling between ventricular and arterial systems did not change. According to **Figure 4-16 - B**, myocardial contractility evolved differently in both groups. Differences in E_{es} mean revealed an initial attenuation for the infarcted heart, which was surpassed in `M3`. In the case of E_a, **Figure 4-17 - B** show an increase in the differences as the chemoreflex was evoked. Visual inspection of **Figure 4-18 - B** confirms an enhancement of the uncoupling over the measurements `M2-3`.

Paradoxically to the heart's dilation to generate sufficient blood flow to overcome the peripheral resistance, stroke volume decreased after lobeline injection (see **Figure C-3**), due to an increase in the afterload volume (V_{es}). Moreover, results show a fall in both myocardial stroke work and oxygen demand, achieved without sacrificing even more Q_{load} and cardiac work efficiency. Visual inspection of **Figure 4-19 - B** and **Figure 4-20 - B** provides evidence that an infarcted heart's response might be compromised in the long-run, when it comes to cardiovascular performance and energetics. Interestingly, both optimality indexes behaved differently. On one hand, differences in CWE means between groups were not found statistically significant (see **Figure 4-21**), which suggests that, even though the cardiac efficiency was lower for the `AMI` group, the chemoreflex affects CWE similarly in both experimental cases. On the other hand, reflex outcomes for Q_{load} were enhanced after acute MI (see **Figure 4-22**). This might suggest the infarcted heart chose to optimize energy transmission to the arterial system over cardiac efficiency (oxygen consumption).

These results suggest that, after acute MI, the lobeline-induced arterial chemoreflex continues to control an increase of arterial pressure of O_2 through an increase in both cardiac contractility and arterial input impedance, while decreasing cardiac performance and heart's oxygen intake. However, this is achieved under an impaired cardiovascular system, with compromised cardiac efficiency and an uncoupled cooperation between ventricle and arterial systems.

von Bezold-Jarisch reflex - Group `AMI`

Injection of ATP after acute MI resulted in a significant decrease in both impaired myocardial contractility and unaffected arterial input impedance. Differences in E_{es} means between groups suggest acute MI compromised how myocardial contractility is affected by the cardiopulmonary reflex, but the same could not be concluded for E_a. Activation of the reflex resulted in an attenuation of the contractility's decrease (see **Figure 4-16 - B**), while arterial input impedance evolved similarly in both groups (see **Figure 4-17 - B**). As before, there was no significant change in ventriculo-arterial coupling, which was already compromised due to heart ischemia.

Visual inspection of **Figure C-11** confirms an increase in stroke volume of an already enlarged left ventricle, at the expense of a decrease in end-systolic volume. Cardiac stroke work and total energy

consumption were reduced, in such a balance that the optimality indexes, though already compromised, remained unchanged throughout the reflex. Visual inspection of **Figure 4-19 - B** provides evidence that the infarcted heart's response was not compromised in cardiovascular workload, even though cardiac stroke work is higher for the diseased group. Regarding the heart's energy expenditure, **Figure 4-20 - B** clearly presents a higher decrease in oxygen intake for the `AMI` group, in both measurements `M2` and `M3`. Moreover, differences in Q_{load} means were not found statistical significant (see **Figure 4-22**), which suggests that, even though the ratio of SW to its theoretical maximum was lower for the diseased group, the von Bezold-Jarisch reflex affects Q_{load} similarly in both experimental cases. Regarding CWE, visual inspection of **Figure 4-21 - B** suggests reflex outcomes were improved after acute MI, which provides evidence that energetic efficiency was more optimized than energy transmission between left ventricle and arterial system.

Overall, results indicate that, in ischemic hearts, activation of ATP-induced von Bezold-Jarisch reflex regulates cardiac contractility, stroke work and oxygen consumption in such a way that reduces workload and energetic demand. This is a cardioprotective reflex, strongly amplified by products of acute myocardial ischemia, that chooses to optimize cardiac energetic efficiency, rather than energy transmission to the arterial system.

CHAPTER 6

Conclusions and Future Prospects

In the first section of this chapter it is acknowledged that the methodology used has a number of potential limitations. Afterwards, rabbit and human cardiac electrical and mechanical functions are compared, to help understand to what extent the results can be inferred to larger mammals. The third and last section summarizes the main conclusions that can be drawn from this thesis and presents possible future research developments to make this approach more applicable in a clinical environment.

6-1 Methodological considerations

It is to be acknowledged that this study has a number of potential limitations.

Potential changes in the mechanical properties of the rabbit's heart, which may vary with age and between genders, were not accounted for. A recent study concluded that E_{es} solely do not provide consistent information regarding myocardial contractile states between men and women of various ages, as normalization is required to cancel out the effect of geometry (Claessens et al., 2007). Redfield et al. (2005) also noticed an increased vascular and ventricular stiffness in female gender and advancing age, even in the absence of cardiovascular disease.

Although body mass is considered determinant of cardiovascular structure and function (Dewey et al., 2008), normalization of the cardiovascular properties in function the body mass (or LV mass) was not performed. In fact, there is no consensus as to the best strategy for normalizing E_{es} or E_a. Dividing either one by the LV mass does not necessarily provide adequate adjustment, because they might not be linearly related. Instead, a preferred approach might be the allometric scaling method (Batterham et al., 1999; Dewey et al., 2008; Nevill and Holder, 1995), in which the elastance is divided by the LV mass raised to a scalar exponent, though it needs further validation.

The experiments were done in open-chest rabbits (Rocha et al., 2003a). Even though this approach is the most frequently used to date, it has some theoretical disadvantages compared to a closed-chest approach. In the closed chest, the lungs remain untouched and the cardiac position remains intact. Lips et al. (2004) published significant differences in SV, V_{es} and V_{ed} and P_{es} between the two approaches,

in mice. However, since the pressure and volume curves were scaled to physiological values, it can be assumed these findings can be extrapolated to the closed-chest approach.

In several rabbits, the PV loops displayed volume changes during the cardiac phases which would be expected to be isovolumic. This may indicate valvular insufficiencies, which is highly unlikely, or could simply be artifacts of the conductance catheter. Despite this, the conductance catheter is considered the gold standard for a reliable measurement of instantaneous LV volume *in vivo* (Burkhoff et al., 2005).

E_{es} values were obtained using Ten Brinke et al.'s single-beat method. Although the method has been validated (Chen et al., 2001) and has recently been applied in a population study on ventricular-arterial coupling (Redfield et al., 2005), it remains an estimate of E_{es} with potential limitations. In a validation study, Kjørstad et al. (2002) discussed that single-beat measurements are insufficient in predicting contractility in a large range of load and frequency situations.

Still in the single-beat method, assessment of isovolumic pressure and P_{MAX} in PV analysis is sensitive to errors and requires high quality LV pressure curves. Although both volume and pressure curves were re-sampled to ensure that the systoles were estimated with minimal error possible, in fact this is an approximation and might not represent the real physiological data. Additionally, the choice of the fitted curve, though it offers a more accurate approximation in case of an asymmetrical LV pressure curve than a cosine wave (Ten Brinke et al., 2010), may also be a limitation. Nevertheless, this does not affect the general idea presented in this study.

Finally, it is unknown whether a linear model of E_{es} with a fixed V_0 is accurate enough for simulations of the relation between pressure and volume of the LV (Burkhoff et al., 2005). Lankhaar et al. (2009) has compared various models in sheep and concluded the best fitting model is the time-varying elastance model, using Akaike information criterion (AIC) and Hamming distance. This model, previously explained in a theoretical study by Drzewiecki et al. (1989), is identical to the classical Suga et al. model except for the intercept V_0, which is allowed to vary with time.

6-2 Inferences towards humans

A critical question the reader may ask is to what extent the results in this study, performed in rabbit LV, can be inferred to larger mammals, such as humans. Historically, dog and pig open-chest preparations were considered the best experimental models for study of cardiac electrophysiology, because of the size similarity of these animal's heart compared with human heart. Larger animals possess HR, cardiac ion channel expressions and ECG morphologies closer to those of humans (Kaese et al., 2013). However, there are some considerable differences, such as inconsistent size of the aortic valve cusps and a higher ratio of wall thicknesses in the myocardial septum, which reduces the clinical relevance of these animals when studying ventricular contractility (Lelovas et al., 2014).

Several new animal models have been introduced, such as rabbit, rat and mouse, due to a higher affordability and availability (Kaese et al., 2013). Although the rabbit weight differ by more than an order of magnitude from a human, several studies in cardiac electrical and mechanical activity have found great similarities between both species. As far as macroscopic electrophysiology is concerned,

Panfilov (2006) found that the effective sizes of rabbit and human hearts, a proposed ratio of heart size to excitation wavelength, were very similar. In fact, the pig and dog hearts would appear to have larger effective sizes than the human heart, probably due to differences in the heart's anatomy and fibrous structure. Furthermore, the rabbit's coronary architecture (Burton et al., 2012) and response to pharmacological interventions or ischaemia (Harken et al., 1981) closely resemble those of human, rather than small rodents. Cardiac cell electrophysiology showed pronounced similarities in the two species, in terms of intracellular ion concentrations and currents determining cardiac action potential properties (Bers, 2002; Hondeghem, 2016; Nerbonne, 2000). Furthermore, regional contractile and diastolic behavior of rabbit hearts is very similar in humans (Jung, 2012), and both species appear to have similar cardiac mechano-electrical coupling mechanisms (Quinn and Kohl, 2016).

All these findings position the rabbit as an optimal model to study basic mechanisms behind ventricular contraction and relaxation and pathophysiology of disease processes, allowing for direct comparisons to be made against humans.

6-3 Conclusions

This thesis aimed at studying left ventricle mechanical properties of the heart during reflex cardiovascular responses, evoked by stimulation of baroreceptors, carotid chemoreceptors and cardiopulmonary fibers, under normal conditions and after acute myocardial infarction (MI), in order to better understand the autonomic balance of the cardiac system in the point of view of cardiovascular efficiency and ventriculo-arterial coupling.

The main accomplishments of this research include an extensive computational software to provide a powerful, accessible framework for researchers and enthusiasts to manage physiological pressure-volume (PV) data and accurately compute a wide variety of indexes that can characterize and quantify chamber contractility and performance. This framework takes full advantage of single-beat method to estimate beat-by-beat cardiovascular indexes, offering new and complementary perspectives for understanding how both heart and arterial systems interact with each other to optimize cardiovascular efficiency and performance, during both systole and diastole. The main value of the software is, undoubtedly, the ability to aggregate PV data in a clear and physiologically relevant picture, and to capture instantaneous and dynamic hemodynamic changes while acute cardiovascular perturbations, including short term reflexes (mechano- and chemoreflexes, see **Figure 3-18**) and diseases (myocadial infarction), are evoked. The engineering robustness of the developed methods significantly increases the software's potential clinical applicability, for instance in drug testing and device therapy.

The close-loop network of cardiovascular reflexes in study revealed a balanced control of induced homeostatic perturbations by modeling both cardiac contractility and arterial input impedance, with consequent changes in stroke work and cardiac output, in such a way that ventriculo-arterial coupling, mechanical ratio and cardiac energetic efficiency were maintained between optimal values. While the cardiac baroreflex enhanced the heart's contractility and the arterial impedance to improve the stroke work, the arterial chemoreflex focused on reducing the heart's oxygen intake, while attempting to main-

tain an adequate perfusion of vital organs. The cardiopulmonary reflex provoked a reduction in both cardiac workload and oxygen demand, as a way to protect the heart from injected ATP. Each reflex optimized the cardiac work and energetic efficiencies dissimilarly. For all reflexes, it was noticeable a reduction of the cardiac output to peripheral organs.

Acute myocardial infarction contributed to considerable changes in heart's mechanical properties. First, cardiac contractility was significantly reduced, due to the death of oxygen-deprived cells from the myocardium. Second, arterial input impedance was not altered by the acute myocardial infarction. This provides evidence that the arterial tone was maintained within the physiological range at the expense of the deterioration of the energy flow between left ventricle and arterial system. As a result of this mismatch, ventriculo-arterial coupling became compromised.

Additionally, as a consequence of left ventricular enlargement to compensate for the depressed contractility, there was an significant increase in end-diastolic and end-systolic volumes. Stroke volume did not change between normal and pathological hearts. Since the heart is no longer able to contract at its full potential due to myocardial necrosis, its work was enhanced as an effort to maintain the arterial tone within the optimal physiological range. Interestingly, results revealed no evidence in deterioration of cardiac work performance between groups. Also, the overall improvement in left ventricle stroke work was obtained at a higher oxygen cost. An unbalanced increase in workload and oxygen consumption resulted in a general depression of cardiac work efficiency and ratio of stroke work to its theoretical maximum.

Activation of cardiovascular reflexes in ischemic hearts revealed similar hemodynamic responses as in the control group, despite an evident impairment of the ventriculo-arterial coupling, as well as of cardiac work and energetic efficiencies. For all reflexes, induced homeostatic perturbations were controlled through modeling both cardiac contractility and arterial input impedance, which in turn affected stroke work and cardiac output. Similarly to normal conditions, the cardiac baroreflex focused in improving the left ventricle stroke work, whereas the lobeline-induced arterial chemoreflex targeted a reduction in the heart's abnormal oxygen intake. The von Bezold-Jarisch reflex reduced heart's workload and energetic demand by choosing to optimize cardiac energetic efficiency, rather than energy transmission to the arterial system.

The proposed methodology disclosed statistically significant results regarding several ventricular and arterial properties that quantitatively predict the impact of various cardiovascular reflexes on dynamic circulatory equilibrium and arterial pressure. To my knowledge, this is the first report of an integrated software capable of quantitatively reproducing baroreflex, chemoreflex and cardiopulmonary-induced dynamic changes in cardiovascular equilibrium, and during acute cardiovascular perturbations.

6-4 Future prospects

The findings of this thesis can be used as a starting point for further research topics. Several suggestions for improving the techniques and methodologies applied in this research are also outlined.

Eliminating random contributions or unwanted features of signals are at the core of signal processing.

The software developed for this study provided two ways of filtering pressure-volume data, but there is room for improvement. The inclusion of adaptive filtering, which involves varying the filter parameters over time to adapt to dynamic signal characteristics, should be targeted as a way to effectively enhance the signal quality (Manolakis et al., 2005).

It would also be beneficial to cross-check the results from this study with those using a time-varying elastance model. Though accepted by the scientific community, the classical elastance model proposed by Suga et al. (1973) has limitations and might not be accurate enough for simulations of the ESPVR. Several studies have shown this relation is nonlinear and that the volume intercept varies substantially Claessens et al. (2006); Kass et al. (1989); Van der Velde et al. (1991). Alternative models have been presented that more accurately reflect the cardiac behavior of pressure and volume variations. Lankhaar et al. (2009) compared various models in sheep and concluded the ESPVR best fitting model is the time-varying elastance formulation, in which the volume intercept V_0 is allowed to vary with time.

With a powerful computational framework that is able to automatically estimate left-ventricle elastance for a set of cardiac cycles using the single-beat method, other cardiovascular properties should be explored. The relationship of $\mathrm{d}P/\mathrm{d}t_{max}$ to V_{ed} is linear and its slope provides a preload-independent contractility index (Little, 1985). It would be interesting to analyze the behavior of $\mathrm{d}P/\mathrm{d}t_{max}$-$V_{ed}$ relation between normal conditions and after MI, as well as during the three reflex stimulations in this study.

Additionally, the isovolumic relaxation of the heart during cardiovascular reflex responses, before and after acute MI, should also be examined. Assessment of LV diastolic function is essential in basic and clinical cardiac studies, because its impairment may cause congestive heart failure in certain heart diseases (Grossman, 1991; Hirota, 1980). A widely used parameter for the relaxation quantification is τ, because it is independent of preload and peak aortic pressure (Varma et al., 1989). However, τ is afterload dependent, so it would be necessary to evaluate this constant over a range of afterloads and plot against V_{ed} (Zile and Brutsaert, 2002).

Recent literature show that activation of cardiovascular carotid chemo and cardiac chemosensitive receptors after MI was partially reversed by losartan microinjection at the level of the NTS, suggesting that its angiotensin receptors are involved in the control of the autonomic outflow of cardiovascular reflexes (Rocha et al., 2003b; Rosario et al., 2003). However, these studies focused on the variations of blood pressure, heart rate and phrenic nerve activity. Given the advantages of the framework developed for this thesis, it is now possible to characterize cardiovascular performance and ventriculo-arterial coupling after losartan injection, during normal conditions and after coronary ligation. This analysis will certainly allow to better understand autonomic modulation of cardiovascular reflexes.

Finally, time-frequency analysis of the left ventricle elastance should be pursued. Since the pioneering work of Sunagawa et al. (1983), the analysis between the left ventricle and the arterial system has focused on time domain, even though originally the arterial load was characterized in the frequency domain (Milnor, 1975; O'Rourke, 1967). Over recent years, with the computational power in our advantage, signal analysis has gradually shifted towards time-frequency distributions, which represent the energy or power of waveform signals in two-dimensional functions of both time and frequency to better reveal subtle variations and patterns in signal morphology (Cohen, 1995). Nowadays, wavelet analysis has been

found particularly useful in the study of biological signals, such as ECG, superseding traditional Fourier methods (Addison, 2005). It is envisaged that the future will see application of the Wavelet Transform to pressure-volume data, as it might present a new tool for a deep understanding of ventricular-arterial coupling.

References

[**1**]: **Abe, S., Ohtomo, J., Yamaguchi, I., Tsuchida, E., Fujinuma, T., Sunagawa, K. and Tomoike, H.** (1995), 'Continuous measurement of left ventricular volume in rabbit, using a two-electrode catheter', *Heart and vessels* **10**(3), 138–145.

[**2**]: **Addison, P. S.** (2005), 'Wavelet transforms and the ecg: a review', *Physiological measurement* **26**(5), R155.

[**3**]: **Akselrod, S., Gordon, D., Madwed, J. B., Snidman, N., Shannon, D. and Cohen, R.** (1985), 'Hemodynamic regulation: investigation by spectral analysis', *American Journal of Physiology-Heart and Circulatory Physiology* **249**(4), H867–H875.

[**4**]: **Anderson, J., Goldman, L. and Ausiello, D.** (2011), 'St segment elevation acute myocardial infarction and complications of myocardial infarction', *Cecil Medicine. Philadelphia, Pa: Saunders Elsevier* .

[**5**]: **Asanoi, H., Kameyama, T. and Ishizaka, S.** (1995), Ventriculo-arterial load matching of failing hearts, *in* 'Cardiac Energetics: From Emax to Pressure-Volume Area', Springer, pp. 157–169.

[**6**]: **Asanoi, H., Sasayama, S. and Kameyama, T.** (1989), 'Ventriculo-arterial coupling in normal and failing heart in humans.', *Circulation Research* **65**(2), 483–493.

[**7**]: **Aviado, D. M. and Aviado, D. G.** (2001), 'The bezold-jarisch reflex', *Annals of the New York Academy of Sciences* **940**(1), 48–58.

[**8**]: **Baan, J., Jong, T. T. A., Kerkhof, P. L., Moene, R. J., D Van Dijk, A., T Van der Velde, E. and Koops, J.** (1981), 'Continuous stroke volume and cardiac output from intra-ventricular dimensions obtained with impedance catheter', *Cardiovascular Research* **15**(6), 328–334.

[**9**]: **Batterham, A., George, K., Whyte, G., Sharma, S. and McKenna, W.** (1999), 'Scaling cardiac structural data by body dimensions: a review of theory, practice, and problems', *International journal of sports medicine* **20**(08), 495–502.

[**10**]: **Benarroch, E. E.** (2008), 'The arterial baroreflex functional organization and involvement in neurologic disease', *Neurology* **71**(21), 1733–1738.

[**11**]: **Berne, R. M., Koeppen, B. M. and Stanton, B. A.** (2008), *Berne & Levy Physiology*, Elsevier Brasil.

[**12**]: **Bers, D. M.** (2002), 'Cardiac na/ca exchange function in rabbit, mouse and man: what's the difference?', *Journal of molecular and cellular cardiology* **34**(4), 369–373.

[**13**]: **Bland, J. M. and Altman, D.** (1986), 'Statistical methods for assessing agreement between two methods of clinical measurement', *The lancet* **327**(8476), 307–310.

[**14**]: **Borlaug, B. A. and Kass, D. A.** (2011), 'Ventricular–vascular interaction in heart failure', *Cardiology clinics* **29**(3), 447–459.

[**15**]: **Borow, K. M., Neumann, A. and Wynne, J.** (1982), 'Sensitivity of end-systolic pressure-dimension and pressure-volume relations to the inotropic state in humans.', *Circulation* **65**(5), 988–997.

[**16**]: **Boulpaep, E. L., Boron, W. F., Caplan, M. J., Cantley, L., Igarashi, P., Aronson, P. S. and Moczydlowski, E. G.** (2009), 'Medical physiology: a cellular and molecular approach', *Signal Transduction* **48**, 27.

[**17**]: **Bowes, G., Townsend, E. R., Kozar, L. F., Bromley, S. M. and Phillipson, E. A.** (1981), 'Effect of carotid body denervation on arousal response to hypoxia in sleeping dogs', *Journal of Applied Physiology* **51**(1), 40–45.

[**18**]: **Brown, H. and Prescott, R.** (2014), *Applied mixed models in medicine*, John Wiley & Sons.

[**19**]: **Burkhoff, D., Mirsky, I. and Suga, H.** (2005), 'Assessment of systolic and diastolic ventricular properties via pressure-volume analysis: a guide for clinical, translational, and basic researchers', *American Journal of Physiology-Heart and Circulatory Physiology* **289**(2), H501–H512.

[**20**]: **Burkhoff, D. and Sagawa, K.** (1986), 'Ventricular efficiency predicted by an analytical model', *American Journal of Physiology-Regulatory, Integrative and Comparative Physiology* **250**(6), R1021–R1027.

[**21**]: **Burton, R. A., Schneider, J. E., Bishop, M. J., Hales, P. W., Bollensdorff, C., Robson, M. D., Wong, K. C., Morris, J., Quinn, T. A. and Kohl, P.** (2012), 'Microscopic magnetic resonance imaging reveals high prevalence of third coronary artery in human and rabbit heart', *Europace* **14**(suppl 5), v73–v81.

[**22**]: **Calvelo, M. G., Abboud, F. M., Bollard, D. R. and Abdel-Sayed, W.** (1970), 'Reflex vascular responses to stimulation of chemoreceptors with nicotine and cyanide activation of adrenergic constriction in muscle and noncholinergic dilatation in dog's paw', *Circulation research* **27**(2), 259–276.

[**23**]: **Carvalho, A. et al.** (2014), *Estatísticas da Saúde 2014.*, Instituto Nacional de Estatística, I.P. - Statistics Portugal.

[**24**]: **Cavalcanti, S. and Belardinelli, E.** (1996), 'Modeling of cardiovascular variability using a differential delay equation', *Biomedical Engineering, IEEE Transactions on* **43**(10), 982–989.

[**25**]: **Chantler, P. D. and Lakatta, E.** (2012), 'Arterial–ventricular coupling with aging and disease', *Frontiers in physiology* **3**, 90.

[**26**]: **Chantler, P. D., Lakatta, E. G. and Najjar, S. S.** (2008), 'Arterial-ventricular coupling: mechanistic insights into cardiovascular performance at rest and during exercise', *Journal of applied physiology* **105**(4), 1342–1351.

[**27**]: **Chen, C.-H., Fetics, B., Nevo, E., Rochitte, C. E., Chiou, K.-R., Ding, P.-A., Kawaguchi, M. and Kass, D. A.** (2001), 'Noninvasive single-beat determination of left ventricular end-systolic elastance in humans', *Journal of the American College of Cardiology* **38**(7), 2028–2034.

[**28**]: **Cheney, E. W. and Kincaid, D. R.** (2012), *Numerical mathematics and computing*, Nelson Education.

[**29**]: **Claessens, T. E., Georgakopoulos, D., Afanasyeva, M., Vermeersch, S. J., Millar, H. D., Stergiopulos, N., Westerhof, N., Verdonck, P. R. and Segers, P.** (2006), 'Nonlinear isochrones in murine left ventricular pressure-volume loops: how well does the time-varying elastance concept hold?', *American Journal of Physiology-Heart and Circulatory Physiology* **290**(4), H1474–H1483.

[**30**]: **Claessens, T. E., Rietzschel, E. R., De Buyzere, M. L., De Bacquer, D., De Backer, G., Gillebert, T. C., Verdonck, P. and Segers, P.** (2007), 'Noninvasive assessment of left ventricular and myocardial contractility in middle-aged men and women: disparate evolution above the age of 50?', *American Journal of Physiology-Heart and Circulatory Physiology* **292**(2), H856–H865.

[**31**]: **Cohen, L.** (1995), *Time-frequency analysis*, Vol. 778, Prentice hall.

[**32**]: **Cohen-Solal, A., Caviezel, B., Himbert, D. and Gourgon, R.** (1994), 'Left ventricular-arterial coupling in systemic hypertension: analysis by means of arterial effective and left ventricular elastances.', *Journal of hypertension* **12**(5), 591–600.

[**33**]: **Cohn, P. F., Liedtke, A. J., Serur, J., Sonnenblick, E. H. and Urschel, C. W.** (1972), 'Maximal rate of pressure fall (peak negative dp/dt) during ventricular relaxation', *Cardiovascular research* **6**(3), 263–267.

[**34**]: **Coleridge, H. M. and Coleridge, J. C. G.** (1980), 'Cardiovascular afferents involved in regulation of peripheral vessels', *Annual Review of Physiology* **42**(1), 413–427.

[**35**]: **Cooper, L. L., Odening, K. E., Hwang, M.-S., Chaves, L., Schofield, L., Taylor, C. A., Gemignani, A. S., Mitchell, G. F., Forder, J. R., Choi, B.-R. et al.** (2012), 'Electromechanical and structural alterations in the aging rabbit heart and aorta', *American Journal of Physiology-Heart and Circulatory Physiology* **302**(8), H1625–H1635.

[**36**]: **Curtis, J. P., Sokol, S. I., Wang, Y., Rathore, S. S., Ko, D. T., Jadbabaie, F., Portnay, E. L., Marshalko, S. J., Radford, M. J. and Krumholz, H. M.** (2003), 'The association of left ventricular ejection fraction, mortality, and cause of death in stable outpatients with heart failure', *Journal of the American College of Cardiology* **42**(4), 736–742.

[**37**]: **Daly, M. d. B.** (1997), Reflex effects on the cardiovascular system: role of changes in respiration, *in* 'Peripheral Arterial Chemoreceptors and Respiratory–Cardiovascular Integration', Clarendon Press, Oxford, pp. 161–181.

[**38**]: **Dampney, R., Horiuchi, J., Tagawa, T., Fontes, M., Potts, P. and Polson, J.** (2003), 'Medullary and supramedullary mechanisms regulating sympathetic vasomotor tone', *Acta physiologica Scandinavica* **177**(3), 209–218.

[**39**]: **Dawes, G. S. and Comroe, J. H.** (1954), 'Chemoreflexes from the heart and lungs', *Physiological reviews* **34**(2), 167–201.

[**40**]: **De Tombe, P. P., Jones, S., Burkhoff, D., Hunter, W. C. and Kass, D. A.** (1993), 'Ventricular stroke work and efficiency both remain nearly optimal despite altered vascular loading', *American Journal of Physiology-Heart and Circulatory Physiology* **264**(6), H1817–H1824.

[**41**]: **Dewey, F. E., Rosenthal, D., Murphy, D. J., Froelicher, V. F. and Ashley, E. A.** (2008), 'Does size matter? clinical applications of scaling cardiac size and function for body size', *Circulation* **117**(17), 2279–2287.

[**42**]: **Diggle, P.** (2002), *Analysis of longitudinal data*, Oxford University Press.

[**43**]: **Dodd, J. and Role, L. W.** (1991), 'The autonomic nervous system', *Principles of neural science* **3**, 761–775.

[**44**]: **Drzewiecki, G., Karam, E. and Welkowitz, W.** (1989), 'Physiological basis for mechanical time-variance in the heart: special consideration of non-linear function', *Journal of theoretical biology* **139**(4), 465–486.

[**45**]: **Dworkin, B. R., Dworkin, S. and Tang, X.** (2000), 'Carotid and aortic baroreflexes of the rat: I. open-loop steady-state properties and blood pressure variability', *American Journal of Physiology-Regulatory, Integrative and Comparative Physiology* **279**(5), R1910–R1921.

[**46**]: **Fitzgerald, R. S. and Lahiri, S.** (1986), 'Reflex responses to chemoreceptor stimulation', *Handbook of Physiology: The Respiratory System Control of Breathing* **2**, 313–362.

[**47**]: **Fitzmaurice, G. M. and Ravichandran, C.** (2008), 'A primer in longitudinal data analysis', *Circulation* **118**(19), 2005–2010.

[48]: **Franchini, K. G., Oliveira, V. L. and Krieger, E. M.** (1997), 'Hemodynamics of chemoreflex activation in unanesthetized rats', *Hypertension* **30**(3), 699–703.

[49]: **Frank, O.** (1895), *Zur Dynamik des Herzmuskels*, Druck v. R. Oldenbourg.

[50]: **Frank, O.** (1899), 'Die grundform des arteriellen pulses', *Z Biol* **37**(483-526), 459.

[51]: **Gaddam, K. K. and Oparil, S.** (2009), 'Diastolic dysfunction and heart failure with preserved ejection fraction: rationale for raas antagonist/ccb combination therapy', *Journal of the American Society of Hypertension* **3**(1), 52–68.

[52]: **Gelfand, R. and Lambertsen, C.** (1973), 'Dynamic respiratory response to abrupt change of inspired co2 at normal and high po2.', *Journal of Applied Physiology* **35**(6), 903–913.

[53]: **Georgakopoulos, D., Mitzner, W. A., Chen, C.-H., Byrne, B. J., Millar, H. D., Hare, J. M. and Kass, D. A.** (1998), 'In vivo murine left ventricular pressure-volume relations by miniaturized conductance micromanometry', *American Journal of Physiology-Heart and Circulatory Physiology* **274**(4), H1416–H1422.

[54]: **Glower, D. D., Spratt, J. A., Snow, N. D., Kabas, J., Davis, J., Olsen, C., Tyson, G., Sabiston, D. and Rankin, J.** (1985), 'Linearity of the frank-starling relationship in the intact heart: the concept of preload recruitable stroke work.', *Circulation* **71**(5), 994–1009.

[55]: **Gould, B.** (1855), 'On peirce's criterion for the rejection of doubtful observations, with tables for facilitating its application', *The Astronomical Journal* **4**, 81–87.

[56]: **Grossman, W.** (1991), 'Diastolic dysfunction in congestive heart failure', *New England Journal of Medicine* **325**(22), 1557–1564.

[57]: **Grossman, W., Haynes, F., Paraskos, J. A., Saltz, S., Dalen, J. E. and Dexter, L.** (1972), 'Alterations in preload and myocardial mechanics in the dog and in man', *Circulation research* **31**(1), 83–94.

[58]: **Guarracino, F., Baldassarri, R. and Pinsky, M. R.** (2013), 'Ventriculo-arterial decoupling in acutely altered hemodynamic states', *Crit Care* **17**(2), 213.

[59]: **Guarracino, F., Cariello, C., Danella, A., Doroni, L., Lapolla, F., Stefani, M., Baldassarri, R. and Vullo, C.** (2007), 'Effect of levosimendan on ventriculo-arterial coupling in patients with ischemic cardiomyopathy', *Acta anaesthesiologica Scandinavica* **51**(9), 1217–1224.

[60]: **Gueorguieva, R. and Krystal, J. H.** (2004), 'Move over anova: Progress in analyzing repeated-measures data andits reflection in papers published in the archives of general psychiatry', *Archives of general psychiatry* **61**(3), 310–317.

[61]: **Gupta, K. B., Bavaria, J., Ratcliffe, M., Edmunds, L. and Bogen, D.** (1989), 'Measurement of end-systolic pressure-volume relations by intra-aortic balloon occlusion.', *Circulation* **80**(4), 1016–1028.

[62]: **Hall, J. E.** (2015), *Guyton and Hall textbook of medical physiology*, Elsevier Health Sciences.

[63]: **Hansson, G.** (2009), 'Inflammatory mechanisms in atherosclerosis', *Journal of Thrombosis and Haemostasis* **7**(s1), 328–331.

[64]: **Hansson, G. K.** (2005), 'Inflammation, atherosclerosis, and coronary artery disease', *New England Journal of Medicine* **352**(16), 1685–1695.

[65]: **Harken, A., Simson, M., Haselgrove, J., Wetstein, L., Harden III, W. and Barlow, C.** (1981), 'Display of oxygen diffusion zone (borderzone) in the rabbit, dog, pig, and monkey', *Am J Physiol* **241**, 202–210.

[66]: **Hayashi, K., Shigemi, K., Shishido, T., Sugimachi, M. and Sunagawa, K.** (2000), 'Single-beat estimation of ventricular end-systolic elastance–effective arterial elastance as an index of ventricular mechanoenergetic performance', *The Journal of the American Society of Anesthesiologists* **92**(6), 1769–1776.

[67]: **Hayes, A. F.** (2009), *Statistical methods for communication science*, Routledge.

[68]: **Heymans, C.** (1958), 'Baroceptor and chemoceptor reflexes in monkeys', *Circ Res* **6**(5), 567–569.

[69]: **Hild, R. and Sick, L.** (1955), 'Das druck-volumen-diagramm des isolierten spontan schlagenden katzenherzens', *Z. Biol* **107**, 51.

[70]: **Hirota, Y.** (1980), 'A clinical study of left ventricular relaxation.', *Circulation* **62**(4), 756–763.

[71]: **Hofmanis, J., Caspary, O., Louis-Dorr, V., Ranta, R. and Maillard, L.** (2013), 'Denoising depth eeg signals during dbs using filtering and subspace decomposition', *Biomedical Engineering, IEEE Transactions on* **60**(10), 2686–2695.

[72]: **Hokanson, J.** (2014), 'Adinstrument-to-matlab sdk'.
URL: *https://github.com/JimHokanson/adinstruments_sdk_matlab, last accessed on May 1st, 2016*

[73]: **Holt, J., Allensworth, J., Diana, J., Collins, D. and Kines, H.** (1957), 'Regulation of the degree of emptying of the left ventricle by the force of ventricular contraction', *Circulation research* **5**(3), 281–287.

[74]: **Hondeghem, L. M.** (2016), 'Disturbances of cardiac wavelength and repolarization precede torsade de pointes and ventricular fibrillation in langendorff perfused rabbit hearts', *Progress in biophysics and molecular biology* **121**(1), 3–10.

[75]: **Hull, S., Vanoli, E., Adamson, P. B., Verrier, R. L., Foreman, R. D. and Schwartz, P. J.** (1994), 'Exercise training confers anticipatory protection from sudden death during acute myocardial ischemia.', *Circulation* **89**(2), 548–552.

[76]: **Hunt, S. A., Baker, D. W., Chin, M. H., Cinquegrani, M. P., Feldman, A. M., Francis, G. S., Ganiats, T. G., Goldstein, S., Gregoratos, G., Jessup, M. L. et al.** (2001), 'Acc/aha guidelines for the evaluation and management of chronic heart failure in the adult: a report of the american college of cardiology/american heart association task force on practice guidelines, developed in collaboration with the international society for heart and lung transplantation endorsed by the heart failure society of america', *Journal of the American College of Cardiology* **38**(7), 2101–2113.

[77]: **Jegger, D., Mallik, A. S., Nasratullah, M., Jeanrenaud, X., Da Silva, R., Tevaearai, H., Von Segesser, L. K. and Stergiopulos, N.** (2007), 'The effect of a myocardial infarction on the normalized time-varying elastance curve', *Journal of Applied Physiology* **102**(3), 1123–1129.

[78]: **Jordan, J., Tank, J., Shannon, J. R., Diedrich, A., Lipp, A., Schröder, C., Arnold, G., Sharma, A. M., Biaggioni, I., Robertson, D. et al.** (2002), 'Baroreflex buffering and susceptibility to vasoactive drugs', *Circulation* **105**(12), 1459–1464.

[79]: **Jung, B.** (2012), 'Optimal fixed cost subsidies in melitz-type models', *Empirica* **39**(1), 87–108.

[80]: **Kaese, S., Frommeyer, G., Verheule, S., van Loon, G., Gehrmann, J., Breithardt, G. and Eckardt, L.** (2013), 'The ecg in cardiovascular-relevant animal models of electrophysiology', *Herzschrittmachertherapie+ Elektrophysiologie* **24**(2), 84–91.

[81]: **Kalia, M., Mesulam, M. et al.** (1980), 'Brain stem projections of sensory and motor components of the vagus complex in the cat: Ii. laryngeal, tracheobronchial, pulmonary, cardiac, and gastrointestinal branches', *Journal of Comparative Neurology* **193**(2), 467–508.

[**82**]: **Kameyama, T., Asanoi, H., Ishizaka, S., Yamanishi, K., Fujita, M. and Sasayama, S.** (1992), 'Energy conversion efficiency in human left ventricle.', *Circulation* **85**(3), 988–996.

[**83**]: **Kandel, E. R., Schwartz, J. H., Jessell, T. M. et al.** (2000), *Principles of neural science*, Vol. 4, McGraw-hill New York.

[**84**]: **Kara, T., Narkiewicz, K. and Somers, V.** (2003), 'Chemoreflexes–physiology and clinical implications', *Acta physiologica Scandinavica* **177**(3), 377–384.

[**85**]: **Kass, D.** (1992), 'Clinical evaluation of left heart function by conductance catheter technique', *European heart journal* **13**(suppl E), 57–64.

[**86**]: **Kass, D. A.** (2002), 'Age-related changes in venticular–arterial coupling: pathophysiologic implications', *Heart failure reviews* **7**(1), 51–62.

[**87**]: **Kass, D. A., Beyar, R., Lankford, E., Heard, M., Maughan, W. L. and Sagawa, K.** (1989), 'Influence of contractile state on curvilinearity of in situ end-systolic pressure-volume relations.', *Circulation* **79**(1), 167–178.

[**88**]: **Kass, D. A. and Maughan, W. L.** (1988), 'From'emax'to pressure-volume relations: a broader view.', *Circulation* **77**(6), 1203–1212.

[**89**]: **Kass, D., Maughan, W., Guo, Z. M., Kono, A., Sunagawa, K. and Sagawa, K.** (1987), 'Comparative influence of load versus inotropic states on indexes of ventricular contractility: experimental and theoretical analysis based on pressure-volume relationships.', *Circulation* **76**(6), 1422–1436.

[**90**]: **Kelly, R. P., Ting, C.-T., Yang, T.-M., Liu, C.-P., Maughan, W. L., Chang, M.-S. and Kass, D. A.** (1992), 'Effective arterial elastance as index of arterial vascular load in humans.', *Circulation* **86**(2), 513–521.

[**91**]: **Kincaid, C.** (2005), Guidelines for selecting the covariance structure in mixed model analysis, *in* 'Thirtieth Annual SAS Users Group International Conference', number 198-30.

[**92**]: **Kind, T., Ruiter, G., Faes, T. J., Handoko, L. M., Schalij, I., Noordegraaf, A. V. and Westerhof, N.** (2011), 'Estimation of right ventricular isovolumic pressure in experimental pulmonary hypertension from a single ejecting beat', *European Respiratory Journal* **38**(Suppl 55), p1520.

[**93**]: **Kjørstad, K. E., Korvald, C. and Myrmel, T.** (2002), 'Pressure-volume-based single-beat estimations cannot predict left ventricular contractility in vivo', *American Journal of Physiology-Heart and Circulatory Physiology* **282**(5), H1739–H1750.

[**94**]: **Kleiger, R. E., Stein, P. K. and Bigger, J. T.** (2005), 'Heart rate variability: measurement and clinical utility', *Annals of Noninvasive Electrocardiology* **10**(1), 88–101.

[**95**]: **Knowlton, F. and Starling, E.** (1912), 'The influence of variations in temperature and blood-pressure on the performance of the isolated mammalian heart', *The Journal of physiology* **44**(3), 206–219.

[**96**]: **Kono, A., Maughan, W. L., Sunagawa, K., Hamilton, K., Sagawa, K. and Weisfeldt, M.** (1984), 'The use of left ventricular end-ejection pressure and peak pressure in the estimation of the end-systolic pressure-volume relationship.', *Circulation* **70**(6), 1057–1065.

[**97**]: **Korner, P., Bobik, A., Oddie, C. and Friberg, P.** (1993), 'Sympathoadrenal system is critical for structural changes in genetic hypertension.', *Hypertension* **22**(2), 243–252.

[**98**]: **Krayer, O.** (1961), 'The history of the bezold-jarisch effect', *Naunyn-Schmiedebergs Archiv für experimentelle Pathologie und Pharmakologie* **240**(5), 361–368.

[**99**]: **Krüger, C., Kalenka, A., Haunstetter, A., Schweizer, M., Maier, C., Rühle, U., Ehmke, H., Kübler, W. and Haass, M.** (1997), 'Baroreflex sensitivity and heart rate variability in conscious rats with myocardial infarction', *American Journal of Physiology-Heart and Circulatory Physiology* **273**(5), H2240–H2247.

[**100**]: **Kubota, T., Alexander, J., Itaya, R., Todaka, K., Sugimachi, M., Sunagawa, K., Nose, Y. and Takeshita, A.** (1992), 'Dynamic effects of carotid sinus baroreflex on ventriculoarterial coupling studied in anesthetized dogs.', *Circulation research* **70**(5), 1044–1053.

[**101**]: **Kumar, P. and Prabhakar, N. R.** (2012), 'Peripheral chemoreceptors: function and plasticity of the carotid body', *Comprehensive Physiology* .

[**102**]: **Laird, N. M. and Ware, J. H.** (1982), 'Random-effects models for longitudinal data', *Biometrics* pp. 963–974.

[**103**]: **Lankhaar, J.-W., Rövekamp, F. A., Steendijk, P., Faes, T. J., Westerhof, B. E., Kind, T., Vonk-Noordegraaf, A. and Westerhof, N.** (2009), 'Modeling the instantaneous pressure–volume relation of the left ventricle: a comparison of six models', *Annals of biomedical engineering* **37**(9), 1710–1726.

[**104**]: **La Rovere, M. T., Bigger, J. T., Marcus, F. I., Mortara, A., Schwartz, P. J., Tone, A. A., Investigators, R. A. M. I. et al.** (1998), 'Baroreflex sensitivity and heart-rate variability in prediction of total cardiac mortality after myocardial infarction', *The Lancet* **351**(9101), 478–484.

[**105**]: **Lee, T., Kuo, J. and Chai, C.** (1972), 'Central integrating mechanism of the bezold-jarisch and baroceptor reflexes', *American Journal of Physiology–Legacy Content* **222**(3), 713–720.

[**106**]: **Lelovas, P. P., Kostomitsopoulos, N. G. and Xanthos, T. T.** (2014), 'A comparative anatomic and physiologic overview of the porcine heart', *Journal of the American Association for Laboratory Animal Science* **53**(5), 432–438.

[**107**]: **Levy, M. and Martin, P.** (1996), 'Autonomic control of cardiac conduction and automaticity', *Nervous control of the heart. Amsterdam: Harwood Academic Publishers* pp. 201–226.

[**108**]: **Lips, D. J., vd Nagel, T., Steendijk, P., Palmen, M., Janssen, B. J., Dantzig, J.-M. v., de Windt, L. J. and Doevendans, P. A.** (2004), 'Left ventricular pressure–volume measurements in mice: Comparison of closed–chest versus open–chest approach', *Basic research in cardiology* **99**(5), 351–359.

[**109**]: **Littell, R. C., Pendergast, J. and Natarajan, R.** (2000), 'Tutorial in biostatistics: modelling covariance structure in the analysis of repeated measures data', *Statistics in medicine* **19**(1793), 1819.

[**110**]: **Little, W. C.** (1985), 'The left ventricular dp/dtmax-end-diastolic volume relation in closed-chest dogs.', *Circulation research* **56**(6), 808–815.

[**111**]: **Maeder, M. T. and Kaye, D. M.** (2009), 'Heart failure with normal left ventricular ejection fraction', *Journal of the American College of Cardiology* **53**(11), 905–918.

[**112**]: **Mahler, F., Covell, J. W. and Ross, J.** (1975), 'Systolic pressure—diameter relations in the normal conscious dog', *Cardiovascular research* **9**(4), 447–455.

[**113**]: **Majure, D. T. and Teerlink, J. R.** (2011), 'Update on the management of acute decompensated heart failure', *Current treatment options in cardiovascular medicine* **13**(6), 570–585.

[**114**]: **Manolakis, D. G., Ingle, V. K. and Kogon, S. M.** (2005), *Statistical and adaptive signal processing: spectral estimation, signal modeling, adaptive filtering, and array processing*, Vol. 46, Artech House Norwood.

[**115**]: **Mark, A. L.** (1983), 'The bezold-jarisch reflex revisited: clinical implications of inhibitory reflexes originating in the heart', *Journal of the American College of Cardiology* **1**(1), 90–102.

[**116**]: **Markwalder, J. and Starling, E.** (1914), 'On the constancy of the systolic output under varying conditions', *The Journal of physiology* **48**(4), 348.

[**117**]: **Marshall, J. M.** (1994), 'Peripheral chemoreceptors and cardiovascular regulation', *Physiological Reviews* **74**(3), 543–595.

[**118**]: **Martin, G., Gimeno, J., Cosin, J. and Guillem, M.** (1984), 'Time constant of isovolumic pressure fall: new numerical approaches and significance', *American Journal of Physiology-Heart and Circulatory Physiology* **247**(2), H283–H294.

[**119**]: **Matsubara, H., Takaki, M., Yasuhara, S., Araki, J. and Suga, H.** (1995), 'Logistic time constant of isovolumic relaxation pressure–time curve in the canine left ventricle better alternative to exponential time constant', *Circulation* **92**(8), 2318–2326.

[**120**]: **Maughan, W., Sunagawa, K., Hunter, W. and Sagawa, K.** (1985), Instantaneous but not end-systolic pressure-volume relationship (espvr) depends on afterload, *in* 'Federation Proceedings', Vol. 44, Federation Amer Soc Exp Biol 9650 Rockville Pike, Bethesda, MD 20814-3998 USA, pp. 1017–1017.

[**121**]: **McKinley, M. P. and O'loughlin, V. D.** (2012), *Human anatomy*, McGraw-Hill Higher Education.

[**122**]: **Mendis, S. et al.** (2014), *Global status report on noncommunicable diseases 2014.*, World Health Organization.

[**123**]: **Mifflin, S. W.** (1992), 'Arterial chemoreceptor input to nucleus tractus solitarius', *American Journal of Physiology-Regulatory, Integrative and Comparative Physiology* **263**(2), R368–R375.

[**124**]: **Milnor, W. R.** (1975), 'Arterial impedance as ventricular afterload.', *Circulation research* **36**(5), 565–570.

[**125**]: **Mirsky, I.** (1984), 'Assessment of diastolic function: suggested methods and future considerations.', *Circulation* **69**(4), 836–841.

[**126**]: **Molaee-Ardekani, B., Shamsollahi, M. B., Tirel, O., Vosoughi-Vahdat, B., Wodey, E. and Senhadji, L.** (2010), 'Investigation of the modulation between eeg alpha waves and slow/fast delta waves in children in different depths of desflurane anesthesia', *Irbm* **31**(1), 55–66.

[**127**]: **Monroe, R. G. and French, G. N.** (1960), 'Ventricular pressure-volume relationships and oxygen consumption in fibrillation and arrest', *Circulation research* **8**(1), 260–266.

[**128**]: **Monroe, R. G. and French, G. N.** (1961), 'Left ventricular pressure-volume relationships and myocardial oxygen consumption in the isolated heart', *Circulation research* **9**(2), 362–373.

[**129**]: **Morris, C. E.** (1990), 'Mechanosensitive ion channels', *Journal of Membrane Biology* **113**(2), 93–107.

[**130**]: **Mullen, T. J., Appel, M. L., Mukkamala, R., Mathias, J. M. and Cohen, R. J.** (1997), 'System identification of closed-loop cardiovascular control: effects of posture and autonomic blockade', *American Journal of Physiology-Heart and Circulatory Physiology* **272**(1), H448–H461.

[**131**]: **Nerbonne, J. M.** (2000), 'Molecular basis of functional voltage-gated k+ channel diversity in the mammalian myocardium', *The Journal of Physiology* **525**(2), 285–298.

[**132**]: **Nevill, A. M. and Holder, R. L.** (1995), 'Scaling, normalizing, and per ratio standards: an allometric modeling approach', *Journal of Applied Physiology* **79**(3), 1027–1031.

[**133**]: **Niazmand, S., Esparham, M., Hassannia, T., Derakhshan, M. et al.** (2011), 'Cardiovascular effects of teucrium polium l. extract in rabbit', *Pharmacognosy magazine* **7**(27), 260.

[**134**]: **Ning, X.-H., Xu, C.-S., Song, Y. C., Childs, K. F., Xiao, Y., Bolling, S. F., Lupinetti, F. M. and Portman, M. A.** (1998), 'Temperature threshold and modulation of energy metabolism in the cardioplegic arrested rabbit heart', *Cryobiology* **36**(1), 2–11.

[**135**]: **Oppenheim, A. V., Schafer, R. W., Buck, J. R. et al.** (1989), *Discrete-time signal processing*, Vol. 2, Prentice hall Englewood Cliffs, NJ.

[**136**]: **O'Rourke, M. F.** (1967), 'Pressure and flow waves in systemic arteries and the anatomical design of the arterial system.', *Journal of Applied Physiology* **23**(2), 139–149.

[**137**]: **Osterziel, K. J., Hänlein, D., Willenbrock, R., Eichhorn, C., Luft, F. and Dietz, R.** (1995), 'Baroreflex sensitivity and cardiovascular mortality in patients with mild to moderate heart failure.', *British heart journal* **73**(6), 517–522.

[**138**]: **Panfilov, A. V.** (2006), 'Is heart size a factor in ventricular fibrillation? or how close are rabbit and human hearts?', *Heart Rhythm* **3**(7), 862–864.

[**139**]: **Parent, M.-E. and Lepage, S.** (2015), 'A heart stopping case of the bezold-jarisch reflex', *Case reports in cardiology* **2015**.

[**140**]: **Patterson, S., Piper, H. and Starling, E.** (1914), 'The regulation of the heart beat', *The Journal of physiology* **48**(6), 465–513.

[**141**]: **Patterson, S. and Starling, E.** (1914), 'On the mechanical factors which determine the output of the ventricles', *The Journal of physiology* **48**(5), 357.

[**142**]: **Peirce, B.** (1852), 'Criterion for the rejection of doubtful observations', *The Astronomical Journal* **2**, 161–163.

[**143**]: **Quinn, T. A. and Kohl, P.** (2016), 'Rabbit models of cardiac mechano-electric and mechano-mechanical coupling', *Progress in biophysics and molecular biology* .

[**144**]: **Rabiner, L. and Herrmann, O.** (1973), 'The predictability of certain optimum finite-impulse-response digital filters', *IEEE Transactions on Circuit Theory* **20**(4), 401–408.

[**145**]: **Raff, G. L. and Glantz, S. A.** (1981), 'Volume loading slows left ventricular isovolumic relaxation rate', *Circ Res* **48**(6 Pt 1), 813–24.

[**146**]: **Redfield, M. M., Jacobsen, S. J., Borlaug, B. A., Rodeheffer, R. J. and Kass, D. A.** (2005), 'Age-and gender-related ventricular-vascular stiffening a community-based study', *Circulation* **112**(15), 2254–2262.

[**147**]: **Regen, D. M., Howe, W. C., Peterson, J. T. and Little, W. C.** (1993), 'Characteristics of single isovolumic left-ventricular pressure waves of dog hearts in situ', *Heart and vessels* **8**(3), 136–148.

[**148**]: **Riordon, J., Zubritsky, E. and Newman, A.** (2000), 'Top 10 articles.', *Analytical chemistry* **72**(9), 324–A.

[**149**]: **Rocha, I., Brás-Rosário, L., Amparo-Barros, M. and Silva-Carvalho, L.** (2003b), 'Angiotensin at1 receptor antagonist losartan and the defence reaction in the anaesthetised rat. effect on the carotid chemoreflex', *Experimental physiology* **88**(03), 309–314.

[**150**]: **Rocha, I., Rosário, L., De Oliveira, E., Barros, M. and Silva-Carvallho, L.** (2003a), 'Enhancement of carotid chemoreceptor reflex and cardiac chemosensitive reflex in the acute phase of myocardial infarction of the anesthetized rabbit', *Basic research in cardiology* **98**(3), 175–180.

[**151**]: **Rocha, I., Tarata, M. and Silva-Carvalho, L.** (2009), 'On measuring the absolute ventricular volumes for the estimation of end systolic pressure-volume relation in rabits', *Proceedings of the 7th International Conference, Smolenice, Slovakia* .

[**152**]: **Rosario, L., Rocha, I. and Silva-Carvalho, L.** (2003), Effect of losartan microinjections into the nts on the cardiovascular components of chemically evoked reflexes in a rabbit model of acute heart ischemia, *in* 'Chemoreception', Springer, pp. 423–431.

[**153**]: **Ross, S. M.** (2003), 'Peirce's criterion for the elimination of suspect experimental data', *Journal of Engineering Technology* **20**(2), 38–41.

[**154**]: **Rousseau, M., Veriter, C., Detry, J., Brasseur, L. and Pouleur, H.** (1980), 'Impaired early left ventricular relaxation in coronary artery disease: effects of intracornary nifedipine.', *Circulation* **62**(4), 764–772.

[**155**]: **Rowell, L.** (1993), 'Reflex control during orthostasis', *Human cardiovascular control. Oxford University Press, New York* pp. 37–80.

[**156**]: **Sagawa, K.** (1978), 'The ventricular pressure-volume diagram revisited.', *Circulation Research* **43**(5), 677–687.

[**157**]: **Sagawa, K.** (1981), 'Editorial: The end-systolic pressure-volume relation of the ventricle: definition, modifications and clinical use', *Circulation* **63**(6).

[**158**]: **Sagawa, K., Suga, H., Shoukas, A. A. and Bakalar, K. M.** (1977), 'End-systolic pressure/volume ratio: a new index of ventricular contractility', *The American journal of cardiology* **40**(5), 748–753.

[**159**]: **Savitzky, A. and Golay, M. J.** (1964), 'Smoothing and differentiation of data by simplified least squares procedures.', *Analytical chemistry* **36**(8), 1627–1639.

[**160**]: **Schafer, R. W.** (2011), 'What is a savitzky-golay filter?[lecture notes]', *Signal Processing Magazine, IEEE* **28**(4), 111–117.

[**161**]: **Schwartz, P. J. and De Ferrari, G. M.** (2011), 'Sympathetic–parasympathetic interaction in health and disease: abnormalities and relevance in heart failure', *Heart failure reviews* **16**(2), 101–107.

[**162**]: **Schwartz, P. J., Zaza, A., Pala, M., Locati, E., Beria, G. and Zanchetti, A.** (1988), 'Baroreflex sensitivity and its evolution during the first year after myocardial infarction', *Journal of the American College of Cardiology* **12**(3), 629–636.

[**163**]: **Segers, P., Georgakopoulos, D., Afanasyeva, M., Champion, H. C., Judge, D. P., Millar, H. D., Verdonck, P., Kass, D. A., Stergiopulos, N. and Westerhof, N.** (2005), 'Conductance catheter-based assessment of arterial input impedance, arterial function, and ventricular-vascular interaction in mice', *American Journal of Physiology-Heart and Circulatory Physiology* **288**(3), H1157–H1164.

[**164**]: **Senzaki, H., Chen, C.-H. and Kass, D. A.** (1996), 'Single-beat estimation of end-systolic pressure-volume relation in humans a new method with the potential for noninvasive application', *Circulation* **94**(10), 2497–2506.

[**165**]: **Shek, D. T. and Ma, C.** (2011), 'Longitudinal data analyses using linear mixed models in spss: concepts, procedures and illustrations', *The Scientific World Journal* **11**, 42–76.

[**166**]: **Shepherd, J.** (1982), 'Reflex control of arterial blood pressure', *Cardiovasc Res* **16**(357), 87–97.

[**167**]: **Shishido, T., Hayashi, K., Shigemi, K., Sato, T., Sugimachi, M. and Sunagawa, K.** (2000), 'Single-beat estimation of end-systolic elastance using bilinearly approximated time-varying elastance curve', *Circulation* **102**(16), 1983–1989.

[**168**]: **Singer, J. D. and Willett, J. B.** (2003), *Applied longitudinal data analysis: Modeling change and event occurrence*, Oxford university press.

[**169**]: **Smith, C. A., Forster, H. V., Blain, G. M. and Dempsey, J. A.** (2010), 'An interdependent model of central/peripheral chemoreception: evidence and implications for ventilatory control', *Respiratory physiology & neurobiology* **173**(3), 288–297.

[**170**]: **Smith, S. W. et al.** (1997), 'The scientist and engineer's guide to digital signal processing'.

[**171**]: **Sodums, M. T., Badke, F. R., Starling, M. R., Little, W. C. and O'Rourke, R. A.** (1984), 'Evaluation of left ventricular contractile performance utilizing end-systolic pressure-volume relationships in conscious dogs.', *Circulation Research* **54**(6), 731–739.

[**172**]: **Somers, V. K. and Abboud, F. M.** (1995), 'Neurocardiogenic syncope.', *Advances in internal medicine* **41**, 399–435.

[**173**]: **Somers, V. K., Mark, A. L. and Abboud, F. M.** (1991), 'Interaction of baroreceptor and chemoreceptor reflex control of sympathetic nerve activity in normal humans.', *Journal of Clinical Investigation* **87**(6), 1953.

[**174**]: **Somers, V. K., Mark, A. L., Zavala, D. C. and Abboud, F. M.** (1989), 'Influence of ventilation and hypocapnia on sympathetic nerve responses to hypoxia in normal humans.', *Journal of applied physiology (Bethesda, Md.: 1985)* **67**(5), 2095–2100.

[**175**]: **Sonnenblick, E. H.** (1962), 'Force-velocity relations in mammalian heart muscle', *American Journal of Physiology–Legacy Content* **202**(5), 931–939.

[**176**]: **Sonnenblick, E. H., Spiro, D. and Spotnitz, H. M.** (1964), 'The ultrastructural basis of starling's law of the heart. the role of the sarcomere in determining ventricular size and stroke volume', *American heart journal* **68**(3), 336–346.

[**177**]: **Spyer, K.** (1989), 'Neural mechanisms involved in cardiovascular control during affective behaviour', *Trends in neurosciences* **12**(12), 506–513.

[**178**]: **Spyer, K. M.** (1981), Neural organisation and control of the baroreceptor reflex, *in* 'Reviews of Physiology, Biochemistry and Pharmacology, Volume 88', Springer, pp. 23–124.

[**179**]: **Stahl, L. D., Weiss, H. R. and Becker, L. C.** (1988), 'Myocardial oxygen consumption, oxygen supply/demand heterogeneity, and microvascular patency in regionally stunned myocardium.', *Circulation* **77**(4), 865–872.

[**180**]: **Starling, M. R.** (1993), 'Left ventricular-arterial coupling relations in the normal human heart', *American heart journal* **125**(6), 1659–1666.

[**181**]: **Steinier, J., Termonia, Y. and Deltour, J.** (1972), 'Smoothing and differentiation of data by simplified least square procedure', *Analytical Chemistry* **44**(11), 1906–1909.

[**182**]: **Suga, H.** (1969), 'Time course of left ventricular pressure-volume relationship under various end-diastolic volumes', *Japanese heart journal* **10**(6), 509–515.

[**183**]: **Suga, H.** (1970), 'Time course of left ventricular pressure-volume relationship under various extents of aortic occlusion', *Japanese heart journal* **11**(4), 373–378.

[**184**]: **Suga, H.** (1971), 'Theoretical analysis of a left-ventricular pumping model based on the systolic time-varying pressure/volume ratio', *Biomedical Engineering, IEEE Transactions on* (1), 47–55.

[**185**]: **Suga, H.** (1990), 'Ventricular energetics', *Physiological reviews* **70**(2), 247–277.

[**186**]: **Suga, H.** (1995), 'How we view systolic function of the heart: Emax and pva', *Systolic and diastolic function of the heart. Amsterdam: IOS Press and Ohmsha* .

[**187**]: **Suga, H.** (2003), 'Global cardiac function: mechano-energetico-informatics', *Journal of biomechanics* **36**(5), 713–720.

[**188**]: **Suga, H., Hayashi, T. and Shirahata, M.** (1981), 'Ventricular systolic pressure-volume area as predictor of cardiac oxygen consumption', *American Journal of Physiology-Heart and Circulatory Physiology* **240**(1), H39–H44.

[**189**]: **Suga, H., Hisano, R., Goto, Y., Yamada, O. and Igarashi, Y.** (1984), 'Effect of positive inotropic agents on the relation between oxygen consumption and systolic pressure volume area in canine left ventricle.', *Circulation research* **53**(3), 306–318.

[**190**]: **Suga, H., Hisano, R., Hirata, S., Hayashi, T., Yamada, O. and Ninomiya, I.** (1983), 'Heart rate-independent energetics and systolic pressure-volume area in dog heart', *American Journal of Physiology-Heart and Circulatory Physiology* **244**(2), H206–H214.

[**191**]: **Suga, H. and Sagawa, K.** (1974), 'Instantaneous pressure-volume relationships and their ratio in the excised, supported canine left ventricle', *Circulation research* **35**(1), 117–126.

[**192**]: **Suga, H., Sagawa, K. and Shoukas, A. A.** (1973), 'Load independence of the instantaneous pressure-volume ratio of the canine left ventricle and effects of epinephrine and heart rate on the ratio', *Circulation research* **32**(3), 314–322.

[**193**]: **Sugimachi, M. and Sunagawa, K.** (1997), Optimal afterload that maximizes external work and optimal heart that minimizes o2 consumption, *in* 'Cardiac-Vascular Remodeling and Functional Interaction', Springer, pp. 189–202.

[**194**]: **Sunagawa, K., Maughan, W. L., Burkhoff, D. and Sagawa, K.** (1983), 'Left ventricular interaction with arterial load studied in isolated canine ventricle', *American Journal of Physiology-Heart and Circulatory Physiology* **245**(5), H773–H780.

[**195**]: **Sunagawa, K., Maughan, W. L. and Sagawa, K.** (1985), 'Optimal arterial resistance for the maximal stroke work studied in isolated canine left ventricle.', *Circulation research* **56**(4), 586–595.

[**196**]: **Sunagawa, K., Yamada, A., Senda, Y., Kikuchi, Y., Nakamura, M., Shibahara, T. and Nose, Y.** (1980), 'Estimation of the hydromotive source pressure from ejecting beats of the left ventricle', *Biomedical Engineering, IEEE Transactions on* (6), 299–305.

[**197**]: **Tabachnick, B. G. and Fidell, L. S.** (2007), 'Using multivariate statistics, 5th', *Needham Height, MA: Allyn & Bacon* .

[**198**]: **Takeuchi, M., Igarashi, Y., Tomimoto, S., Odake, M., Hayashi, T., Tsukamoto, T., Hata, K., Takaoka, H. and Fukuzaki, H.** (1991), 'Single-beat estimation of the slope of the end-systolic pressure-volume relation in the human left ventricle.', *Circulation* **83**(1), 202–212.

[**199**]: **Templeton, G. H., Ecker, R. R. and Mitchell, J. H.** (1972), 'Left ventricular stiffness during diastole and systole: the influence of changes in volume and inotropic state', *Cardiovascular research* **6**(1), 95–100.

[**200**]: **Ten Brinke, E., Klautz, R., Verwey, H., Van Der Wall, E., Dion, R. and Steendijk, P.** (2010), 'Single-beat estimation of the left ventricular end-systolic pressure–volume relationship in patients with heart failure', *Acta physiologica* **198**(1), 37–46.

[**201**]: **Thorén, P.** (1979), Role of cardiac vagal c-fibers in cardiovascular control, *in* 'Reviews of Physiology, Biochemistry and Pharmacology, Volume 86', Springer, pp. 1–94.

[**202**]: **Thygesen, K., Alpert, J. S., Jaffe, A. S., White, H. D., Simoons, M. L., Chaitman, B. R., Katus, H. A., Apple, F. S., Lindahl, B., Morrow, D. A. et al.** (2012), 'Third universal definition of myocardial infarction', *Journal of the American College of Cardiology* **60**(16), 1581–1598.

[**203**]: **Thygesen, K., Alpert, J. S. and White, H. D.** (2007), 'Universal definition of myocardial infarction', *Journal of the American College of Cardiology* **50**(22), 2173–2195.

[**204**]: **Toller, W. G. and Stranz, C.** (2006), 'Levosimendan, a new inotropic and vasodilator agent', *The Journal of the American Society of Anesthesiologists* **104**(3), 556–569.

[**205**]: **Tortora, G. J. and Derrickson, B. H.** (2008), *Principles of anatomy and physiology*, John Wiley & Sons.

[**206**]: **Townend, J. and Littler, W.** (1995), 'Cardiac vagal activity: a target for intervention in heart disease', *The Lancet* **345**(8955), 937–938.

[**207**]: **Twisk, J. W.** (2013), *Applied longitudinal data analysis for epidemiology: a practical guide*, Cambridge University Press.

[**208**]: **Ullrich, K., Riecker, G. and Kramer, K.** (1954), 'Das druckvolumdiagramm des warmblüterherzens', *Pflügers Archiv European Journal of Physiology* **259**(6), 481–498.

[**209**]: **Van der Velde, E., Burkhoff, D., Steendijk, P., Karsdon, J., Sagawa, K. and Baan, J.** (1991), 'Nonlinearity and load sensitivity of end-systolic pressure-volume relation of canine left ventricle in vivo.', *Circulation* **83**(1), 315–327.

[**210**]: **Vanoli, E., De Ferrari, G. M., Stramba-Badiale, M., Hull, S., Foreman, R. D. and Schwartz, P. J.** (1991), 'Vagal stimulation and prevention of sudden death in conscious dogs with a healed myocardial infarction.', *Circulation Research* **68**(5), 1471–1481.

[**211**]: **Varma, S. K., Owen, R. M., Smucker, M. L. and Feldman, M. D.** (1989), 'Is tau a preload-independent measure of isovolumetric relaxation?', *Circulation* **80**(6), 1757–1765.

[**212**]: **Verberne, A. and Guyenet, P. G.** (1992), 'Medullary pathway of the bezold-jarisch reflex in the rat', *American Journal of Physiology-Regulatory, Integrative and Comparative Physiology* **263**(6), R1195–R1202.

[**213**]: **Wade, J. G., Larson Jr, C. P., Hickey, R. F., Ehrenfeld, W. K. and Severinghaus, J. W.** (1970), 'Effect of carotid endarterectomy on carotid chemoreceptor and baroreceptor function in man', *New England Journal of Medicine* **282**(15), 823–829.

[**214**]: **Weiss, J. L., Frederiksen, J. W. and Weisfeldt, M. L.** (1976), 'Hemodynamic determinants of the time-course of fall in canine left ventricular pressure.', *Journal of Clinical Investigation* **58**(3), 751.

[**215**]: **Wiggers, C. J.** (1915), *Modern Aspects of the Circulation in Health and Disease*, Lea & Febiger.

[**216**]: **Yamakawa, K., Zhou, W., Ko, Y., Benharash, P., Takemoto, M. and Mahajan, A.** (2014), 'Improved cardioprotection using a novel stepwise ischemic preconditioning protocol in rabbit heart', *Journal of Surgical Research* **188**(2), 381–386.

[**217**]: **Yamazaki, T., Shimada, Y., Taenaka, N., Ohsumi, H., Takezawa, J. and Yoshiya, I.** (1982), 'Circulatory responses to afterloading with phenylephrine in hyperdynamic sepsis.', *Critical care medicine* **10**(7), 432–435.

[**218**]: **Zile, M. R. and Brutsaert, D. L.** (2002), 'New concepts in diastolic dysfunction and diastolic heart failure: Part i diagnosis, prognosis, and measurements of diastolic function', *Circulation* **105**(11), 1387–1393.

[**219**]: **Zimetbaum, P. J. and Josephson, M. E.** (2003), 'Use of the electrocardiogram in acute myocardial infarction', *New England Journal of Medicine* **348**(10), 933–940.

APPENDIX A

`DataPhysioBeat` **Object**

In order to store all important variables, a custom object structure was created in Matlab ® 2014b. Named `DataPhysioBeat`, its several properties are updated throughout each stage of the preprocessing pipeline. **Figure A-1** presents the structure of the `DataPhysioBeat` object.

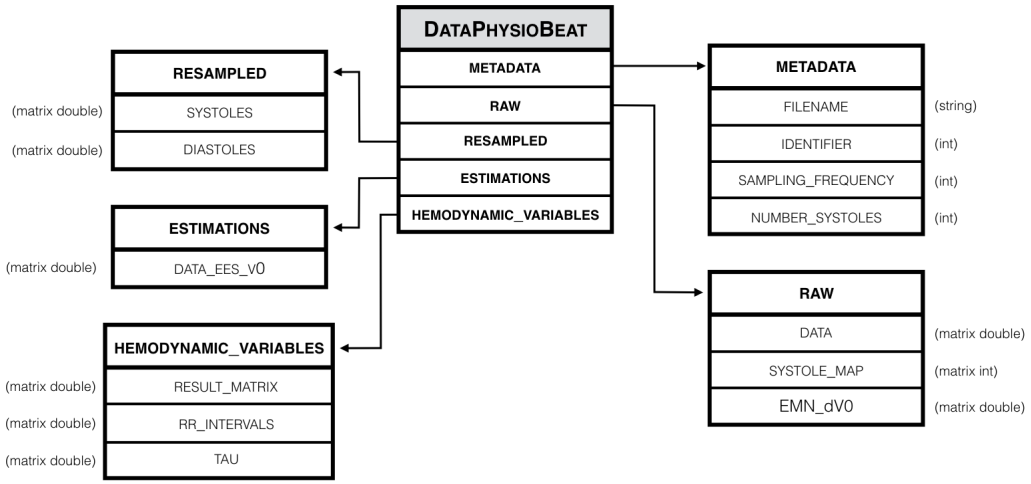

Figure A-1: `DataPhysioBeat` object's structure.

The **metadata** property stores the original file's name, an identifier in case multiple analysis are performed using the same filename, the sampling frequency, and the number of systoles identified in the analysis. The **raw** property contains all the raw PV data, such as a time vector t, LV $P(t)$, LV $V(t)$, $BP(t)$, and normalized LV $E(t)$. Additionally, it also contains a systole map to store the indexes of both beginning and ending of all systoles. After resampling the raw data (both systoles and diastoles) for more precise estimations, the results are stored in the **resampled** property. The **estimations** property is where the estimations for LV elastance and volume-intercept are stored, before preliminary statistical analysis. The variables which are computed using the estimations are stored in the **hemodynamic variables** property, together with information regarding instantaneous heart rate (RR intervals).

Matlab ® code from DataPhysioBeat.m:

```
classdef DataPhysioBeat
    % dataPhysioBeat stores properties that are related to Pressure-Volume data.
    properties
        metadata
        raw
        resampled
        estimations
        hemodynamics
    end
    methods
        function dataPhysioBeat = DataPhysioBeat
            % File identication
            dataPhysioBeat.metadata.filename = 'empty';                % Filename
            dataPhysioBeat.metadata.identifier = 0;                    % Identifier
            dataPhysioBeat.metadata.sampling_frequency = 0;            % Double
            dataPhysioBeat.metadata.number_systoles = 0;               % Double

            % Systole data
            dataPhysioBeat.raw.data = [];                              % nx4
            dataPhysioBeat.raw.systole_map = [];                       % (nrCycles)x2
            dataPhysioBeat.raw.EMN_dV0 = [];                           % Nx4

            % Resampled data for N = 1000 each cycle
            dataPhysioBeat.resampled.systoles = [];                    % (nrCycles)x2xN
            dataPhysioBeat.resampled.diastoles = [];                   % (nrCycles)x2xN

            % Initial estimations of Ees and V0
            dataPhysioBeat.estimations = [];                           % (nrCycles)x2

            % Hemodynamic properties
            dataPhysioBeat.hemodynamics.results = [];                  % (nrCycles)x20
            dataPhysioBeat.hemodynamics.RRint = [];                    % (nrCycles)x1
            dataPhysioBeat.hemodynamics.Tau.half = [];                 % (nrCycles)x1
            dataPhysioBeat.hemodynamics.Tau.weiss = [];                % (nrCycles)x2
            dataPhysioBeat.hemodynamics.Tau.glantz = [];               % (nrCycles)x3
            dataPhysioBeat.hemodynamics.Tau.levenberg_marquardt = [];  % (nrCycles)x4
            dataPhysioBeat.hemodynamics.Tau.logistic = [];             % (nrCycles)x4
        end
    end
end
```

APPENDIX B

Pseudocode

Pseudocode is an informal, efficient and environment-independent description of the key principles of an algorithm. Though it uses the structural conventions of a normal programming language, it is intended for human reading, omitting details such as variable declarations and system-specific code. It is commonly used in scientific publications in which various algorithms are documented.

B-1 Lankhaar et al.'s algorithm for estimation of end-diastolic and end-systolic points

Algorithm B.1 Detection of corner points of pressure-volume loops (Lankhaar et al., 2009). The point with the maximal distance to the center is defined as the corner point.

Require: V and P are the volume and pressure of **one** PV loop, with equal length N.

function ESTIMATION OF CORNER POINTS(V, P)
  $w \leftarrow \max(V) - \min(V)$
  $h \leftarrow \max(P) - \min(P)$
  $V_{center} \leftarrow w/2$
  $P_{center} \leftarrow h/2$
  for $i \leftarrow 1$ **to** N **do**
    if $P[i] \geq P_{center} \wedge V[i] \leq V_{center}$ **then** ▷ Upper-left corner
      $d_{ES}[i] = \sqrt{((V[i] - V_{center})/(w))^2 + ((P[i] - P_{center})/(h))^2}$
    end if
    if $P[i] \leq P_{center} \wedge V[i] \geq V_{center}$ **then** ▷ Lower-right corner
      $d_{ED}[i] = \sqrt{((V[i] - V_{center})/(w))^2 + ((P[i] - P_{center})/(h))^2}$
    end if
  end for
  $C_{ES} \leftarrow \arg\max(d_{ES})$ ▷ Index of the end-systolic point
  $C_{ED} \leftarrow \arg\max(d_{ED})$ ▷ Index of the end-diastolic point
end function

B-2 Ten Brinke et al.'s single-beat method

Algorithm B.2 Single-beat estimation of LV end-systolic elastance, by fitting a fifth-order polynomial to the pressure curve (Ten Brinke et al., 2010).

Require: P is the pressure of **one** PV loop, with length M, between the onset and end of the systole. t is the time vector with length M.

function ESTIMATION OF $P_{MAX}(t, P)$
  $dP \leftarrow dP/dt$ ▷ First-derivative of the pressure curve.
  $dP_{max} \leftarrow \max(dP)$
  $dP_{min} \leftarrow \min(dP)$
  $c \leftarrow 1$
  for $i \leftarrow 1$ **to** M **do**
    if $dP[i] < dP_{max} \vee (dP[i] > dP_{min} \wedge dP[i] < 0.85 dP_{min})$ **then**
      $P_s[c] \leftarrow P[i]$
      $t_s[c] \leftarrow t[i]$
      $c \leftarrow c + 1$
    end if
  end for
  $\{\min_{c_1,\ldots,c_6} \sum_{k=1}^{N} (P_s[k] - F(t_s[k], c_1, \ldots, c_6))^2\}$ ▷ Least-squares fit.
  $P_{MAX} \leftarrow \max(F(t_s, c_1, \ldots, c_6))$ ▷ Isovolumic PV point.
  $E_{es} = (P_{MAX} - P_{es})/(V_{ed} - V_{es})$ ▷ LV end-systolic elastance.
end function

B-3 Peirce's criterion for outlier removal

Algorithm B.3 Detection and rejection of outliers in input data, using Peirce's method with Ross (2003) updated tables.

Require: x is a vector with length N.

function OUTLIER REJECTION(x)
  $\mu \leftarrow \text{mean}(x)$
  $\sigma \leftarrow \text{std}(x)$
  $\gamma \leftarrow 1$ ▷ Start with **one** doubtful observation.
  while `true` **do**
    $k \leftarrow 0$ ▷ Number of outliers detected.
    $R \leftarrow \text{TABLE}_{\text{ROSS}}(N - 1, \gamma + 1)$ ▷ Maximum allowable deviation.
    for $i \leftarrow 1$ **to** N **do**
      if $|x[i] - \mu| > R \cdot \sigma$ **then** ▷ Threshold for detection of an outlier.
        $x[i] \leftarrow$ `null` ▷ The outlier is rejected.
        $k \leftarrow k + 1$
      end if
    end for
    $\gamma \leftarrow \gamma + k$
    if $k = 0$ **then**
      `false`
    end if
  end while
end function

APPENDIX C

Left-ventricle Volume and Pressure

The plots presented in this chapter are complementary to those presented in **Chapter 4**, as they represent beat-to-beat variations in the pressure-volume data in each *stimulation*, for all three *measurements*. However, no perfect assessment index of the contractility of the heart can be obtained from volume or pressure measurements alone. In fact, these measurements on their own are neither sufficient to characterize the heart's performance during systole, nor they cannot solely define contractility. Simultaneous pressure and volume measurements are necessary to provide valuable functional parameters, such as E_{es} or SW.

For each of the following pages, the first plot displays V_{ed}, V_{es} and SV variations. The y-axis limits were set to [$0;\ 6$] mL for better readability and comparison between different reflex responses, and between groups `NOR` and `AMI`. In the second plot, P_{ed}, P_{es} and $P_{baseline}$ are represented. Baseline pressure, or $P_{baseline}$, corresponds to the mean of the pressure curve for each cardiac beat, and thus may not be directly proportional to the mean between P_{es} and P_{ed}. The y-axis limitst were set to [$0;\ 150$] $mmHg$ so that it is easier to read and compare different *datasets*.

Note that the fit coefficients a, b correspond to the intercept and slope parameters, respectively, estimated using linear mixed-effects model. The coefficient of determination R^2 measures how well the estimated straight line can replicate the data in analysis.

To see the results, please go to the next page.

C-1 The BR Dataset

Normal conditions:

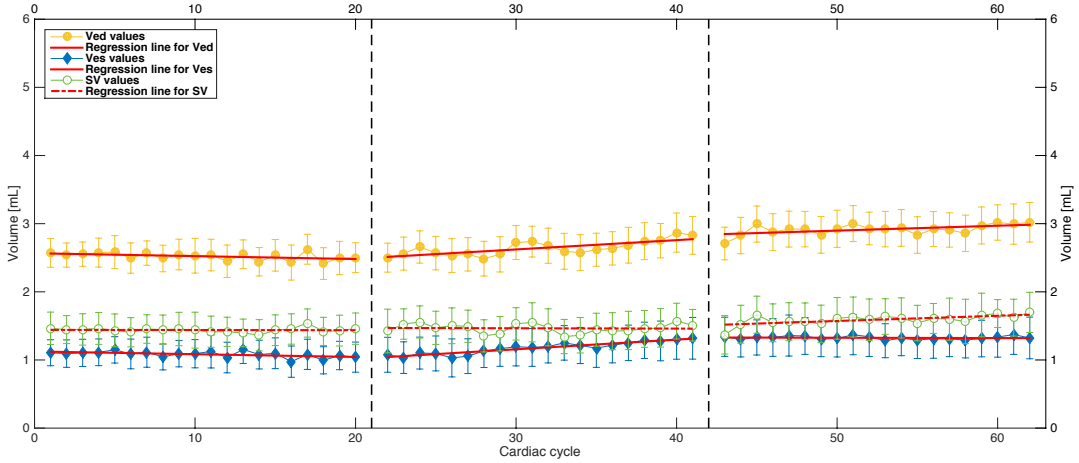

Figure C-1: Beat-to-beat mean V_{ed}, V_{es} and SV during three 20-beat measurements, evoked during aorta occlusion ($n = 42$) under normal conditions (`NOR`). Bars denote standard deviation. Y-axis limits were set to $[0;\ 6]\ mL$.

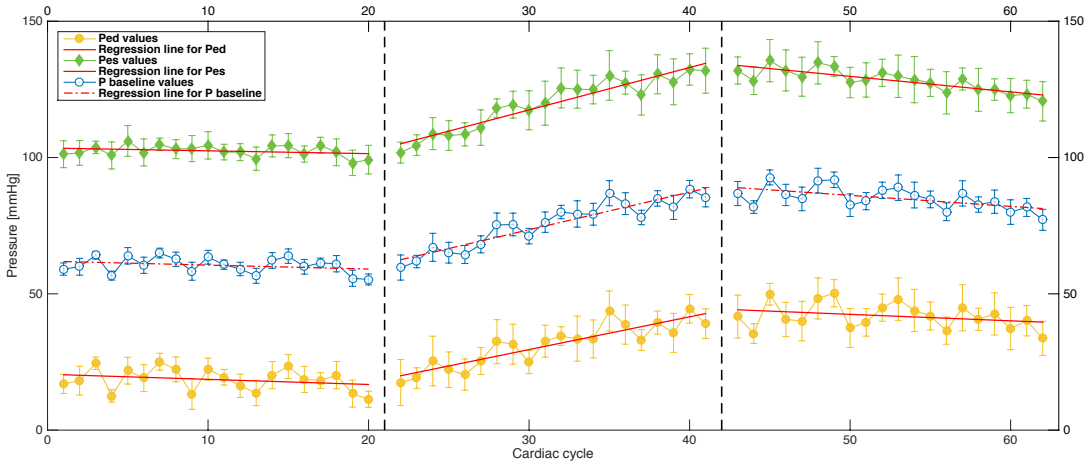

Figure C-2: Beat-to-beat mean P_{ed}, P_{es} and $P_{baseline}$, evoked on the unloading of carotid baroreceptors ($n = 42$) under normal conditions (`NOR`), for *measurements* `M1-3`. Bars denote standard deviation. Y-axis limits were set to $[0;\ 150]\ mmHg$.

	Measurement M1					**Measurement M2**					**Measurement M3**				
	μ	σ	a	b	R^2	μ	σ	a	b	R^2	μ	σ	a	b	R^2
V_{ed}	2.436	0.059	-0.001	2.445	0.007	2.595	0.146	0.019	1.983	0.617	2.801	0.132	-0.003	2.941	0.014
V_{es}	0.981	0.041	-0.001	0.991	0.019	1.374	0.269	0.041	0.088	0.808	1.726	0.129	-0.005	1.999	0.057
SV	1.456	0.034	0.000	1.454	0.001	1.221	0.135	-0.021	1.896	0.878	1.075	0.036	0.003	0.942	0.170
P_{ed}	18.530	4.112	-0.187	20.496	0.073	31.353	7.977	1.201	-6.494	0.794	41.879	4.753	-0.238	54.357	0.087
P_{es}	102.407	2.079	-0.103	103.488	0.086	119.798	9.658	1.555	70.829	0.907	128.358	4.107	-0.570	158.297	0.675
$P_{baseline}$	60.468	2.927	-0.145	61.992	0.086	75.575	8.737	1.378	32.168	0.871	85.118	4.156	-0.404	106.327	0.331

Table C-1: Mean (μ), standard deviation (σ) and fit coefficients (a, b and R^2) for V_{ed}, V_{es}, SV, P_{ed}, P_{es} and $P_{baseline}$ in baroreflex *stimulation* of group `NOR` ($n = 42$), discriminated by measurement.

After Myocardial Infarction:

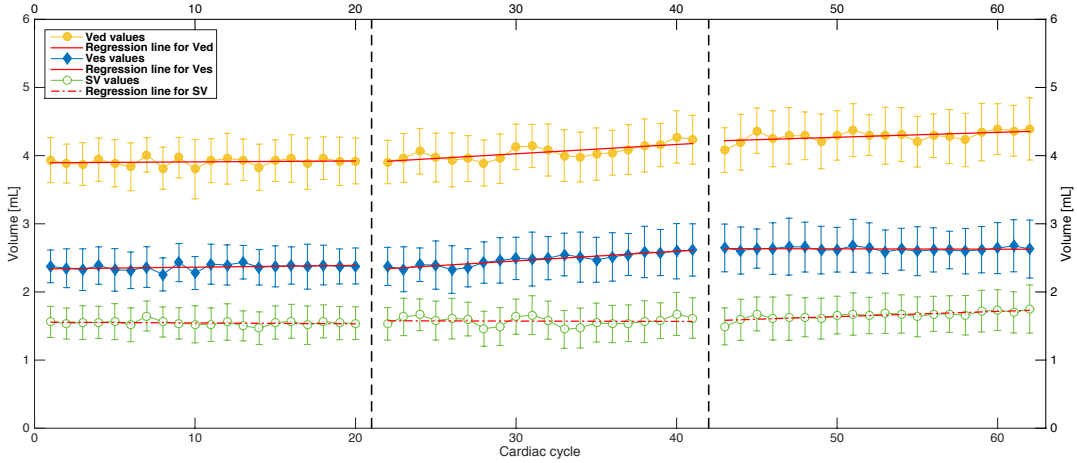

Figure C-3: Beat-to-beat mean V_{ed}, V_{es} and SV during three 20-beat measurements, due inflation of a balloon in the descending aorta ($n = 27$) after acute myocardial infarction (`AMI`). Bars denote standard deviation. Y-axis limits were set to $[0;\ 6]\ mL$.

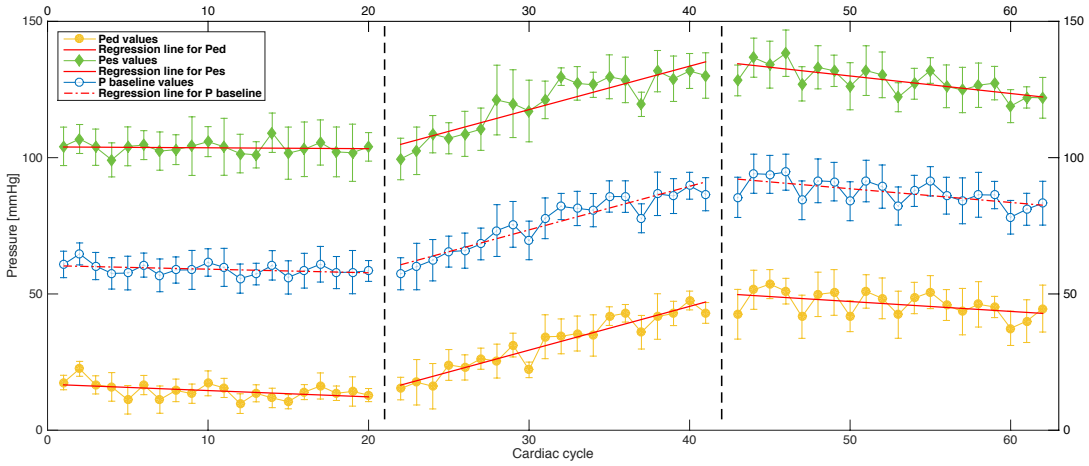

Figure C-4: Beat-to-beat mean P_{ed}, P_{es} and $P_{baseline}$, caused by aorta occlusion ($n = 27$) after acute myocardial infarction (`AMI`), for *measurements* `M1-3`. Bars denote standard deviation. Y-axis limits were set to $[0;\ 150]\ mmHg$.

	Measurement M1					**Measurement M2**					**Measurement M3**				
	μ	σ	a	b	R^2	μ	σ	a	b	R^2	μ	σ	a	b	R^2
V_{ed}	4.290	0.109	-0.007	4.361	0.135	4.315	0.125	-0.004	4.436	0.033	4.288	0.160	-0.004	4.524	0.028
V_{es}	2.748	0.112	-0.006	2.815	0.114	3.016	0.167	0.018	2.458	0.396	3.147	0.165	-0.007	3.494	0.056
SV	1.544	0.047	0.000	1.541	0.001	1.298	0.136	-0.022	1.978	0.881	1.141	0.036	0.002	1.030	0.119
P_{ed}	14.447	2.981	-0.231	16.878	0.211	31.800	9.991	1.604	-18.736	0.902	46.318	4.503	-0.363	65.385	0.228
P_{es}	103.600	2.230	-0.032	103.940	0.007	120.009	10.435	1.594	69.802	0.817	128.354	5.152	-0.642	162.076	0.544
$P_{baseline}$	59.023	2.140	-0.132	60.409	0.133	75.905	10.003	1.599	25.533	0.895	87.336	4.672	-0.503	113.731	0.405

Table C-2: Mean (μ), standard deviation (σ) and fit coefficients (a, b and R^2) for V_{ed}, V_{es}, SV, P_{ed}, P_{es} and $P_{baseline}$ in baroreflex *stimulation* of group `AMI` ($n = 27$), discriminated by measurement.

C-2 The CR Dataset

Normal conditions:

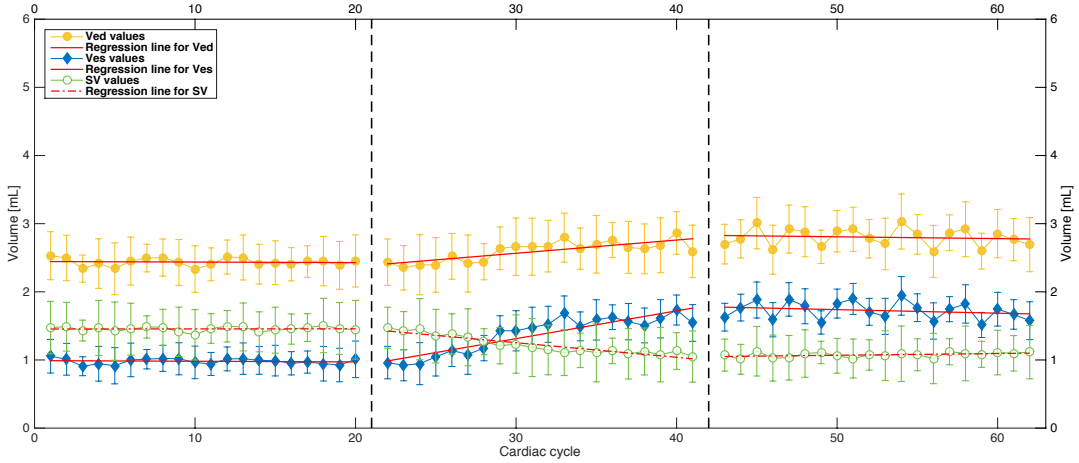

Figure C-5: Beat-to-beat mean V_{ed}, V_{es} and SV during three 20-beat measurements, evoked on the stimulation of the carotid chemoreceptors ($n = 26$) under normal conditions (`NOR`). Bars denote standard deviation. Y-axis limits were set to $[0;\ 6]\ mL$.

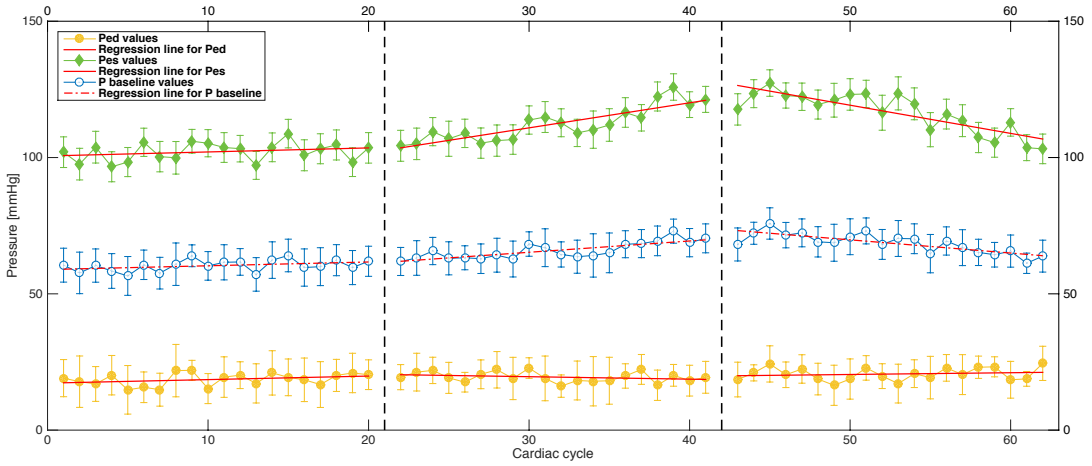

Figure C-6: Beat-to-beat mean P_{ed}, P_{es} and $P_{baseline}$, as response to the activation of the chemoreceptors with lobeline ($n = 26$) under normal conditions (`NOR`), for *measurements* `M1-3`. Bars denote standard deviation. Y-axis limits were set to $[0;\ 150]\ mmHg$.

	Measurement M1					Measurement M2					Measurement M3				
	μ	σ	a	b	R^2	μ	σ	a	b	R^2	μ	σ	a	b	R^2
V_{ed}	2.521	0.056	-0.004	2.566	0.201	2.642	0.107	0.014	2.212	0.566	2.916	0.078	0.007	2.539	0.300
V_{es}	1.082	0.046	-0.004	1.125	0.273	1.178	0.090	0.014	0.731	0.871	1.325	0.025	-0.000	1.350	0.012
SV	1.439	0.035	-0.000	1.441	0.001	1.464	0.068	-0.001	1.481	0.002	1.591	0.072	0.008	1.189	0.391
P_{ed}	18.598	2.316	0.130	17.235	0.110	19.466	1.898	-0.090	22.313	0.079	20.574	2.365	0.065	17.182	0.026
P_{es}	102.120	3.358	0.148	100.568	0.068	112.267	6.283	0.918	83.344	0.748	116.610	7.360	-1.034	170.890	0.691
$P_{baseline}$	60.359	2.124	0.139	58.901	0.150	65.867	3.091	0.414	52.828	0.628	68.592	3.651	-0.485	94.036	0.617

Table C-3: Mean (μ), standard deviation (σ) and fit coefficients (a, b and R^2) for V_{ed}, V_{es}, SV, P_{ed}, P_{es} and $P_{baseline}$ in chemoreflex *stimulation* of group `NOR` ($n = 26$), for each measurement.

After Myocardial Infarction:

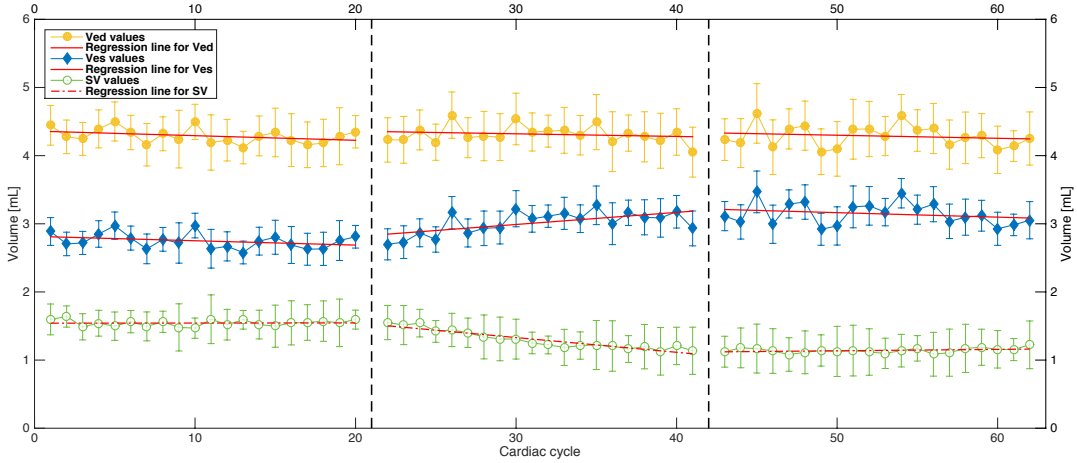

Figure C-7: Beat-to-beat mean V_{ed}, V_{es} and SV during three 20-beat measurements, caused by stimulation of the carotid chemoreceptors ($n = 11$) after acute myocardial infarction (`AMI`). Bars denote standard deviation. Y-axis limits were set to $[0;\ 6]\ mL$.

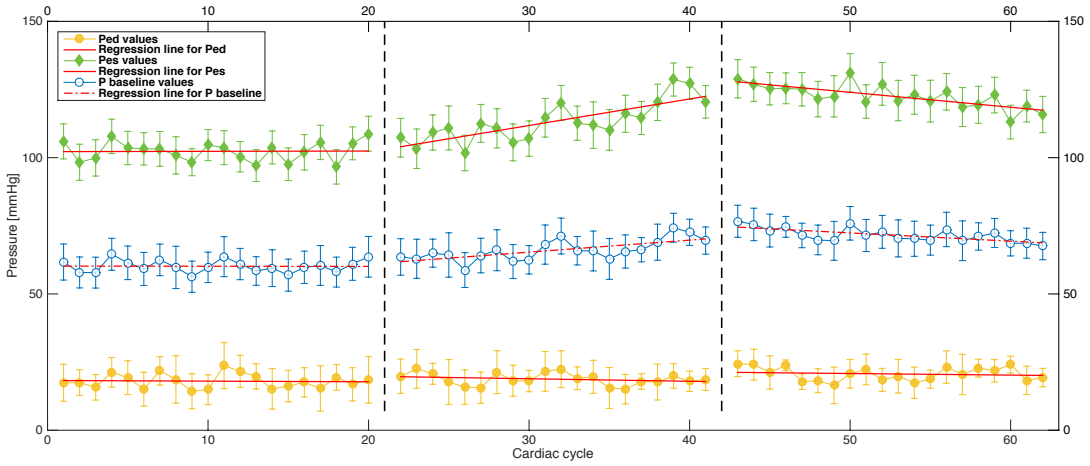

Figure C-8: Beat-to-beat mean P_{ed}, P_{es} and $P_{baseline}$, as response to the activation of the chemoreceptors with lobeline ($n = 11$) after myocardial infarction (`AMI`), for *measurements* `M1-3`. Bars denote standard deviation. Y-axis limits were set to $[0;\ 150]\ mmHg$.

	Measurement M1					**Measurement M2**					**Measurement M3**				
	μ	σ	a	b	R^2	μ	σ	a	b	R^2	μ	σ	a	b	R^2
V_{ed}	3.909	0.056	0.001	3.894	0.022	4.048	0.107	0.014	3.617	0.566	4.288	0.078	0.007	3.911	0.300
V_{es}	2.365	0.046	0.003	2.337	0.116	2.476	0.090	0.014	2.029	0.871	2.631	0.025	-0.000	2.656	0.012
SV	1.544	0.035	-0.001	1.557	0.043	1.572	0.068	-0.001	1.588	0.002	1.657	0.057	0.008	1.255	0.640
P_{ed}	18.005	2.667	-0.023	18.250	0.003	18.751	2.252	-0.093	21.685	0.060	20.668	2.527	-0.059	23.739	0.019
P_{es}	102.320	3.576	0.011	102.203	0.000	113.256	7.253	0.973	82.592	0.630	122.602	4.381	-0.548	151.366	0.548
$P_{baseline}$	60.163	2.297	-0.006	60.226	0.000	66.004	3.844	0.440	52.139	0.459	71.635	2.624	-0.303	87.553	0.467

Table C-4: Mean (μ), standard deviation (σ) and fit coefficients (a, b and R^2) for V_{ed}, V_{es}, SV, P_{ed}, P_{es} and $P_{baseline}$ in chemoreflex *stimulation* in group `AMI` ($n = 11$), for each measurement.

C-3 The BJR Dataset

Normal conditions:

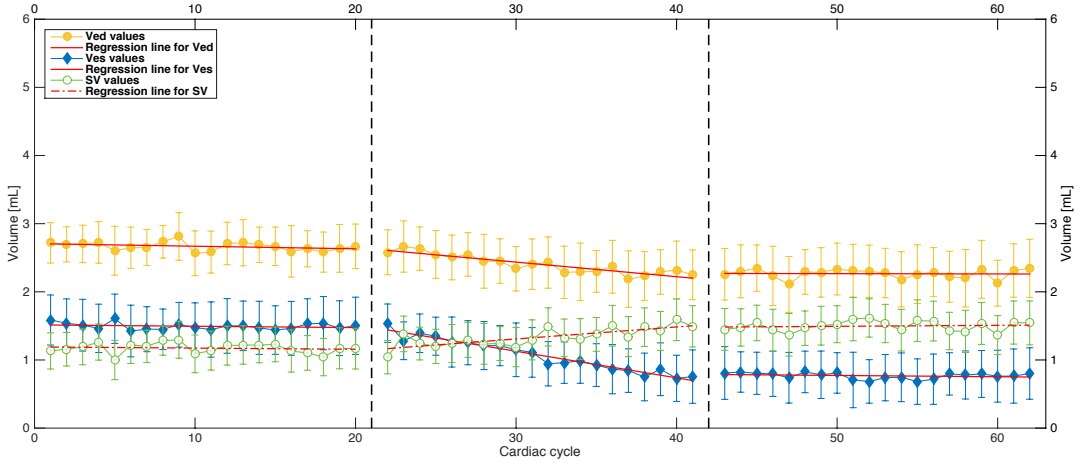

Figure C-9: Beat-to-beat mean V_{ed}, V_{es} and SV during three 20-beat measurements, evoked on the stimulation of the pulmonary afferent fibers ($n = 23$) under normal conditions (NOR). Bars denote standard deviation. Y-axis limits were set to $[0;\ 6]\ mL$.

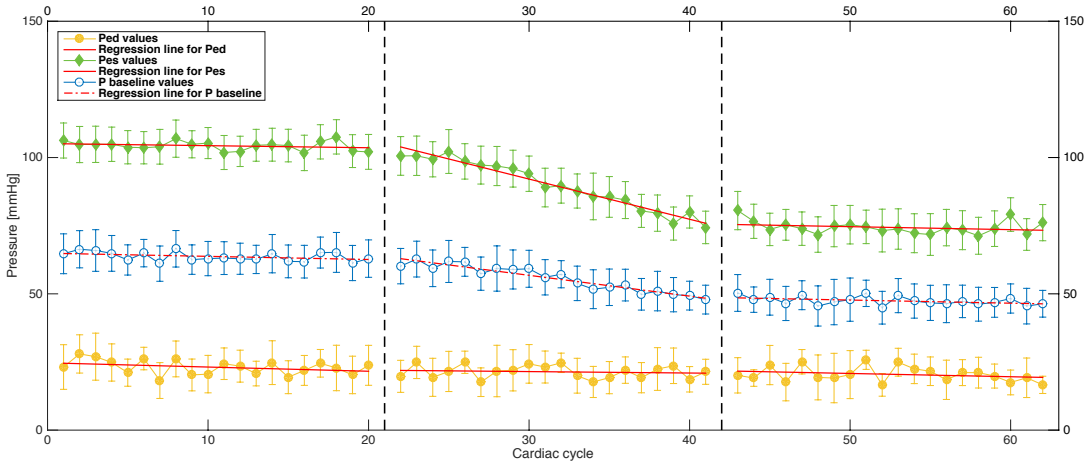

Figure C-10: Beat-to-beat mean P_{ed}, P_{es} and $P_{baseline}$, as response to activation of the Bezold-Jarisch reflex with ATP ($n = 23$) under normal conditions (NOR), for *measurements* M1-3. Bars denote standard deviation. Y-axis limits were set to $[0;\ 150]\ mmHg$.

	Measurement M1					Measurement M2					Measurement M3				
	μ	σ	a	b	R^2	μ	σ	a	b	R^2	μ	σ	a	b	R^2
V_{ed}	2.667	0.063	-0.004	2.707	0.124	2.404	0.140	-0.021	3.078	0.821	2.265	0.068	-0.000	2.288	0.001
V_{es}	1.494	0.048	-0.002	1.515	0.061	1.069	0.238	-0.039	2.299	0.945	0.768	0.044	-0.002	0.868	0.064
SV	1.173	0.077	-0.002	1.191	0.018	1.334	0.134	0.018	0.779	0.607	1.497	0.074	0.001	1.420	0.014
P_{ed}	23.065	2.704	-0.154	24.685	0.114	21.398	2.377	-0.053	23.069	0.017	20.489	2.763	-0.120	26.806	0.066
P_{es}	104.316	1.663	-0.076	105.116	0.073	89.887	8.910	-1.474	136.313	0.958	74.365	2.391	-0.109	80.113	0.073
$P_{baseline}$	63.690	1.699	-0.115	64.900	0.161	55.642	4.750	-0.763	79.691	0.904	47.427	1.560	-0.115	53.460	0.190

Table C-5: Mean (μ), standard deviation (σ) and fit coefficients (a, b and R^2) for V_{ed}, V_{es}, SV, P_{ed}, P_{es} and $P_{baseline}$ in BJR reflex *stimulation* of group NOR ($n = 23$), discriminated by measurement.

After Myocardial Infarction:

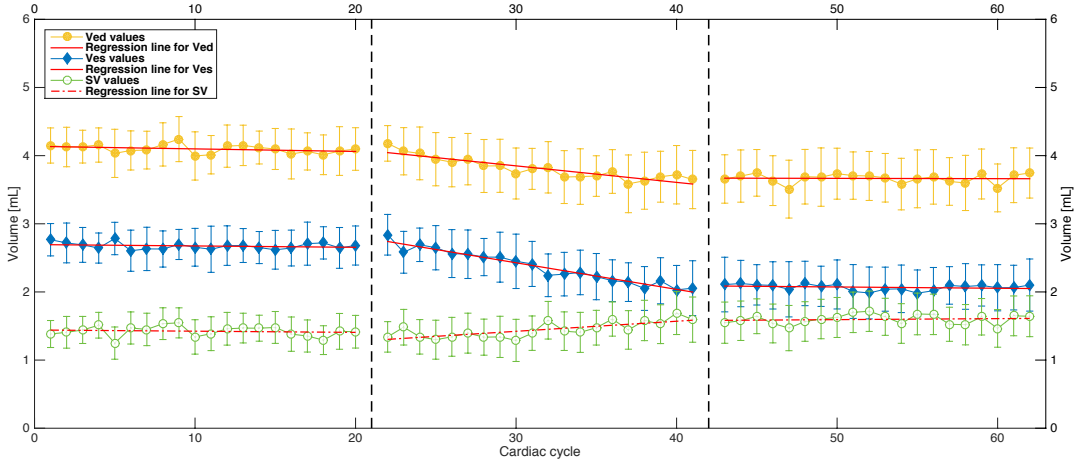

Figure C-11: Beat-to-beat mean V_{ed}, V_{es} and SV during three 20-beat measurements, caused by activation of the cardiopulmonary reflex ($n = 13$) after acute myocardial infarction (`AMI`). Bars denote standard deviation. Y-axis limits were set to $[0;\ 6]\ mL$.

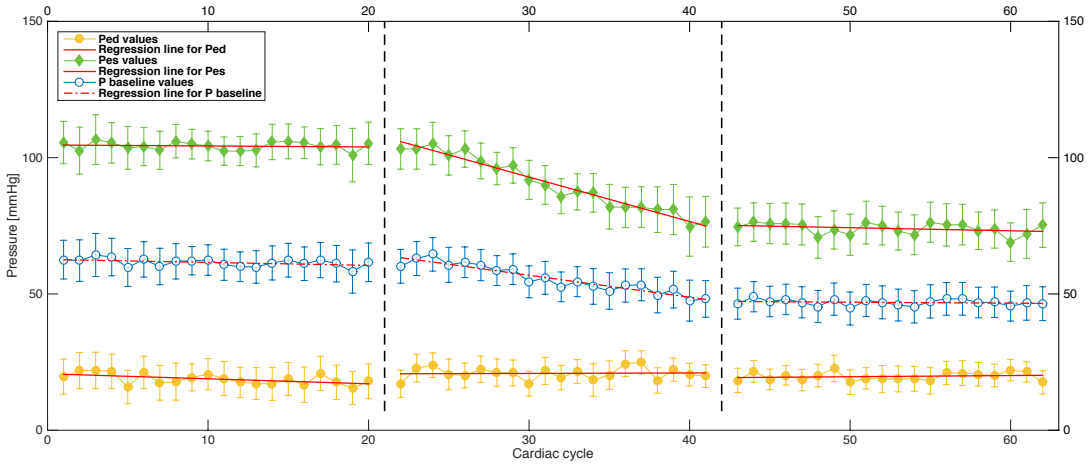

Figure C-12: Beat-to-beat mean P_{ed}, P_{es} and $P_{baseline}$, as response to the activation of the Bezold-Jarisch reflex ($n = 13$) after myocardial infarction (`AMI`), for *measurements* `M1-3`. Bars denote standard deviation. Y-axis limits were set to $[0;\ 150]\ mmHg$.

	Measurement M1					**Measurement M2**					**Measurement M3**				
	μ	σ	a	b	R^2	μ	σ	a	b	R^2	μ	σ	a	b	R^2
V_{ed}	4.097	0.063	-0.004	4.137	0.124	3.814	0.159	-0.024	4.578	0.816	3.665	0.068	-0.000	3.688	0.001
V_{es}	2.674	0.048	-0.002	2.695	0.061	2.369	0.238	-0.039	3.599	0.945	2.068	0.044	-0.002	2.168	0.064
SV	1.423	0.077	-0.002	1.441	0.018	1.444	0.117	0.015	0.979	0.556	1.597	0.074	0.001	1.520	0.014
P_{ed}	18.780	2.035	-0.183	20.701	0.283	20.870	2.214	0.016	20.362	0.002	19.747	1.525	0.043	17.506	0.027
P_{es}	104.270	1.559	-0.036	104.653	0.019	90.425	9.853	-1.629	141.753	0.957	74.019	2.096	-0.114	80.008	0.104
$P_{baseline}$	61.525	1.451	-0.110	62.677	0.200	55.648	5.056	-0.807	81.057	0.891	46.883	1.129	-0.036	48.757	0.035

Table C-6: Mean (μ), standard deviation (σ) and fit coefficients (a, b and R^2) for V_{ed}, V_{es}, SV, P_{ed}, P_{es} and $P_{baseline}$ in BJR reflex *stimulation* of group `AMI` ($n = 13$), discriminated by measurement.